DYNAMIC BEHAVIOUR OF COMPOSITE STRUCTURES CONTAINING VISCOELASTIC MATERIALS, WITH APPLICATIONS TO SOLID FUEL ROCKET MOTORS.

A thesis submitted for the degree of Doctor of Philosophy.

by

Wendy Edwards.

March 1975.

Synopsis

The object of the research was to study the effect of forced harmonic vibration on solid fuel rocket motors. A rocket motor consists of the motor case (which contains the propellant) and the blast tube attached to the aft end. The propellant is a viscoelastic material, no reliable data on the complex modulii of the propellants were available so a method was developed to measure it - the admittance method. This consists of vibrating a rod longitudinally, the applied force is kept constant the acceleration at the free end and the phase difference between force and acceleration are measured. The frequency is varied and a set of measurements obtained for each frequency. These data are then used in a computer program to iterate to the complex modulus necessary to give the particular acceleration and phase at the particular frequency. Thus values of complex modulus are obtained for each frequency at which measurements are made. The modulus thus measured was used to calculate

(i) the acceleration and phase at the forced end of the rod in longitudinal vibration

(ii) the acceleration and phase at both ends of the rod in transverse vibration

(iii) the acceleration along the length of the full scale sample.

The calculations compared very well with measured data.

The rocket motor was then analysed as rigidly connected beams. The equations used were the Timoshenko beam equations which include the effect of shear deformation and rotary inertia. The unknown coefficients were found from the end conditions of the beams.

Analyses were carried out on four different motor designs, experimental data were available for three of them. The calculated and measured results were in good agreement even though the data were not detailed enough to give an accurate representation of the constraints.

3. Case bonded motors - theoretical approach

results of computer analysis

comparison with measurements

5. Conclusions and proposals for further work

Appendices A The Euler-Bernoulli equations for transverse vibrations of beams

B The Timoshenko equations for transverse vibrations of beams

C Comparison of "direct" and "modal analysis" methods

D Gauss elimination

E FORTRAN listing of the program which obtains the dynamic modulus from experimental measurements

References

Acknowledgements

List of Figures

Notation

A	Area (m^2)
a_m	Maximum acceleration (at frequency fm) (m/s^2)
B_1, B_2 etc	Unknown coefficients in the solution of Timoshenko equation (m)
B_j	$1/K_j$ for Kelvin viscoelastic model (m/N)
b	γl, variable used in the iteration routine
b_o	Initial estimate for b
b_n	n^{th} iterated value of b
$\bar{b}$	Solution of frequency equation
c	Damping constant for a viscous damper (Ns/m)
c_j	Damping constant for the viscous damper of element j in viscoelastic model (Ns/m)
$D_{crp}(t)$	Creep compliance (m^2/N)
$D^*(\omega)$	Dynamic compliance or complex compliance (m^2/N)
d_1	Distance of accelerometer from bonded edge of mass m_1 (m)
d_2	Distance of accelerometer from bonded edge of mass m_2 (m)
E	Young's modulus (N/m^2)
$E_{rel(t)}$	Relaxation modulus (N/m^2)
$E^*(\omega)$	Dynamic modulus or complex modulus (N/m^2)
$E(s)$	$Q(s)/P(s)$
E_1	Real part of E^* (N/m^2)
E_2	Imaginary part of E^* (N/m^2)
$\lvert E^* \rvert$	Modulus of E^* $= \sqrt{(E_1^2 + E_2^2)}$ (N/m^2)
$E_2/E_1 = \eta =$	$\tan \delta$
F	Applied force (N)
F_o	Amplitude of applied force, $F = F_o e^{i\omega t}$ (N)
f	Frequency (Hz)
$f(x,t) = \ddot{U}(x,t)$	Acceleration (m/s^2)

f_m	Frequency where the acceleration is a maximum (Hz)
f_n	Undamped natural frequency (Hz)
f_1	Frequency where the acceleration is pa_m or $a_m/\sqrt{2}$ (Hz)
f_2	Frequency where the acceleration is $a_m/\sqrt{2}$ (Hz)
G^*	Complex shear modulus $G^* = E^*/(2(1 + \nu^*))$ (N/m^2)
I	Moment of inertia (kgm^2) and second moment of area (m^4)
i	$\sqrt{-1}$
K	Stiffness of elastic spring (N/m)
K_j	Stiffness of elastic spring of element j in viscoelastic model (N/m)
k'	Shape factor in Timoshenko equations
L_1	Length of mass m_1 (m)
L_2	Length of mass m_2 (m)
L_3	Distance between point of application of force and free edge (m)
l	Length of rod or beam (m)
M(x,t)	Bending moment (Nm)
m_1	Mass of the block at the forced end of the rod (kg)
m_2	Mass of the block at the free end of the rod (kg)
N_1	$m_1/\rho Al$ ratio of end mass : beam mass
N_2	$m_2/\rho Al$
P	measured acceleration at the free end of the rod in longitudinal vibration $P = \|P\| e^{i\theta}$ (m/s^2)
P_1	Acceleration of mass m_1 at a distance d_1 from the bonded edge (m/s^2)
P_2	Acceleration of mass m_2 at a distance d_2 from the bonded edge (m/s^2)
$\underline{p}$	$\sum p_k \frac{\partial^k}{\partial t^k}$, differential operator used in viscoelastic stress-strain relations
P(s)	$\sum p_k s^k$, polynomial in s with the same coefficients as $\underline{p}$
p	proportion of 1, $0 < p < 1$

p_k	Coefficient of $\underline{P}$ and $P(s)$
$Q(x,t)$	Shear force (N)
Q	$1/2\ \xi$, magnification factor
$\underline{Q}$	$\sum q_x \frac{\partial^k}{\partial t^k}$, differential operator used in viscoelastic stress-strain relations
$Q(s)$	$\sum q_k s^k$, polynomial in s with the same coefficients as $\underline{Q}$
q_k	Coefficient of $\underline{Q}$ and $Q(s)$
q_T	Correction factor for the dynamic modulus obtained from the relaxation modulus
R	Parameter of Timoshenko equation solution defined in Appendix B, equation B(19) (1/m)
S	Parameter of Timoshenko equation solution defined in Appendix B, equation B(20) (1/m)
s	Laplace Transform variable
T	Temperature (^oK)
T_o	Reference temperature (^oK)
t	Time (seconds)
$U(x,t)$	Displacement (m)
$u(x)$	Spatial variation of $U(x,t)$ (m)
X_n	Normal modes of free vibration
x	Spatial variable (along the length of the beam) (m)

α	Variable in the solution of the Timoshenko equation, defined in Appendix B, equation B(17) (1/m)
α_j	c_j/K_j , "relaxation time" of element j in viscoelastic model (s)
α_n	Attenuation factor associated with frequency ω_n
α_T	"Shift factor" used in the superposition principle
β	Variable in the solution of the Timoshenko equation, defined in Appendix B, equation B(18) (1/m)
γ	$\omega\sqrt{\rho/E}$ for elastic materials, $\omega\sqrt{\rho/E^*}$ for viscoelastic materials (1/m)
δ	$\tan^{-1} E_2/E_1$
ϵ	A small quantity
ϵ_x	Strain in the x-direction
η	E_2/E_1
θ	Phase difference (radians)
ν	Poisson's ratio of elastic material
ν^*	Complex Poisson's ratio of viscoelastic material
ξ	Damping ratio $\xi = C/C_c = C/2\sqrt{km} = 1/2Q$
ρ	Mass density (kg/m^3)
σ_x	Stress in the x-direction (N/m^2)
ϕ_n	Generalised coordinate
$\psi(x,t)$	Slope of the neutral axis of a beam in bending
Ω	f_1/f_m
ω	frequency (radians/s)
ω_n	resonant frequency (radians/s)

Chapter I

INTRODUCTION

1.1 Rocket Motors and the Problems of Environmental Vibrations

1.1.1 Missiles

The rocket motors manufactured at Summerfield Research Station (SRS) are used to power guided tactical missiles. SRS motors are used in most of the British weapon systems e.g.

British Aircraft Corporation:	Thunderbird and Rapier (ground-to-air missiles)
	Swingfire, Vigilant and Hawkswing (anti-tank)
Hawker Siddeley Dynamics:	Seadart and Seaslug (ship-to-air)
	SRAAM (air-to-air)
Short Bros. and Harland:	Seacat (ship-to-air)
	Tigercat (ground-to-air)

Many of these systems have been sold overseas, also a number of contracts have been won by SRS for motors to power missiles developed in other countries.

1.1.2 Rocket Motors

A missile usually has two stages of powered flight - a boost phase and a sustain phase. The boost is high thrust/short burn for the initial lift off and the sustain is low thrust/long burn time to convey the missile to its target, rocket motors may be used for both phases. The missile can have separate boost and sustainer motors or a dual purpose motor. Rocket motors can be powered by solid or liquid fuel. Only solid fuel motors will be considered in the present work since this is the type manufactured at SRS.

A motor consists of the propellant, the case, an igniter and a blast tube or nozzle. There are facilities at SRS for the manufacture and assembly of all the components.

1.1.3 Propellant

The fuel used in the motors manufactured at SRS is cast double base (CDB)propellant i.e. it is made by a casting process, the basic

ingredients being nitroglycerine and nitrocellulose. There are two types of CDB propellant, conventional and composite modified, the latter has the double base matrix with large proportions of aluminium and oxidiser, it has a higher energy rating than the conventional CDB propellant. Other proprietary ingredients are added to the fuels to improve ballistic performance, to ensure it is safe to handle and to inhibit adverse chemical changes.

The propellant is a viscoelastic material, it has a high coefficient of expansion, most properties are temperature dependent, it is homogeneous, virtually incompressible and the density is about 1/5 that of steel.

1.1.4 Motor designs

There are two types of motor design - cartridge loaded and case bonded.

With a cartridge loaded motor the propellant is cast into a cylindrical mould which has a loose lining of inhibitor (a material which does not burn); as the propellant solidifies the inhibitor bonds to it on the outer surface (with an end face left free). When removed from the mould the propellant plus inhibitor is called the 'charge'. The charge is loaded into the case; it can be loosely inserted (with no restraints), located in place on spigots or bolted and/or bonded to the case at the forward end.

With a case bonded motor the propellant is cast directly into the case (which has a bonded inhibitor lining).

A charge can either be solid or have a central aperture down the length (called a conduit). A solid charge is ignited at the rear and burns along the length - hence the alternative name of "cigarette burner". The other type is ignited at the forward end and burns radially outwards along the entire length. The shape of the conduit is designed to give a variation of burning surface which results in the specified performance.

Solid charges are always cartridge loaded but radial burners can be case bonded or cartridge loaded.

Because there is a larger burning surface, a radial burner burns more quickly than a solid charge of the same propellant.

The coefficient of expansion of propellant is about 18 times that of steel (from which the case is usually made) and the motor must withstand ambient temperatures from -40°C to +60°C. As the motor cools the propellant shrinks more than the case, with a case bonded radial burning charge deformation of the inner surface helps to alleviate the stress on the bonded interface. If the bond between the propellant and the inhibited case is broken then the burning surface is increased and when ignited the motor will not perform as designed.

If a solid charge was bonded to the case, a drop in temperature would cause the propellant to pull away from the case or break itself; this is why solid charges are cartridge loaded and not case bonded. Since solid charges burn longer, when a long burn time is required the design is a cartridge loaded motor.

1.1.5 Qualification tests

Before production begins on a new motor design, it has to pass a series of customer specified 'qualification tests'. These are to show that the performance is as required (e.g. burning rate, burning time, thrust, total impulse etc) and to ensure that the motor will withstand environmental conditions without deterioration of safety or performance standards. The environmental tests include temperature cycling, high humidity, drop tests, bump tests and environmental vibration tests. If the motor design does not pass all these qualification tests then penalties are incurred while problems are rectified - hence a series of pre-qualification trials are completed to ensure that the motors will not fail.

1.1.6 Environmental vibration tests

These trials are to simulate the transport vibrations encountered while the motor is being carried on a lorry, plane, ship etc. The

actual test is specified by the customer but is usually low frequency forced vibrations (10 Hz to 1 000 Hz) for a long duration (several hours). It can consist of random or sinusoidal vibration. The sinusoidal vibration may consist of forcing the motor at one frequency (usually a resonance) or sweeping up and down through a specific frequency range. The whole vibration specification can contain just some or all of these and usually tests are carried out at several temperatures.

1.1.7 The problem

In 1970 during the pre-qualification environmental vibration trials of one particular motor (A), there were several failures. The motors were stripped down after the trials to be inspected and it was found that motors tested at the high temperature (40°C) were damaged. Motor (A) was a cartridge loaded motor - it was about 2.5 m long in total, the propellant within it about 1.5 m. The propellant was bolted and bonded to the forward end plate which was rigidly connected to the case, otherwise the charge was free to move within the constraints of the case. At 20°C the gap between the charge and the case was 1 mm and at 40°C it was 0.64 mm. The damage was about 1 m from the fixed end and was in the form of a radial crack in the inhibitor.

Several modifications were made and after about three months the problem was overcome by supporting the charge along the length with rubber strips (thus still allowing room for expansion). This was considered to be a temporary expedient, so in 1971 the topic of 'The vibrations of rocket motors' was offered to the University of Aston as an IHD project. It was hoped to discover how the charge was damaged and devise a method for detecting and removing problems at the design stage with future motors.

1.2 Viscoelasticity

1.2.1 General

A viscoelastic material is one for which the mechanical behaviour exhibits viscous and delayed elastic response to stress in addition to instantaneous elasticity, the strain being dependent on the rate of loading as well as the level of load and, in general, not all of the strain being recoverable.

The material displays creep under static loads and the response to dynamic loads is damped (because of the viscous effects).

If the material is subjected to a constant applied load then the plot of strain/stress vs time gives the 'creep compliance' $D_{crp}(t)$, see Figure 1.1(a).

If the material is subjected to a constant strain then stress/strain vs time gives the 'relaxation modulus' $E_{rel}(t)$, see Figure 1.1(b).

There also exists a dynamic modulus E^* and a dynamic compliance D^*:

for a harmonically varying stress and strain,

$$E^* = \frac{\text{stress}}{\text{strain}}$$

and

$$D^* = \frac{\text{strain}}{\text{stress}}$$

then

$$D^* = \frac{1}{E^*}$$

E^* and D^* vary with frequency ω since the strain is dependent on the rate of loading.

As the response is damped the strain is not in phase with the stress so E^* and D^* are complex numbers (they are also known as the complex modulus and the complex compliance).

i.e. for a harmonically varying stress,

$$\sigma_x(t) = \sigma_o e^{i\omega t}$$

the resulting strain,

$$\epsilon_x(t) = \epsilon_o e^{-i\theta} e^{i\omega t}$$

where θ is the phase difference between stress and strain, the strain always lagging behind the stress.

then $$E^* = \frac{\sigma_x(t)}{\epsilon_x(t)} = \frac{\sigma_o}{\epsilon_o} e^{i\theta}$$

which is complex .

The compliances and moduli are, in general, also temperature dependent.

Note: These moduli apply for simple extension, there are equivalent moduli for shear deformation, bulk longitudinal deformation and bulk compression and dilation. The present research deals only with the case of simple extension so the others will not be discussed here, they are related to the extension moduli and are fully covered in Ferry (48).

1.2.2 Stress-strain relationships

For a linear elastic material the stress σ_x is related to the strain ϵ_x by Hooke's Law, i.e.

$$\sigma_x = E\epsilon_x \qquad 1.2(1)$$

where E is Young's modulus.

For a linear viscoelastic material the relation can be written as

$$\underline{P}(\sigma_x) = \underline{Q}(\epsilon_x) \qquad 1.2(2)$$

where $\underline{P}$ and $\underline{Q}$ are differential operators,

with $$\underline{P} = \sum_{k=1}^{m} p_k \frac{\partial^k}{\partial t^k}$$

and $$\underline{Q} = \sum_{k=1}^{n} q_k \frac{\partial^k}{\partial t^k}$$

see Flügge (49).

1.2.3 Viscoelastic moduli and compliances

The Laplace Transform of Equation 1.2(2) is

$$P(s)\,\bar{\sigma}_x = Q(s)\,\bar{\epsilon}_x \qquad 1.2(3)$$

where $P(s) = \sum_{k=1}^{m} p_k s^k$

and $Q(s) = \sum_{k=1}^{n} q_k s^k$

i.e. P(s) and Q(s) are polynomials in s with the same coefficients as $\underline{P}$ and $\underline{Q}$.

and $\bar{\sigma}_x$ and $\bar{\epsilon}_x$ represent the Laplace Transforms of σ_x and ϵ_x respectively.

Then $$\bar{\sigma}_x = \frac{Q(s)}{P(s)}\ \bar{\epsilon}_x$$

or $$\bar{\sigma}_x = E(s)\bar{\epsilon}_x \qquad 1.2(4)$$

where $$E(s) = \frac{Q(s)}{P(s)}$$

1.2.4 Creep compliance

A constant stress, $\sigma_x(t) = \sigma_o$, is applied and the variation of strain with time, $\epsilon_x(t)$, is measured to give the creep compliance

$$D_{crp}(t) = \frac{\epsilon_x(t)}{\sigma_o}$$

Since $$\epsilon(t) = D_{crp}(t)\,\sigma_o$$

then $$\bar{\epsilon}_x = \bar{D}_{crp}(s)\,\sigma_o$$

and since $\sigma_x(t) = \sigma_o$

then $$\bar{\sigma}_x = \sigma_o/s$$

substituting in 1.2(3) gives

$$\bar{D}_{crp}(s) = \frac{P(s)}{sQ(s)} = \frac{1}{sE(s)} \qquad 1.2(5)$$

1.2.5 Relaxation modulus

A constant strain, ϵ_o, is maintained and the relaxation modulus is found from the variation of stress with time,

$$E_{rel}(t) = \frac{\sigma_x(t)}{\epsilon_o}$$

Since $\sigma_x(t) = E_{rel}(t)\,\epsilon_o$

then $\bar{\sigma}_x = \bar{E}_{rel}(s)\,\epsilon_o$

and since $\epsilon_x(t) = \epsilon_o$

then $\bar{\epsilon}_x = \epsilon_o/s$

Substituting in 1.2.(3),

$$\bar{E}_{rel}(s) = \frac{Q(s)}{P(s)\,s} = E(s)/s \qquad 1.2(6)$$

1.2.6 Dynamic modulus

If it is assumed that the stress is varying harmonically with frequency ω i.e. $\sigma = \sigma_o e^{i\omega t}$, then by substitution into 1.2.(2):

$$\left(\sum_{k=o}^{m} p_k \frac{\partial^k}{\partial t^k}\right)\left(\sigma_o e^{i\omega t}\right) = \left(\sum_{k=o}^{n} q_k \frac{\partial^k}{\partial t^k}\right)\left(\epsilon_o e^{i\omega t}\right)$$

therefore $\sum_{k=o}^{m} p_k (i\omega)^k \sigma_o e^{i\omega t} = \sum_{k=o}^{n} q_k (i\omega)^k \epsilon_o e^{i\omega t}$

i.e. $\left[P(s)\right]_{s=i\omega} \sigma_x = \left[Q(s)\right]_{s=i\omega} \epsilon_x$

$$\sigma_x = \left[\frac{Q(s)}{P(s)}\right]_{s=i\omega} \epsilon_x$$

or $\sigma_x = E^* \epsilon_x$.

Where $E^* = \left[E(s)\right]_{s=i\omega} = \left[s\,\bar{E}_{rel}(s)\right]_{s=i\omega}$ 1.2(7)

1.2.7 Elastic and viscoelastic analyses

If we consider the analysis of a continuous medium, there are three types of equations which formulate the problem:

1. Equilibrium conditions
2. Strain-displacement relationships
3. Stress-strain relationships

and the only difference between an elastic analysis and that for a viscoelastic substance is the third, the constitutive equation. For a linear elastic material this is $\sigma_x = E\epsilon_x$ and for a linear viscoelastic material it can be written

$$\underline{P}(\sigma_x) = \underline{Q}(\epsilon_x)$$

It has been shown in section 1.2.3 that in the transformed domain

$$\overline{\sigma}_x = E(s)\,\overline{\epsilon}_x ,$$

thus it can be seen that the analysis for a viscoelastic material can be obtained from the solution of the corresponding elastic problem by replacing the unknown variable with its Laplace Transform, replacing E with E(s), and then inverting back into the time domain. This is known as the 'correspondence principle'. See refs. (11), (48) and (49).

Because of the complicated nature of the viscoelastic problems, the inversion will probably have to be carried out numerically. See refs. (8) and (37).

If the stress varies harmonically with time the constitutive equation is $\sigma = E^*\epsilon$ (equation 1.2(7)), therefore in dealing with vibration analysis, the correspondence principle states that: The solution to a viscoelastic problem can be obtained from that of an elastic material by replacing the elastic constants with the equivalent complex, frequency-varying functions. (See refs. (35) and (43)).

The present research considers forced vibrations so this latter form of the correspondence principle is used throughout. The Young's modulus E is replaced by the complex modulus $E^*(\omega)$.

If free vibrations are considered, E is replaced with $E^* (\omega_n + i\alpha_n)$ since the natural frequencies are complex because the free vibrations are damped; ω_n is the frequency and α_n is the attenuation factor.

1.2.8 Viscoelastic models

The solutions to most viscoelastic problems that have been solved, have been arrived at by using simple models - a combination of elastic springs and viscous dampers. (See refs. (10), (19), (20) and (50)). The simplest are the Maxwell and Kelvin elements, refs. (11), (49).

The Maxwell element is a spring and damper in series and the Kelvin element is a spring and damper in parallel.

The stress-strain relationship for the Maxwell element is

$$\left(1 + \frac{c}{K}\frac{d}{dt}\right)\sigma_x = \left(c\frac{d}{dt}\right)\epsilon_x$$

then $$E(s) = \frac{cs}{1+\frac{c}{K}s}$$

$$E_{rel}(t) = K e^{-\frac{K}{c}t}$$

$$D_{crp}(t) = \left(\frac{c}{K} + t\right)\Big/c$$

$$E^*(\omega) = \frac{\omega^2 c^2/K}{1+\frac{c^2\omega^2}{K^2}} + i\,\frac{c\omega}{1+\frac{c^2\omega^2}{K^2}}$$

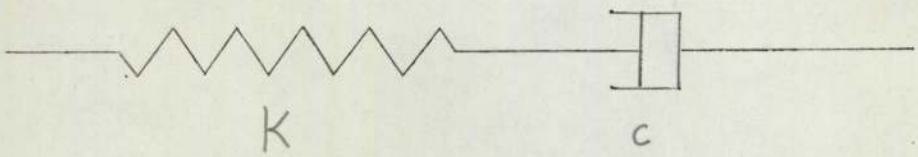

Maxwell element

The stress-strain relationship for the Kelvin element is:

$$\sigma_x = (K + c\frac{d}{dt})\epsilon_x$$

then $E(s) = K + cs$

and $E_{rel}(t) = K + c\delta(t)$

where $\delta(t)$ is the Dirac delta function

$$D_{crp}(t) = \frac{1}{K}(1-e^{-K/ct})$$

$$E^*(\omega) = K + ic\omega$$

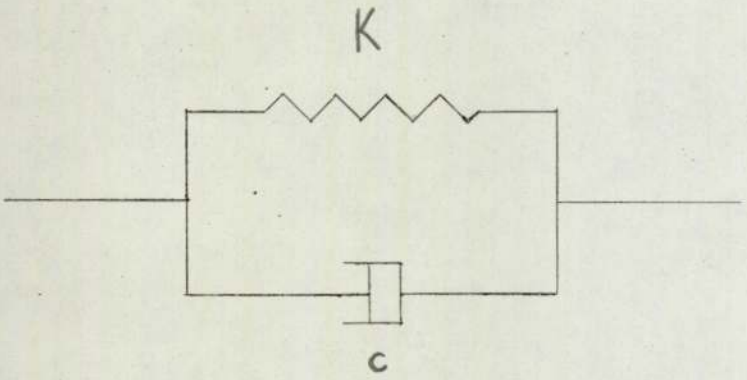

Kelvin element

Clearly such simple models do not adequately describe the behaviour of real materials so they have been extended; the'Maxwell Model'consists of n Maxwell elements in parallel and the 'Kelvin Model' consists of n Kelvin elements in series. (11), (49).

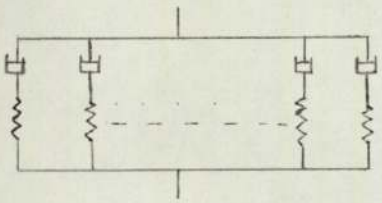

Maxwell model

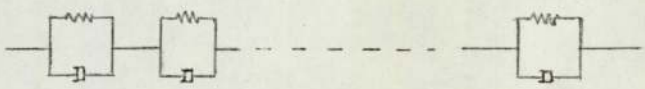

Kelvin model

The Maxwell Model is used when the relaxation modulus $E_{rel}(t)$ or the dynamic modulus E^* is required as they are easily derived as:

$$E_{rel}(t) = \sum_{j=1}^{n} K_j \, e^{-t/\alpha_j}$$

and $$E^*(\omega) = \sum_{j=1}^{n} \left[\frac{\alpha_j^2 \omega^2 K_j}{1+\alpha_j^2 \omega^2} + i \frac{\omega K_j \alpha_j}{1+\omega^2 \alpha_j^2} \right]$$ (See Ferry (48))

where K_j is analogous to the stiffness of the spring in element j. α_j is the ratio of the damping factor (c_j) of the dashpot in element j to the spring stiffness K_j.

The Kelvin Model is used when the creep compliance $D_{crp}(t)$ or the dynamic compliance D^* is required since they are simply expressed as:

$$D_{crp}(t) = \sum_{j=1}^{n} B_j \, (1-e^{-t/\alpha_j})$$

$$D^*(\omega) = \sum_{j=1}^{n} \left[\frac{B_j}{1+\omega^2 \alpha_j^2} + i \frac{B_j \omega \alpha_j}{1+\omega^2 \alpha_j^2} \right]$$

where $B_j = 1/K_j$

1.2.9 Fitting viscoelastic models

The method used to find the parameters of these models for a particular material is to measure one of the moduli and to fit the model's formula for that modulus to the measured values.

e.g. If a Maxwell element is to be used, the relaxation modulus of the material can be measured and the curve $E_{rel}(t) = K \, e^{-tK/c}$ is either fitted to two measured points or a least squares method is used to fit the curve through several points.

The moduli are all interrelated and, in theory, having obtained one, the others can be evaluated:

from equation 1.2(5) $\quad \bar{D}_{crp}(s) = 1/s\, E(s)$

from equation 1.2(6) $\quad \bar{E}_{rel}(s) = E(s)/s$

from equation 1.2(7) $\quad E^*(\omega) = 1/G^*(\omega) = \left[E(s) \right]_{s=i\omega}$

1.2.10 Time-temperature superposition principle (Refs.(11) and (48))

There are difficulties in determining the relaxation modulus and creep compliance in that the values change so rapidly with time that it is impractical to measure them accurately. See, for example, the relaxation modulus in fig.1.2(b), at $t=10^{-9}$, $E_{rel}(t) = 500$ and at $t=10^{-2}$, $E_{rel}(t) \simeq 18$.

This problem is overcome by using the time-temperature superposition principle:

$$E_{rel}(t,T) = E_{rel}(t/\alpha_T, T_o) \qquad 1.2(8)$$

where T_o is the (arbitrary) reference temperature.

This states that $E_{rel}(t)$ measured at a time t and a temperature T is equivalent to the modulus at a temperature T_o with the time axis shifted by a function α_T (called the 'shift factor').

Thus if the relaxation modulus is measured at several temperatures and plotted against t/α_T, a single composite curve will be formed corresponding to $E_{rel}(t)$ at the temperature T_o. A considerable extension to the time range is achieved in this way.

From the composite curve of the relaxation modulus vs t/α_T at temperature T_o (fig.1.2(b)), and the graph of α_T vs T (fig.1.2(a)), the modulus for any temperature can be found by substituting the particular value of α_T into equation 1.2(8).

A similar process is used to extend the time range of the creep compliance,

$$D_{crp}(t,T) = D_{crp}(t/\alpha_T, T)$$

1.2.11 Frequency-temperature superposition principle

It is difficult to devise an experiment to measure the dynamic modulus (or compliance) over a large frequency range; the range can be greatly expanded by using a similar superposition principle, the frequency-temperature superposition principle:

$$E^*(\omega,T) = E^*(\alpha_T\omega, T_o)$$

and $$D^*(\omega,T) = D^*(\alpha_T\omega, T_o)$$

where α_T is the same as given above.

Thus by making measurements at several temperatures it is possible to achieve a considerable extension to the frequency range in this manner.

See Ferry (48), chapter 11 for a full discussion of the superposition principles (which is called the 'method of reduced variables'). Also described are methods for finding α_T ; several empirical formulae are given.

1.3 Outline of Investigation

The investigation began with experiments at Aston on a piece of inert propellant (i.e. containing no explosive constituents). A rod 0.9 m long with a circular cross section of diameter 0.15 m was used; it was vibrated longitudinally and transversely. The response to forced harmonic vibrations was measured and is reported in section 2.2. Having become familiar with the experimental technique the equipment was transported to IMI Summerfield and the tests repeated on live propellant. These experiments are reported in section 2.3.

The theoretical approach initially used was the lumped parameter method; this can be used for longitudinal and transverse vibrations. A continuous beam is approximated as point masses connected by springs and dampers. It is a useful approximation for complicated elastic systems with little or no damping and gives good agreement with an exact analysis when using only a few point masses. The difficulty was to describe the material properties. It could be done by using Maxwell, Kelvin or more complicated models, however if the model was good enough to describe the material behaviour adequately it was extremely difficult to solve the ensuing matrix equations, see Ref. (29). Since forced harmonic vibrations were being considered it was possible to use the simpler correspondence principle given in section 1.2.7 i.e. substitute E^* for E in the analysis for a similar elastic system. As the test pieces and rocket motors generally consist of uniform beams and cylinders the equations are not difficult to formulate. The difficulty lies not in the shape of the structure but in the propellant's dynamic properties; thus if graphs of E^* vs frequency and temperature are available then for a specific frequency and temperature the value of E^* can be used to calculate the response. There is thus no need to actually categorise either the type of damping or the variation of modulus with frequency and temperature.

Initially the E* graphs were obtained from the relaxation modulus as described in section 1.2.6.

Longitudinal vibrations were analysed using the single degree of freedom equation for a long thin rod, this assumes a constant stress over the cross section.

For transverse vibrations the single degree of freedom Euler-Bernoulli equation was used (see Appendix A). The theoretical predictions did not agree with the measurements on the test piece, it was thought that the complex modulus was not accurate so a method was devised to measure it directly. This is fully discussed in chapter 3, but essentially it consists of forcing a small rod in longitudinal vibrations and measuring the acceleration (both magnitude and phase) of the free end. The complex modulus is obtained from a computer program which iterates to find a value of E* to give the measured response at that particular frequency. In this way E* was measured for frequencies in the range 100-1 000 Hz and temperatures between -10 and +40°C. The modulus thus measured was appreciably different from that calculated from the transform of the relaxation modulus (see fig. 1.3).

The complex modulus was first verified by comparing predicted and measured values of acceleration at the forced end of the rod in longitudinal vibrations. There was good agreement throughout the frequency range. (Section 3.6)

The same rod was then harmonically forced in transverse vibrations and the measured accelerations compared with calculations, up to the first resonance they agreed quite well but not at higher frequencies. The analysis was amended to include the effect of shear deformation and rotary inertia (i.e. the Timoshenko beam equations). The discrepancy between measured and calculated was then within 10% throughout the frequency range. (Section 3.7)

The Timoshenko beam equations were solved for the large test pieces used in the preliminary tests; with these equations and more accurate values of E* the calculated response agreed very well for the first seven bending modes. After this, secondary resonances (coupled bending and radial modes, transverse shear modes etc) were excited; as large displacements cause the problems in rocket motors the low frequencies are much more important, so the bending theory is quite adequate. This is fully discussed in section 3.8.

The modulus measurement technique was also used on a sample of natural rubber, the results are discussed in section 3.9.

The whole motor was then studied, three computer programs were written to analyse the response of motors to forced harmonic vibrations:

1. case bonded motors when the applied forces are specified,
2. case bonded motors when accelerations at control points are specified
3. cartridge loaded motors

The case bonded motor was modelled as two rigidly connected uniform beams (main motor body and blast tube or nozzle). The main motor body is an elastic/visco-elastic composite structure and the blast tube or nozzle is assumed to be elastic.

The cartridge loaded motor was considered to be three rigidly connected uniform beams (motor case, propellant and blast tube or nozzle), the propellant being viscoelastic and the other two beams elastic. The results from these models show good agreement with measurements made on actual motors. These three programs should be adequate for the analysis of all case bonded motors and for all cartridge loaded motors where the propellant is secured to the case at the forward end. All the details of this work is given in chapter 4.

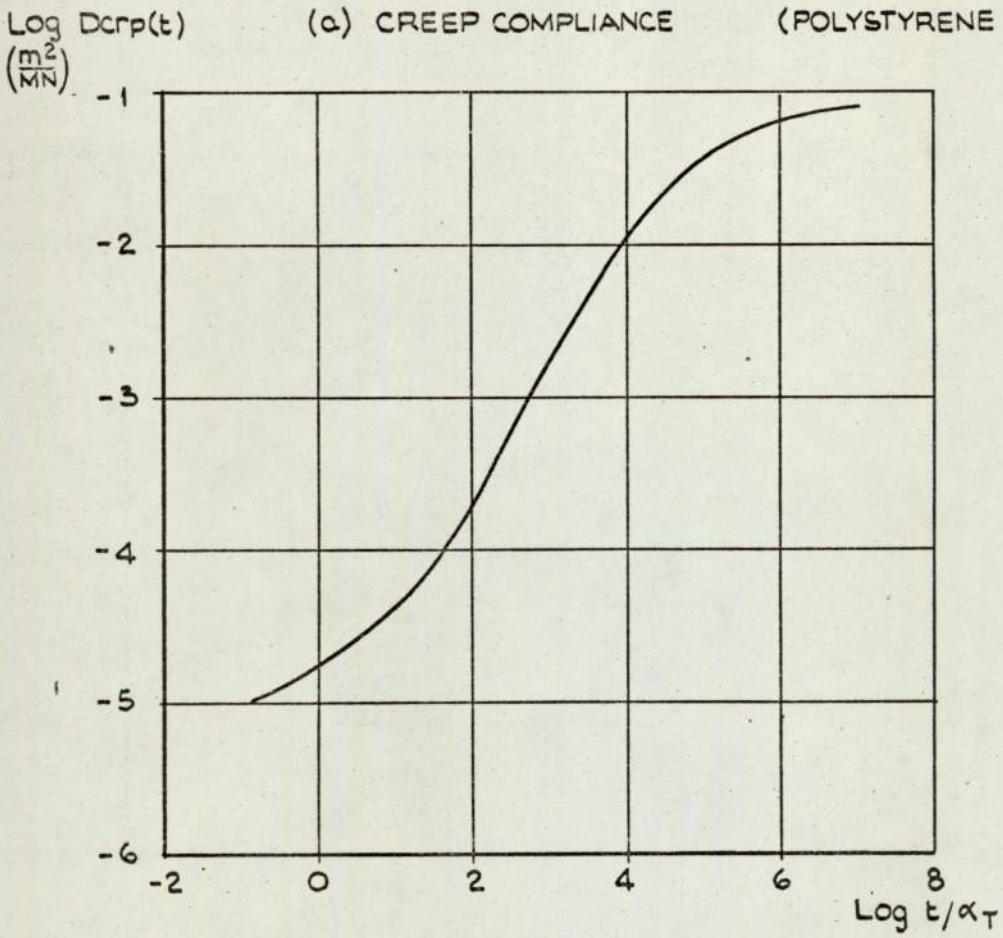

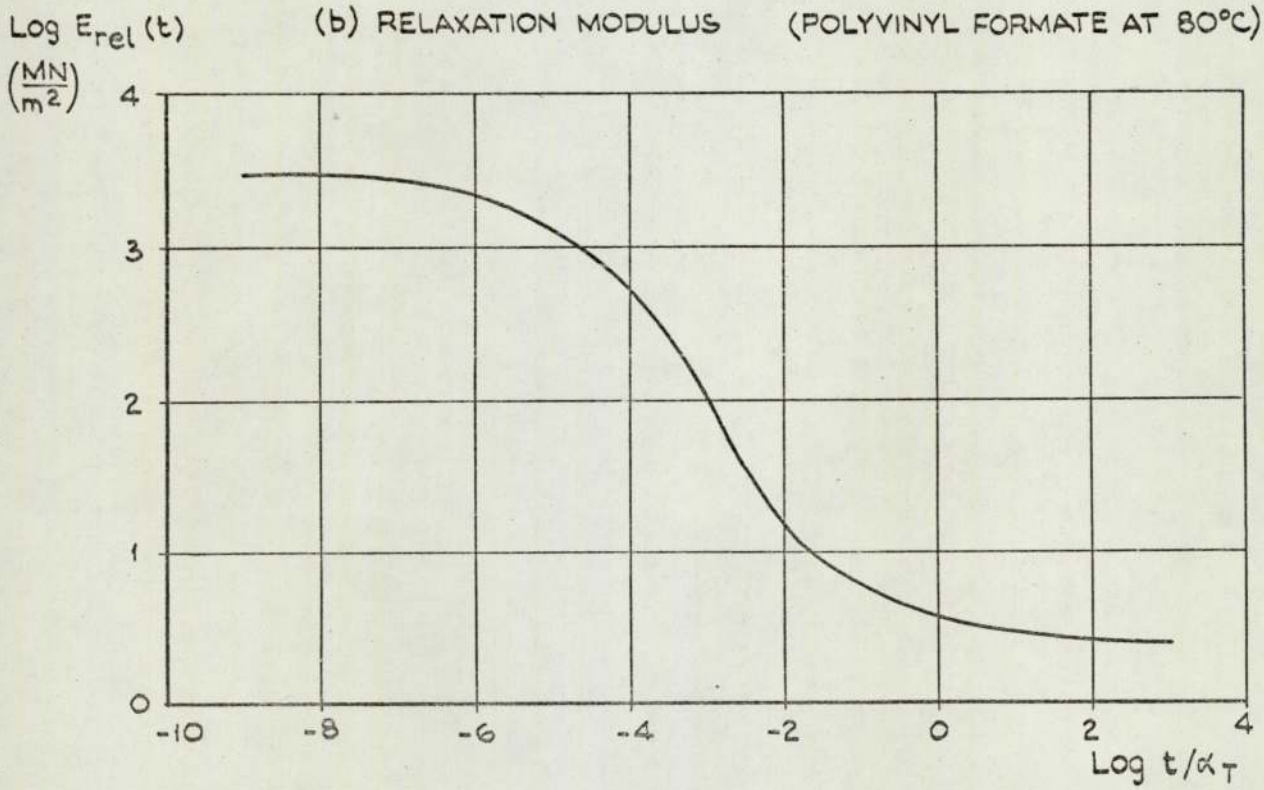

FIG. 1.1 CREEP COMPLIANCE AND RELAXATION MODULUS.

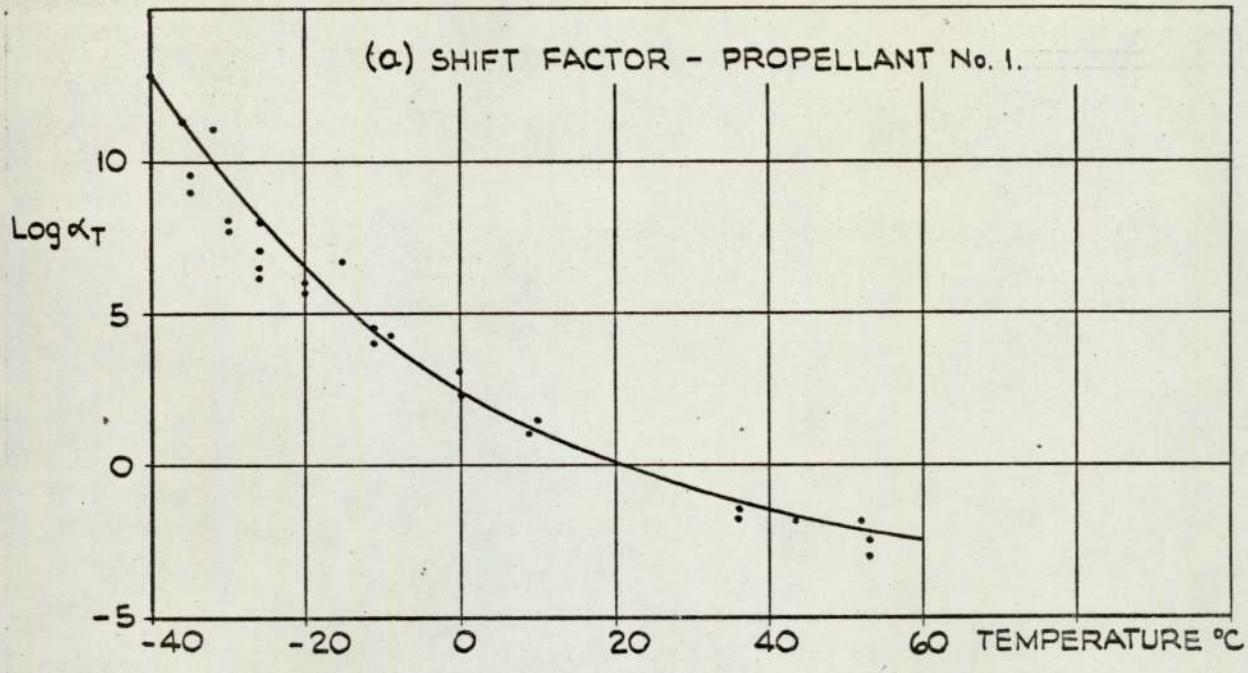

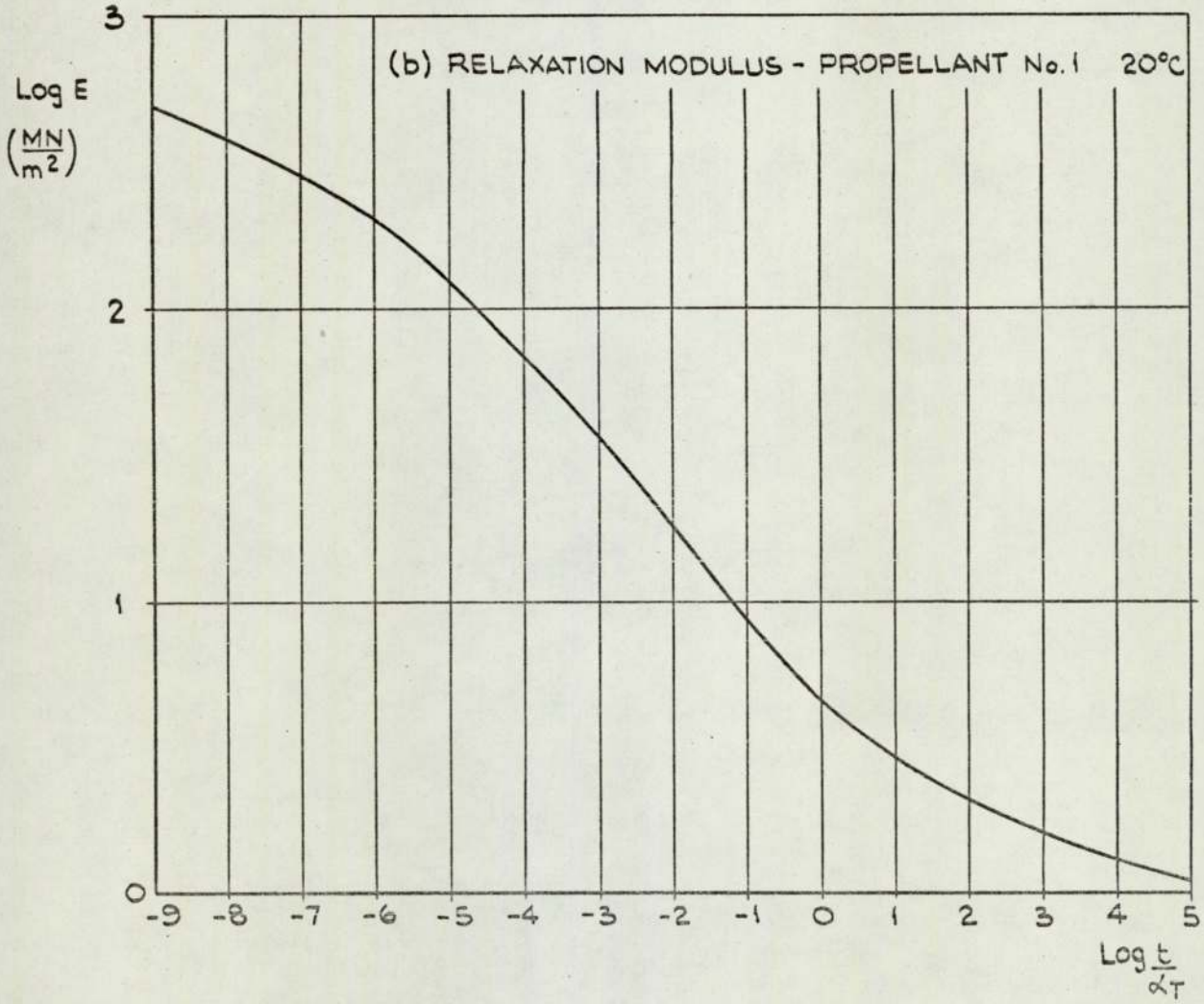

FIG. 1.2 SHIFT FACTOR AND RELAXATION MODULUS OF PROPELLANT No. 1.

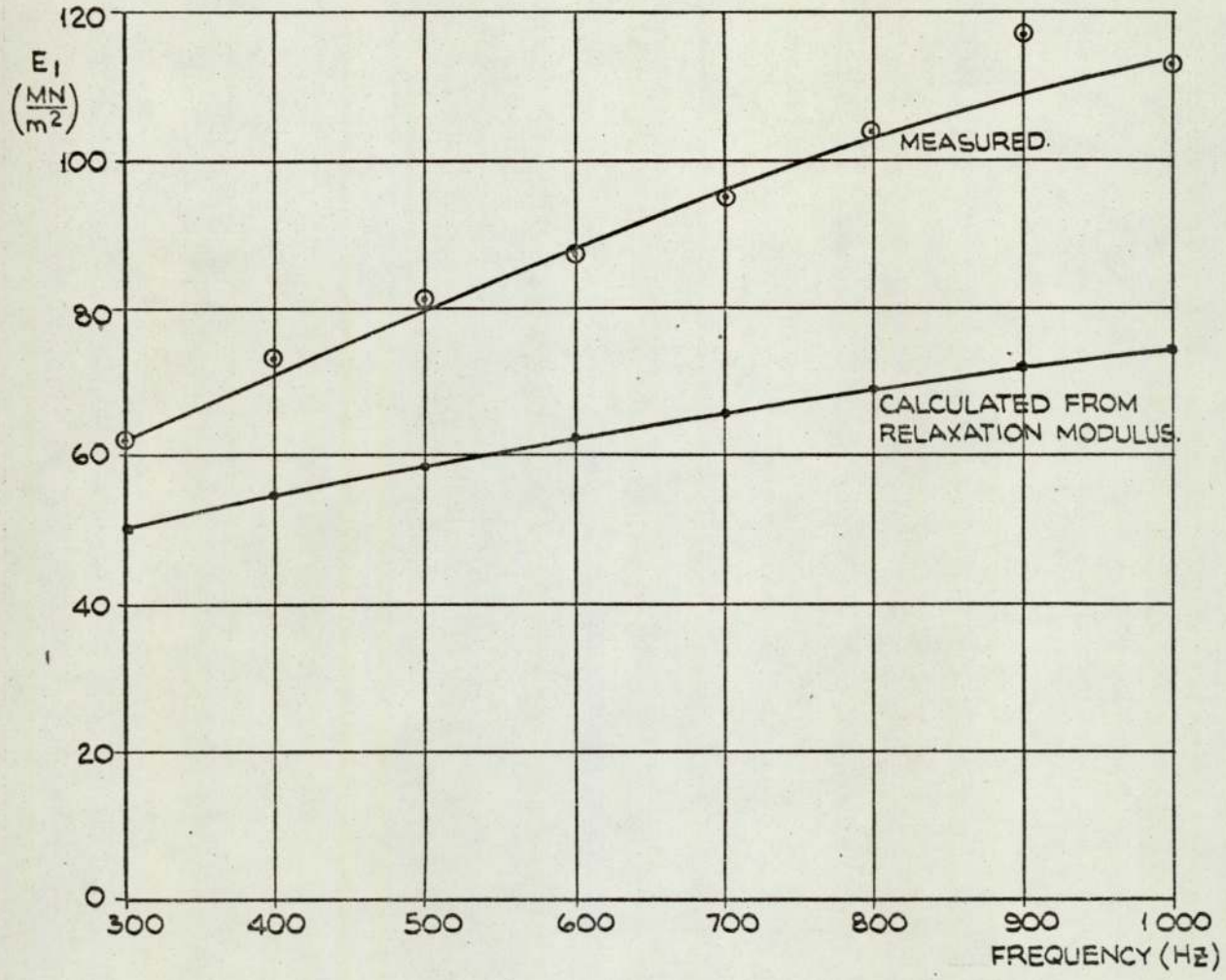

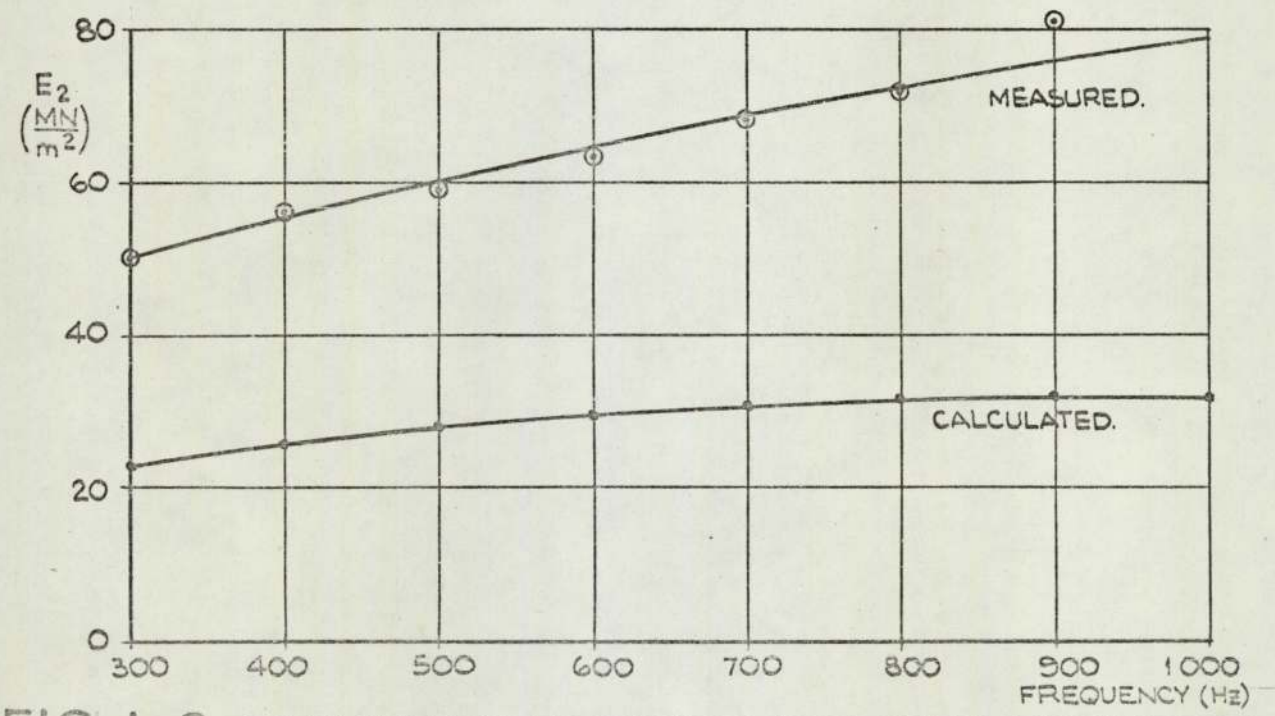

FIG. 1.3 COMPARISON OF E^* OBTAINED FROM DIRECT MEASUREMENTS WITH THAT CALCULATED FROM THE RELAXATION MODULUS ($E^* = E_1 + iE_2$)

Chapter 2

PRELIMINARY EXPERIMENTS ON THE FULL SCALE PROPELLANT SAMPLES

2.1 Experimental set-up and procedure

The equipment used for these preliminary experiments was as follows:

Oscillator	-	Muirhead 2 phase L.F. D-880-A
Amplifier	-	Radford MA 25
Vibrator	-	Goodmans V50
Accelerometers	-	J. Langham-Thompson XA2
Load cell	-	Endevco 2103-100
Charge amplifier	-	Environmental equipment 6 channel CVA-6
Oscilloscope	-	Telequipment D33R
Voltmeters	-	Advance A.C. VM78
A.C. Ammeter 0-2 amps		

A block diagram of the system is shown in fig (2.1). Two test pieces were manufactured one of inert (or 'dummy') propellant and the other of live propellant (No. 1). The dimensions of the two pieces were the same:

Circular cross section, diameter = .15 m

Length = .9 m

A plate was bonded to each end of the beam so that the specimen could be suspended at one end from a crane and coupled to the vibrator at the other end.

Throughout the experiments the force was kept constant and the accelerations at various points were measured. The phase difference between two accelerometer signals (one used as a 'standard' and the other as the variable) was 'estimated' from the oscilloscope i.e. anywhere between 270-0-90 was 'in' and anywhere between 90-180-270 was 'out'.

2.2 Inert Propellant

Longitudinal vibrations: The test piece was suspended above the vibrator which was coupled to the specimen by means of the bottom plate. An accelerometer could be screwed into either the top or bottom plate. The measurements from this experiment are given in fig (2.2).

Transverse vibrations: The vibrator was turned through 90°, a jubilee clip was strapped round the test piece near the bottom plate and the vibrator push rod was coupled to it. The accelerometers were also attached to jubilee clips so they could be moved up and down to measure modal shapes.

The measured responses of 2 points along the beam (at 0.03 m and 0.9 m from the forced end) are given in fig. (2.3). Note that the maximum values of the acceleration do not occur at the same frequency, this is due to the damping in the material. For a lightly damped material (steel, for example) the natural frequency in free vibrations, the maximum acceleration and displacement in forced vibrations all occur at the same frequency, the 'resonant frequency'. Also the maximum will occur at the same frequency wherever the measurements are made. It can be seen that when the damping is not negligible there is no common frequency where all these phenomena occur, hence any allusion to the 'resonant frequency' of a damped material should be carefully defined.

The modal shapes measured at specific frequencies are given in fig. (2.4). The effect of damping is clear here too, the displacement at the forced end is appreciably greater than at the free end, the energy is absorbed as the wave travels along the beam.

2.3 Live propellant (No. 1)

The above equipment was transported to SRS and experiments were carried out on the specimen of live propellant. Only transverse vibrations were studied in this case.

Acceleration vs frequency plots for three points along the length of the beam (at 0.1 m, 0.2 m and 0.3 m from the forced end) are given in fig. (2.5); modal shapes at specific frequencies are given in fig. (2.6).

It can be seen that the live propellant is much more heavily damped than the inert material and the comments on the effects of damping given in the previous section are even more pertinent here.

The main purpose of these preliminary experiments was to discover if the inert and live propellants had similar dynamic properties. It was hoped that they would be similar, then experiments would be carried out using the inert propellant, the results of which could then be used to predict the response of the live materials.

It was decided that the properties were too dissimilar to pursue this plan; also, although the relaxation modulus of most of the live propellants had been measured, there were no similar data for the dummy so it was decided to continue with experiments on live propellant only.

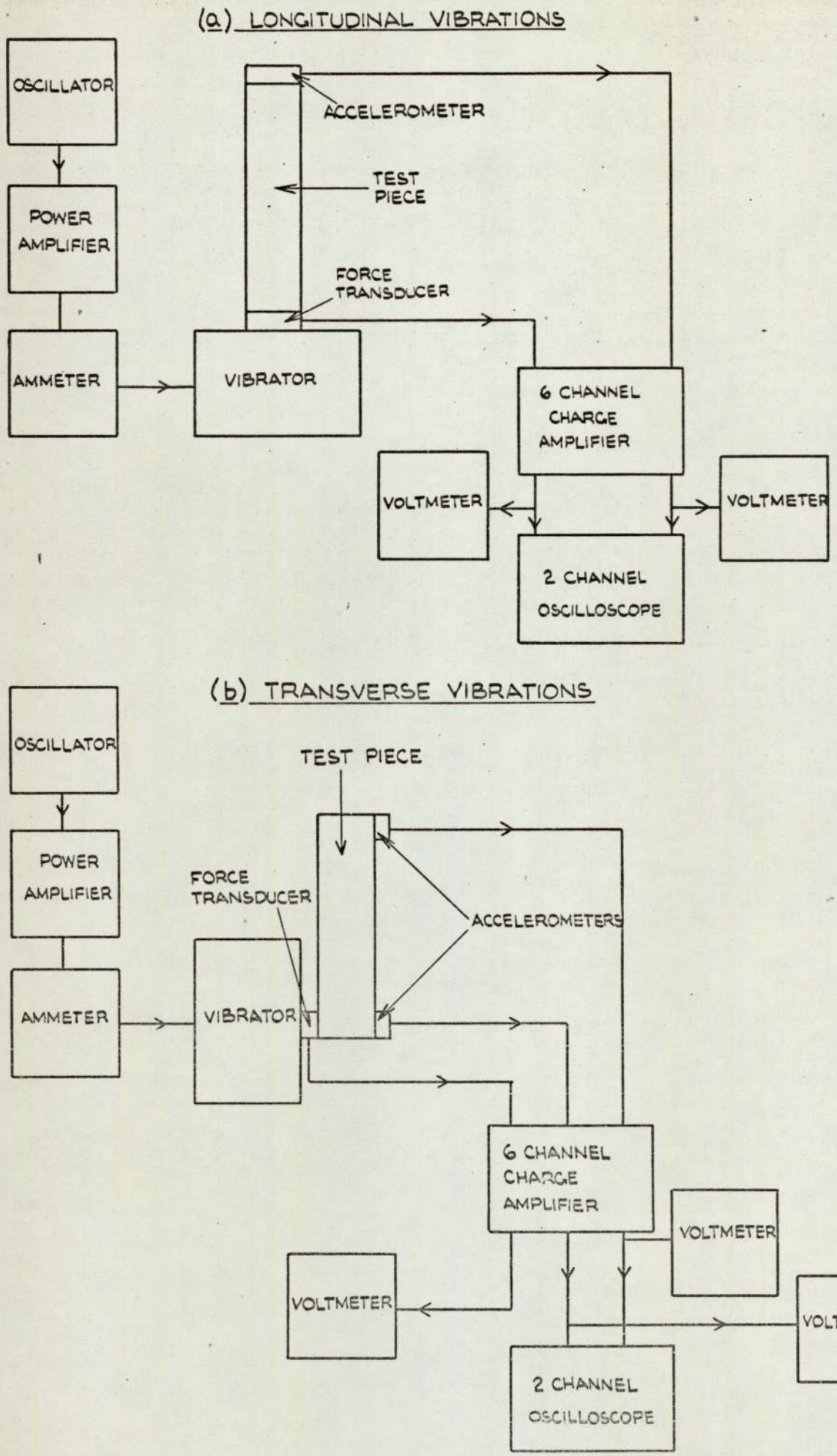

FIG. 2.1 BLOCK DIAGRAM OF SET-UP FOR PRELIMINARY TESTS.

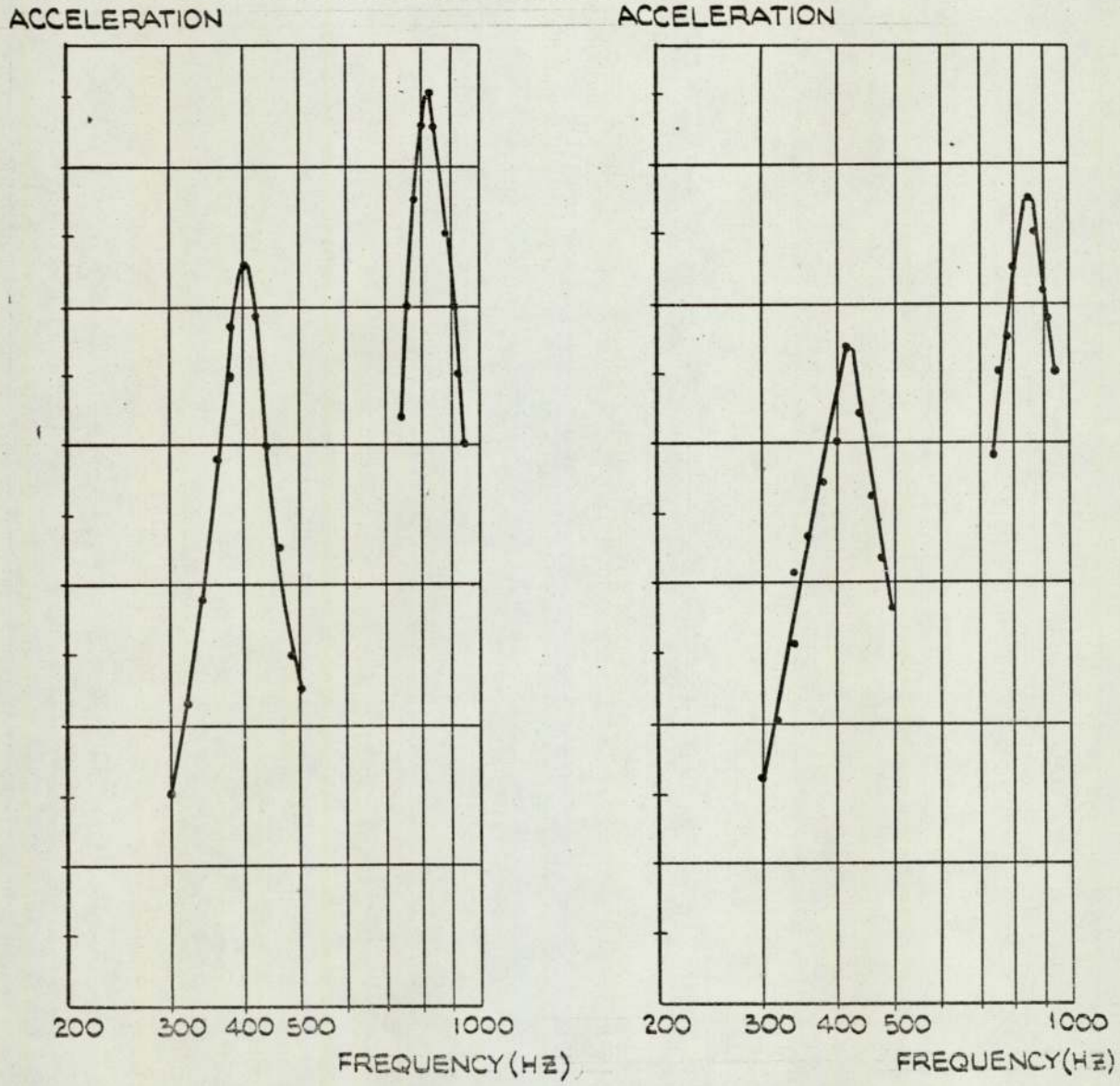

(a) FORCED END.

(b) FREE END.

FIG. 2.2 LONGITUDINAL VIBRATIONS - INERT PROPELLANT.

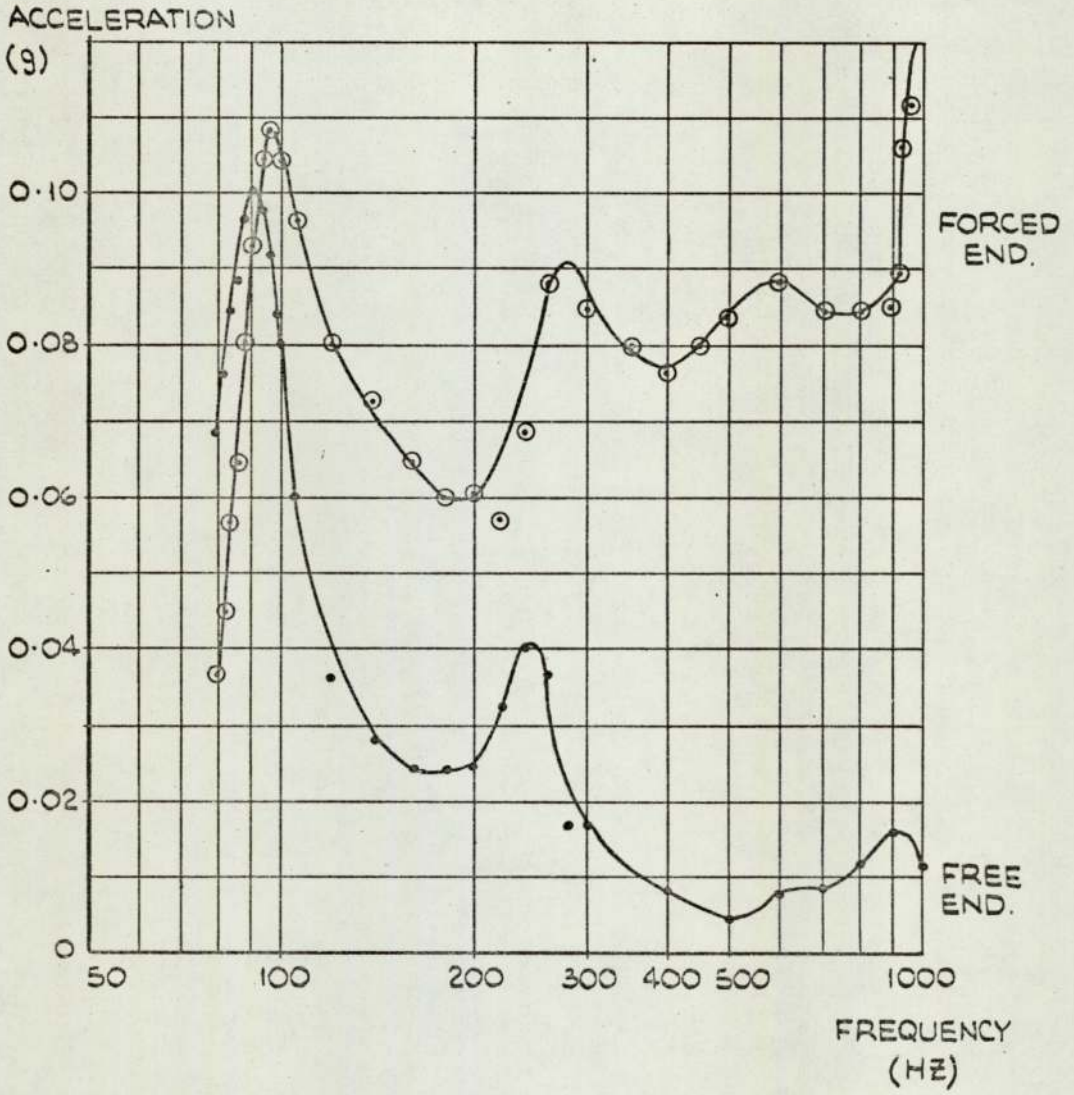

FIG. 2.3 TRANSVERSE VIBRATIONS - INERT PROPELLANT.

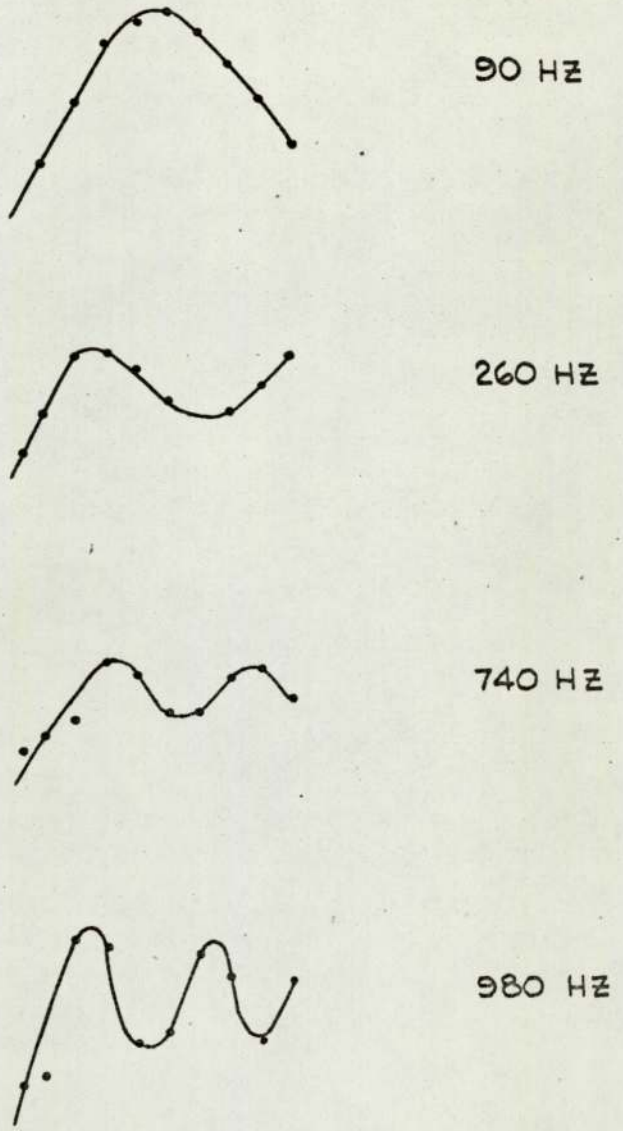

FIG. 2.4 MODAL SHAPES - TRANSVERSE VIBRATIONS INERT PROPELLANT.

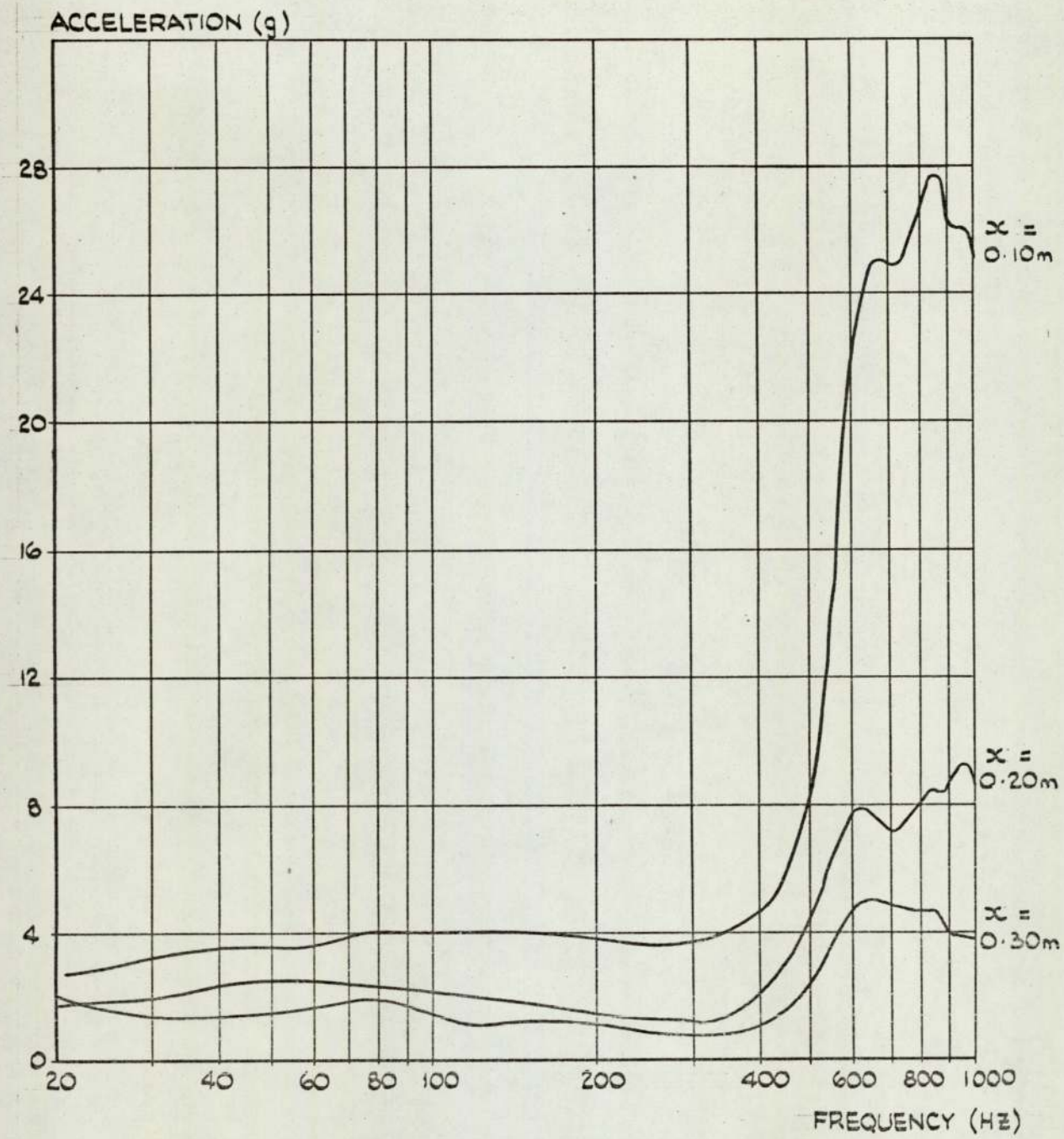

FIG. 2.5 TRANSVERSE VIBRATIONS - PROPELLANT Nº 1
ACCELERATION MEASURED AT $x = 0{\cdot}1\,m, 0{\cdot}2\,m, 0{\cdot}3\,m$
FROM THE FORCED END.

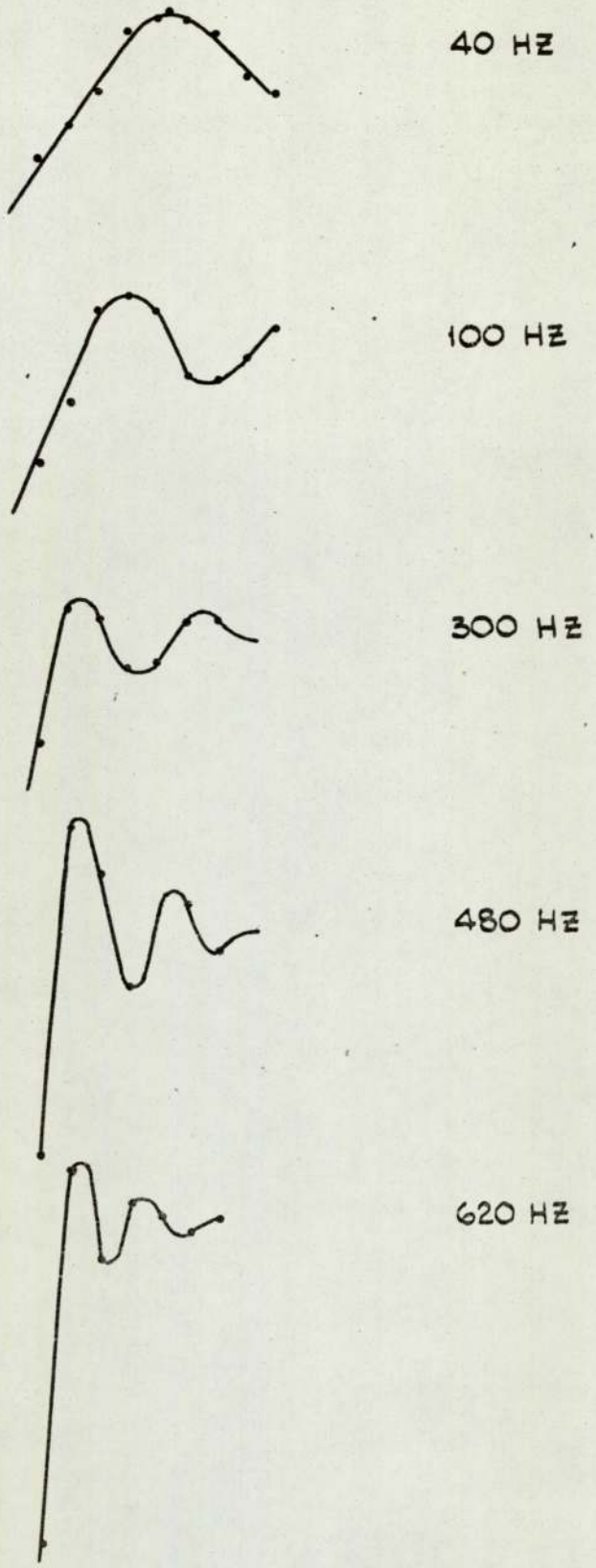

FIG. 2.6 MODAL SHAPES - TRANSVERSE VIBRATIONS - PROPELLANT Nº 1.

Chapter 3

MEASUREMENT OF THE COMPLEX MODULUS

3.1 Introduction and Literature Survey

The present research deals with forced harmonic vibrations of viscoelastic materials. In order to analyse these conditions it is convenient to use the second form of the correspondence principle (see section 1.2.7) - i.e. the solution to a viscoelastic problem can be obtained from that of an elastic material by replacing the elastic constants with the equivalent complex frequency-dependent parameters.

Since the work deals exclusively with beam vibrations, the elastic constant needed for the analyses is Young's Modulus E. For the viscoelastic analysis, E is replaced with the dynamic modulus $E^*(\omega)$.

The relaxation moduli of most of the propellants had previously been measured so it was decided to use these to calculate the dynamic moduli with the equation:

$$E^*(\omega) = \left[s\,\overline{E}_{rel}(s) \right]_{s=i\omega} \qquad 3.1.(1)$$

where $\overline{E}_{rel}(s)$ denotes the Laplace Transform of $E_{rel}(t)$. (see section 1.2.6)

The Maxwell Model in parallel with a spring was used, i.e.

$$E_{rel}(t) = K_o + \sum_{j=1}^{n} K_j\, e^{-t/\alpha_j} \qquad 3.1.(2)$$

and hence from 3.1.(1)

$$E^*(\omega) = K_o + \sum_{j=1}^{n} \frac{K_j \alpha_j^{\,2} \omega^2 + iK_j \alpha_j \omega}{1 + \omega^2 \alpha_j^{\,2}} \qquad 3.1.(3)$$

The K_j and α_j are found by fitting equation 3.1.(2) to the measured relaxation modulus, they were then substituted into equation 3.1.(3) to give $E^*(\omega)$.

$E^*(\omega)$ calculated in this way was used to compute the response to forced transverse vibrations of the large scale specimen used in the preliminary experiments. The response calculation was based on the Euler-Bernoulli equations (see Appendix (A)). The calculated values were

compared with the measured response (reported in Chapter 2); the comparison is shown in fig. (3.1), clearly the agreement is not good. Obtaining $E^*(\omega)$ in this way would be erroneous if the basic assumptions were not valid. Two of the most important assumptions are:

(i) that the material is linearly viscoelastic,
i.e. if a stress σ_x produces a strain ϵ_x,
then a stress $n\sigma_x$ will produce a strain of
$n\,\epsilon_x$, where n is a constant.

The material was found to be linear for the order of displacements encountered in the vibration tests; however, the strain specified for measuring the relaxation modulus is usually 5% and it is thought that the material is non-linear for such large strains.

(ii) that it is possible to perform the time-temperature superposition (see section 1.2.10).

By varying the temperature at which the relaxation modulus is measured it is possible to considerably extend the time range by using the above principle. A plot of α_T vs. T should be a smooth curve passing through the measured values of α_T. Figure (1.2(b)) shows the graph of log α_T vs. log T for propellant No. 1. It can be seen that there are quite large deviations from the smooth curve.

Further doubts arise due to:

(i) the range over which the relaxation modulus is valid;
Ferry (Ref. (48)) advises caution when using values of modulus obtained at temperatures far removed from the reference temperature. In this present work the frequency range of interest is 10 Hz to 1 000 Hz; assuming ω is approximately equivalent to 1/t then the important time range on the relaxation curve is 10^{-4} to 10^{-2} seconds.

This implies temperatures of about -12°C and 0°C (from fig. (1.2(b)), for log a_T = +4, T = -12°C, etc.), assuming actual measurements begin at t = 1 second. The reference temperature is 20°C.

(ii) Practical limitations - at extremes of temperature it is difficult to maintain a constant 5% strain - at high temperatures the propellant is very soft so the strain will easily increase, when cold the material is brittle so the specimen could break before the specified strain level is reached. If the level cannot be achieved, the stress is calculated assuming that the material is linear and scaling up or down as appropriate, i.e. if the strain is 10% and the stress σ_1 then it is assumed that at 5% the stress would have been $\sigma_1/2$.

In view of these uncertainties it was decided to devise a technique for direct measurement of the dynamic modulus. The method is described in the subsequent sections of this Chapter.

A literature search was conducted to find a method to measure the dynamic modulus E*; general surveys of the various techniques are given in References (46), (47), (48), (52).

There are many established methods, they fall into several different categories:

(i) The measurement of the shear modulus G* (see References (1), (4), (9), (23) and (44)), then the use of the equation $E^* = G^* (2(1+\nu^*))$ to obtain E*; it is usually assumed that ν^* is constant and equal to $\frac{1}{2}$. This method was not used because of the necessity to make the assumption about ν^*.

(ii) The measurement of the response of a beam to forced transverse vibrations and the use of the Euler-Bernoulli equations to find E^*. It is found either by approximation (see reference (53) for frequencies below the first resonance) or by an iterative technique (see (5)). Transverse vibrations are inherently more complicated to analyse than longitudinal vibrations, so difficulties are introduced without any obvious advantages. References (31) and (36) describe the limitations on sample geometry for the Euler-Bernoulli equations to be applicable (i.e. when it is possible to ignore the effect of rotary inertia and shear deformation) and it is shown that the equations are valid only for the first few modes of vibration.

(iii) The measurement of resonant frequencies of a beam, using either forced or free, longitudinal or transverse vibrations, (References (54) - (58)). This method is not suitable if the material is highly damped (as the propellant is) - free vibrations are attenuated so rapidly that no useful results can be obtained and with forced vibrations the response curve does not show a sharp peak (possibly no peak at all; see the result reported in Chapter 2), so it is difficult to distinguish where the maximum value occurs.

(iv) The resonant frequency methods can be utilised when the viscoelastic material is used in conjunction with an elastic material in a compound structure. See References (3), (25), (26), (31) and (36) for techniques using viscoelastic/elastic layered beams in transverse vibrations. The same comments apply as in section (ii) with additional complications generated due to the necessity to extract the complex modulus of the

viscoelastic material from the measured 'composite modulus'.

(v) The longitudinal vibrations of a viscoelastic rod with an added end mass also gives measurable resonant frequencies. References (2) and (30) treat the rod as a complex spring with no mass, Reference (38) includes the effect of the mass of the rod. This method as described in the references gives E^* at resonant frequencies only, although by varying the added mass the resonant frequency can be varied.

These various methods were not suitable for the reasons specified so the "admittance method" was devised; a free-free rod with bonded end masses (one to connect the vibrator and the other to facilitate suspension of the sample) is forced in longitudinal vibration. The input force is set at a constant level F_o and the acceleration at the free end ($|P|$) and the phase difference between the two (θ) are measured, then the cross admittance $= \frac{|P|\, e^{i\theta}}{F_o}$. A computer program has been written to compute E^* from these data using an iterative technique. In this way E^* can be measured over a large frequency range and is not dependent on 'resonant frequencies'.

The values of E^* can easily be verified by using them to predict the direct admittance $= \frac{\text{acceleration at the forced end}}{F_o}$ and comparing with measurements (see section 3.6).

E^* can be further proved by calculating the direct and cross admittances of the rod in transverse vibration and comparing with the measured responses (see sections 3.7 and 3.8).

A variation of the "admittance method" is given in Reference (32) (reference was discovered after the present experiment had been designed). The Transfer Impedance method of (32) consists of forcing one end of a rod in longitudinal vibrations, the other end is fixed (i.e. it is attached to a heavy mass). The variables measured are the force at the fixed end, the

acceleration at the forced end and the phase between the two. Using an iterative technique E* is calculated from the transfer impedance:- Acceleration at x = 0 / Force at x = 1. Corrections are necessary to compensate for the finite end mass.

The admittance method was preferable in that it is easier to attain a free end rather than a fixed end. The end masses are incorporated in the present analysis so it is marginally more complicated than that of Reference (32) but with the use of a computer this is unimportant.

3.2 Theoretical basis of the method

3.2.1 Forced longitudinal vibrations of an elastic rod with end masses

It is assumed that the rod has a uniform cross section and that it is long relative to the cross section, then lateral displacements can be ignored and it can be assumed that the stress is constant over the section.

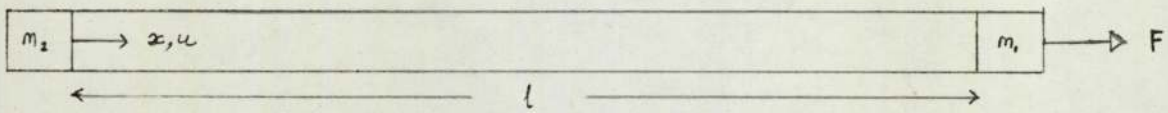

Mass m_1 at $x = l$

Mass m_2 at $x = 0$

Force $F = F_0 e^{i\omega t}$ is applied to mass m_1

Differential equation of motion

Consider an element δx of the rod

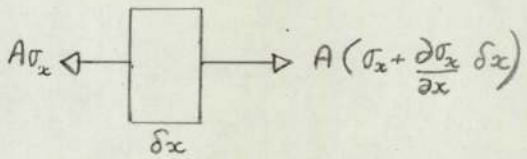

The equilibrium equation for this element is:

$$A\left(\sigma_x + \frac{\partial \sigma_x}{\partial x}\delta x\right) - A\sigma_x = \rho A \delta x \frac{\partial^2 u}{\partial t^2}$$

where σ_x is the stress in the x-direction (N/m^2)

A is the cross sectional area (m^2)

ρ is the density (kg/m^3)

$u(x,t)$ is the displacement (m)

then

$$\frac{\partial \sigma_x}{\partial x} = \rho \frac{\partial^2 u}{\partial t^2} \qquad 3.2.(1)$$

Assuming it is a linear elastic material, then

$$\sigma_x = E\epsilon_x$$

where E is Young's Modulus (N/m^2)

and ϵ_x is the strain in the x-direction

then $$E\frac{\partial \epsilon_x}{\partial x} = \rho\frac{\partial^2 u}{\partial t^2} \qquad 3.2.(2)$$

The strain-displacement relation is:

$$\epsilon_x = \frac{\partial u}{\partial x}$$

Substituting into 3.2.(2) gives:

$$E\frac{\partial^2 u}{\partial x^2} = \rho\frac{\partial^2 u}{\partial t^2} \qquad 3.2.(3)$$

Since the applied force $F = F_o e^{i\omega t}$, it is assumed that the displacement

$$U(x,t) = u(x)\, e^{i\omega t},$$

then equation 3.2.(3) becomes

$$E\frac{d^2 u}{dx^2} = -\rho\omega^2 u$$

or $$\frac{d^2 u}{dx^2} + \gamma^2 u = 0 \qquad 3.2.(4)$$

where $$\gamma^2 = \frac{\rho\omega^2}{E} \qquad 3.2.(5)$$

The general solution to 3.2.(4) is given by

$$u(x) = B_1 \cos \gamma x + B_2 \sin \gamma x \qquad 3.2.(6)$$

Then $$U(x,t) = (B_1 \cos \gamma x + B_2 \sin \gamma x)e^{i\omega t} \qquad 3.2.(7)$$

Boundary Conditions

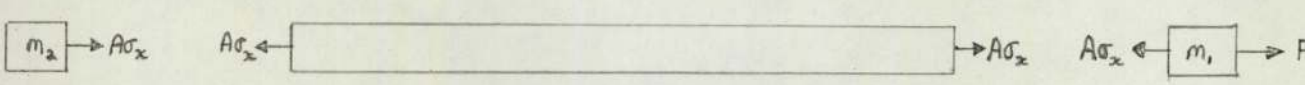

Considering the equilibrium of the end masses, the boundary conditions are given by:

at $x = 0, \quad A\sigma_x = m_2 \frac{\partial^2 u}{\partial t^2}$

at $x = l, \quad F - A\sigma_x = m_1 \frac{\partial^2 u}{\partial t^2}$

Substituting 3.2.(7) into these and solving for B_1 and B_2 gives

$$U(x,t) = -F_o \frac{(AE\gamma \cos \gamma x - m_2\omega^2 \sin \gamma x)\ e^{i\omega t}}{(A^2E^2\gamma^2 - m_1m_2\omega^4)\sin \gamma l + AE\gamma\omega^2(m_1 + m_2) \cos \gamma l} \qquad 3.2.(8)$$

3.2.2 Forced longitudinal vibration of a viscoelastic rod with end masses

For a linear elastic material the constitutive equation is

$$\sigma_x = E\ \epsilon_x,$$

by using the second form of the correspondence principle for viscoelastic materials in forced vibration (see section 1.2.7), the constitutive equation can be written as

$$\sigma_x = E^*\ \epsilon_x$$

where E^* is the complex or dynamic modulus.

Hence, to convert the analysis in the preceding section from an elastic rod to a viscoelastic rod, it is only necessary to replace E with E^*.

Therefore for the forced longitudinal vibrations of a viscoelastic rod with end masses the displacement is given by:

$$U(x,t) = -F_o \frac{(AE^*\gamma \cos \gamma x - m_2\omega^2 \sin \gamma x)\ e^{i\omega t}}{(A^2E^{*2}\gamma^2 - m_1m_2\omega^4)\sin \gamma l + AE^*\gamma\omega^2(m_1 + m_2) \cos \gamma l} \qquad 3.2.(9)$$

where $$\gamma^2 = \frac{\rho\omega^2}{E^*} \qquad 3.2.(10)$$

3.2.3 The calculation of E* from measurements

The acceleration f(x,t) is given by:

$$f(x,t) = \ddot{U}(x,t) = -\omega^2 U(x,t)$$

then
$$f(o,t) = \frac{F_o \omega^2 AE^* y\, e^{i\omega t}}{(A^2E^{*2}y^2 - m_1 m_2 \omega^4)\sin yl + AE^* y\omega^2(m_1 + m_2)\cos yl} \qquad 3.2.(11)$$

But from 3.2.(10)

$$E^* = \frac{\rho\omega^2}{y^2}$$

substituting this into 3.2.(11) and letting $yl = b$

gives
$$f(o,t) = \frac{F_o A\rho e^{i\omega t}}{\left(\frac{A^2\rho^2 l}{b} - \frac{m_1 m_2 b}{l}\right)\sin b + A\rho(m_1 + m_2)\cos b} \qquad 3.2.(12)$$

In the experiment f(o,t) is measured, let it equal $P\, e^{i\omega t}$

where $P = |P|\, e^{i\theta}$,

$|P|$ is the magnitude of the acceleration

θ is the phase difference between force and acceleration

Defining
$$g(b) = \frac{F_o A\rho}{\left(\frac{A^2\rho^2 l}{b} - \frac{m_1 m_2 b}{l}\right)\sin b + A\rho(m_1 + m_2)\cos b} - P \qquad 3.2.(13)$$

it is necessary to find a 'b' such that $g(b) = 0$

i.e.
$$f(o,t) = P\, e^{i\omega t} \qquad 3.2.(14)$$

Using the Newton-Raphson iteration (reference (62)):

$$b_{n+1} = b_n - \frac{g(b_n)}{g'(b_n)}$$

With an initial estimate b_o it is possible to find a b_n such that $g(b_n) \leq \epsilon$ for any small ϵ, provided g(b) is single valued in the region of b_n and g'(b) and g''(b) are non-zero in the region of b_n.

Then from 3.2.(10),

$$E^* = \frac{\rho\omega^2 l^2}{b_n^2} \qquad 3.2.(15)$$

3.3 Experimental set-up and procedure

3.3.1 Test piece (a)

A test piece of propellant No. 1 was manufactured, the dimensions were:

Square cross section: 0.0254 m x 0.0254 m

Length: 0.203 m

The end masses were of aluminium and weighed 0.0446 kg and 0.0107 kg respectively.

Figures (3.2) and (3.3) show the experimental set-up.

Figure (3.4) gives a Block Diagram of the system.

3.3.2 The equipment

The equipment used was:

Sweep oscillator	-	Spectral Dynamics Corporation SD 104-2
Power Amplifier	-	Derritron 250 W.L.F.
Vibrator	-	Derritron VP 5
Force Transducer	-	Kistler 910 / 11
Accelerometer	-	Birchall
Charge Amplifier	-	Environmental Equipment Ltd. CVA 2
Tracking Filters	-	Spectral Dynamics Corporation. Dynamic Analyser SD 101A and SD 101AS
Oscilloscope	-	Telequipment D33R
Voltmeters	-	Brüel and Kjaer Random Noise Voltmeter Type 2417 Advanced AC Transistorised Voltmeter VM 78 Digital Measurements DM 2001 Mk.2
Pre-amplifiers	-	Levell Transistor AC Amplifier Type TA60
Phase Meter	-	Acton Laboratories Inc. 329 BSD
Frequency Counter	-	Advance Type TC 2A

3.3.3 The test procedure

The test procedure was as follows:

1. The oscillator frequency was established using the frequency counter.
2. The Force was measured with the digital voltmeter and the oscillator output was adjusted to give the pre-set force level F_o.
3. The magnitude of the acceleration was read on the B & K voltmeter.
4. The phase meter operates on voltages between 0.5 v and 2 v; the Advance voltmeters measured the inputs to the phase meter - the oscillator output and the pre-amplifiers were adjusted until the phase meter inputs were within the operating range.

   (Note: It is only possible to vary the force without affecting the phase reading if the material is linear. See section 3.3.8)
5. The phase difference between force and acceleration was then measured.
6. The oscillator frequency was changed and the procedure repeated.

Measurements were made at 20 Hz intervals between 40 Hz and 1 000 Hz. An example of the measurements made on test piece (a) is given in Table (3.1) and plotted in fig. (3.5).

3.3.4 Test piece (b)

Another sample of propellant No. 1 was manufactured to see if sample size affected the results. The dimensions were:

Square cross section: 0.0254 m x 0.0254 m

Length: 0.373 m

The aluminium end masses weighed 0.026 kg and 0.020 kg respectively.

An example of the measurements made with this test piece is given in Table (3.2) and plotted in fig. (3.6).

3.3.5 Temperature dependence

E* is not only dependent on frequency but also on temperature (reference (48)). Two thermocouples were inserted into the propellant and an oven was built so that measurements could be made at various temperatures above ambient. For temperatures below ambient the test piece was cooled down in a refrigerator then removed and vibration measurements were made at various temperatures as the sample temperature returned to ambient.

3.3.6 The thermocouples

The thermocouples used were chromel/alumel (nickel/chromium and nickel/aluminium alloys). A Thermos flask containing melting ice was used for the cold junction and the hot junction was inserted well into the propellant (to a depth of about 5 mm).

The sensitivity of a chromel/alumel thermocouple is 40 $\mu V/^{\circ}C$; it has an operating range of $-200^{\circ}C$ to $1\,100^{\circ}C$.

The output voltages were measured with the digital voltmeter, this has a minimum resolution of 50 μV, therefore, the minimum temperature variation that could be measured was $1.25^{\circ}C$.

3.3.7 The oven

The oven (see fig. (3.7)) consisted of a wooden box with a detachable front section. A slit in the top was to allow access to the elastic suspension system and the accelerometer and thermocouple cables. A slit in the bottom section was to permit transmission of the vibrator push rod.

The oven was heated by two 20 watt light bulbs, one on either side of the specimen. Aluminium reflector plates shielded the test piece from direct radiation.

A thermostat was situated on the back wall of the oven to maintain a constant temperature by controlling the input to the bulbs.

The experimental results for various temperatures are given in Table (3.3) and plotted in fig. (3.8).

3.3.8 Material linearity

Tests were carried out to check that the material response was linear. Trials were conducted with pre-set force levels of F, 2F, and 4F - the corresponding accelerations doubled and quadrupled while the phase between force and acceleration remained constant; so the material was linear within the range of displacements reached in these vibration experiments.

3.3.9 Energy dissipation

As the propellant is highly damped, energy is dissipated during vibration. This causes a local temperature increase within the propellant - and hence a change in modulus. The test specimen was vibrated at a constant frequency and with a constant force for about 2 hours. At 15 minute intervals the temperature, acceleration and phase were measured. Table (3.4) and Figure (3.9) give the results of this trial.

3.3.10 Calibration

(i) Accelerometer

The Birchall accelerometer was calibrated against a Standard and the sensitivity was measured as 2.63 pc/g.

(ii) Force transducer

The sensitivity given on the calibration chart of the Kistler force transducer was 48.5 pc/kp; this was checked by attaching a solid mass to the transducer, vibrating it and measuring the acceleration of the mass - A_1. Then the force $F_1 = M A_1$.

Another block of known mass (m) was then put on top of the first mass and the test repeated,

then $F_2 = (M+m) A_2$

therefore $m = F_2/A_2 - F_1/A_1$,

the right hand side was calculated using the given sensitivity and it was exactly equal to m.

Note: The bonded end mass m_1 of section 3.2 consists of the mass of the aluminium block + the mass of the push rod + the effective seismic mass above the piezoelectric element of the force transducer (m_f). The above experiment was also used to determine m_f:

$$F_1 = M A_1 = (M_k + m_f) A_1$$

where M_k was the known attached mass

then $m_f = F_1/A_1 - M_k$

For the Kistler transducer $m_f = 0.015$ kg.

(iii) Tracking filters

There were two tracking filters in the system, the acceleration signal was passed through one and the force signal through the other. The variable gains of the filters were set at 10 for the acceleration and 1 for the force.

(iv) Phase meter

The phase meter was calibrated by feeding in

(a) two signals exactly in phase

and (b) two signals 180° out of phase

and adjusting the meter so that it read 0° and 180° respectively.

Care was taken to ensure that the input voltages were between 0.5 v and 2 v.

3.4 Computer analysis to obtain the dynamic modulus from the measurements

3.4.1 The program

A computer program was written to iterate to a value of E^* which satisfied equation 3.2.(14),

$$f(o,t) = P\, e^{i\omega t}$$

where $f(o,t)$ is given in equation 3.2.(12)

and P is the acceleration measured at $x = 0$.

Thus E^* was evaluated for each frequency at which P was measured.

The iteration was based on the Newton-Raphson technique, i.e.

$$b_{n+1} = b_n - \frac{g(b_n)}{g'(b_n)} \qquad 3.4.(1)$$

where $g(b)$ is defined in equation 3.2.(13)

and $$b = \omega l \sqrt{\frac{\rho}{E^*}} \qquad 3.4.(2)$$

The program read in the following data:

A	cross sectional area (m^2)
ρ	density (kg/m^3)
l	length (m)
F_o	amplitude of applied force (N)
m_1	mass of block at forced end (kg)
m_2	mass of block at free end (kg)

then for each frequency:

f	frequency (Hz)
$\|P\|$	magnitude of acceleration at $x = 0$ (g)
θ	phase difference between force and acceleration (radians)

For every frequency an initial estimate for b (b_o) was obtained (see section 3.4.3) then $g(b_o)$ and $g'(b_o)$ were computed and substituted into equation 3.4.(1) to give b_1. The iteration was repeated until:

$$Re(g(b_n)) \leq \epsilon$$

$$\mathrm{Im}(g(b_n)) \leq \epsilon$$

where ϵ is a small quantity.

Then E* was calculated from equation 3.2.(15), i.e.

$$E^* = \rho\omega^2 l^2 / b_n^2 \qquad 3.4.(3)$$

A FORTRAN listing of the program is given in appendix E.

3.4.2 Accuracy and speed of computation

The program was run with various values of ϵ, for ϵ = 0.1, 0.01, 0.001, 0.0001, the calculated E*'s were equal up to the fourth significant figure throughout the frequency range.

The number of iterations necessary with the different ϵ values was also measured, for ϵ = 0.1 3 iterations were necessary

ϵ = 0.0001 4 iterations were necessary

Hence the value of ϵ was not significant either for accuracy or speed of computation. The present version of the program uses ϵ = 0.001.

3.4.3 Initial estimate for b

It is easiest to estimate b_o for the frequency where the acceleration is a maximum, the program then automatically generates b_o for the succeeding frequencies by either:

1) using the final b_n for one frequency as the initial b_o for the next frequency or

2) using $f/f_m b_o$ as the estimate for frequency f_r

where f is any frequency

f_m is the frequency where the acceleration is the maximum

b_o is the initial estimate of b calculated at frequency f_m.

1) was found to be convenient with the data for propellant No. 1 where E* was changing rapidly with frequency, 2) was used with the natural rubber data where E* was almost constant with frequency. (See note 3, page 40)

The initial estimate for b_o at the frequency f_m :

From f_m and the shape of the response curve an initial estimate for b_o may be obtained as follows:

In general for an elastic beam, at any frequency f,

$$E = \rho 4\pi^2 f^2 l^2 / b^2$$

where $b = \gamma l$

At a resonant frequency f_n, b is the solution of the frequency equation, $\bar{b}$ say.

then at f_n, $E = \dfrac{\rho 4\pi^2 f_n^2 l^2}{\bar{b}^2}$

It has been found that for a viscoelastic beam:

$$|E^*| \simeq \frac{\rho 4\pi^2 f_m^2 l^2}{\bar{b}^2} \qquad 3.4.(4)$$

where $\bar{b}$ is the solution of the frequency equation for a similar elastic beam, and f_m is the frequency at which the acceleration is a maximum.

(a) Free-free beam

For a free-free elastic beam in longitudinal vibrations the frequency equation is:

$b = n\pi$ (see reference (59))

then at the first resonance $\bar{b} = \pi$

therefore for a viscoelastic beam at frequency f_m from equation 3.4.(4)

$$|E^*| \simeq \rho 4 f_m^2 l^2 \qquad 3.4.(5)$$

(b) Free-free beam with bonded end masses m_1 and m_2

For a free-free elastic beam with bonded end masses the frequency equation is:

$$\tan b = \frac{(N_1 + N_2)b}{N_1 N_2 b^2 - 1}$$

where $N_1 = m_1 \Big/ \rho A l$

and $N_2 = m_2 \Big/ \rho A l$ (see reference (59))

Figure (3.10) gives the solution $\bar{b}$ for various values of N_1 and N_2 between 0 and 0.5

(If M and N are larger

$$\bar{b} \simeq \left(\frac{1}{N_1} + \frac{1}{N_2} - \frac{1}{3} \left(\frac{1}{N_1^2} + \frac{1}{N_2^2} - \frac{1}{N_1 N_2} \right) \right)^{\frac{1}{2}}$$

Then from equation 3.4.(4)

$$|E^*| \simeq \frac{\rho 4\pi^2 f_m^2 l^2}{\bar{b}^2} \qquad 3.4.(6)$$

Thus $|E^*|$ may be calculated from the frequency f_m with 3.4.(5) or 3.4.(6). The separate components of E^* i.e. E_1, E_2 are found from the shape of the response curve:

If the acceleration at f_m is a_m

then the frequency f_1 is measured where the acceleration is pa_m (where $p < 1$),

then, if $\Omega = f_1 / f_m$,

it may be shown (see section 3.4.4) that ξ is given by:

$$\xi^2 = \tfrac{1}{2} \left(1 \pm \sqrt{1 - \frac{p^2(1 - 2\Omega^2 + \Omega^4)}{\Omega^4 - p^2(2\Omega^2 - 1)}} \right) \qquad 3.4.(7)$$

where $\xi = \frac{1}{2Q}$ is the "damping ratio".

It may also be shown (see section 3.4.5) that

$$\xi = \tfrac{1}{2} \frac{E_2}{E_1} \qquad 3.4.(8)$$

$$\text{therefore} \quad |E^*| = \sqrt{E_1^2 (1 + 4\xi^2)} \qquad 3.4.(8)$$

$$\text{therefore} \quad E_1 = \frac{|E^*|}{\sqrt{1 + 4\xi^2}} \qquad 3.4.(9)$$

and $$E_2 = 2\xi E_1 \qquad 3.4.(10)$$

Having found an estimate for E^* at f_m, b_o at f_m is given by:

$$b_o = 2\pi f_m l \sqrt{\frac{\rho}{E_{1+i}E_2}} \qquad 3.4.(11)$$

Note 1: if the damping is light then an approximation for ξ may be found from the 'half power points' i.e. the two frequencies f_1 and f_2 where the acceleration is

$$\frac{1}{\sqrt{2}} a_m \ ,$$

then $$\xi = \frac{f_2 - f_1}{2f_m}$$

Note 2: if the damping is light the method described above to estimate E^* is often used as a method for actually measuring E^* at the frequency f_m.

Note 3; if second and higher acceleration maxima are discernable from the response curve then an estimate for $|E^*|$ may be obtained for those frequencies. Using either $\overline{b} = 2\pi$, 3π etc. or curves similar to those in fig.(3.10) for the higher roots, $|E^*|$ may be approximated as above. If estimates can be made for two or more frequencies it will be possible to choose which of 1) or 2) (page 37) to use.

It has been found that if b_o is within $\pm$ 25% of the actual b then the routine will be convergent. The table below gives the number of iterations necessary to reach $b_n = b$ with different starting values. (The frequency was 1 000 Hz and the actual value of b was 4.06 - i 1.11):

Starting value b_o	No. of iterations
3 - 2.i	9
3.5 - 2.i	5
4 - 0.i	5
4 - 5.i	4
4 - 2.i	5
5 - 0.i	11

3.4.4 The derivation of the expression for ξ

The beam is approximated by a single degree of freedom system: a point mass and a Kelvin element (a spring and dashpot in parallel).

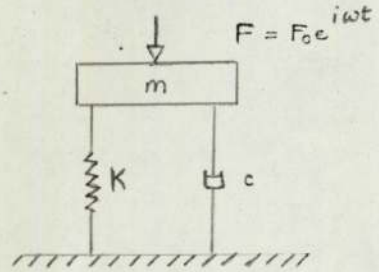

Let it be forced with a harmonic force $F_o\, e^{i\omega t}$,

then the acceleration is given by:

$$a = \frac{-\frac{f^2}{f_n^2}\,\frac{F}{m}}{\sqrt{\left(1 - \frac{f^2}{f_n^2}\right)^2 + 4\xi^2\,\frac{f^2}{f_n^2}}} \qquad \text{see reference (59)} \qquad 3.4.(12)$$

where F is the applied force

m is the point mass

K is the stiffness of the spring

c is the damping constant of the dashpot

ξ is the damping ratio, $\xi = \frac{c}{2\sqrt{Km}}$

By differentiating 3.4.(12) and equating to zero it may be shown that the acceleration is a maximum when

$$f^2 = f_n^2 / (1 - 2\xi^2) = f_m^2 \quad \text{say} \quad . \qquad 3.4.(13)$$

where f_n is the undamped natural frequency

and f_m is the frequency where the acceleration is a maximum.

therefore
$$a_m = \frac{-\frac{1}{1-2\xi^2}\,\frac{F}{m}}{\sqrt{\left(1-\frac{1}{1-2\xi^2}\right)^2 + 4\xi^2\frac{1}{1-2\xi^2}}}$$

$$= \frac{-F/m}{2\xi\sqrt{1-\xi^2}} \qquad 3.4.(14)$$

Let f_1 be the frequency where the acceleration is $p\,a_m$, $p < 1$

then from 3.4.(12) and 3.4.(14)

$$\frac{-p\,F/m}{2\xi\sqrt{1-\xi^2}} = \frac{-f_1^2\,F/m}{f_n^2\sqrt{\left(1-\frac{f_1^2}{f_n^2}\right)^2+4\xi^2\frac{f_1^2}{f_n^2}}}$$

substituting $f_n^2 = f_m^2\,(1 - 2\xi^2)$ from equation 3.4.(13), and letting $f_1/f_m = \Omega$ gives:

$$\xi^4 - \xi^2 + \frac{p^2(1 - 2\Omega^2 + \Omega^4)}{4\Omega^4 - 4p^2(2\Omega^2-1)} = 0$$

i.e
$$\xi^2 = \tfrac{1}{2}\left(1 \pm \sqrt{1 - p^2\frac{(1-2\Omega^2+\Omega^4)}{\Omega^4 - p^2(2\Omega^2-1)}}\right) \qquad 3.4.(15)$$

3.4.5 Derivation of the relationship between ξ and E^*

As in section 3.4.4 the beam is approximated by a single degree of freedom system.

For the Kelvin element $E^* = E_1 + i\,E_2$

$$= K + i\omega c \qquad 3.4.(16)$$

(see section 1.2.8)

where K and c are defined in section 3.4.4.

For the spring-mass-damper system,

$$\xi = \frac{c}{2\sqrt{Km}}$$

and $$f_n = \frac{1}{2\pi}\sqrt{\frac{K}{m}}$$ see reference (59)

Then by substituting from equation 3.4.(16) it may be seen that:

$$\xi = \frac{E_2}{4\pi f \sqrt{E_1 m}}$$

and $$f_n = \frac{1}{2\pi}\sqrt{\frac{E_1}{m}}$$

therefore at $f = f_n$

$$\xi = E_2 / 2E_1$$

therefore at the undamped natural frequency fn,

$$\xi = E_2 / 2E_1 \quad ;$$

for the approximation required in section 3.4.3 it is assumed that f_n is not very different from f_m and that ξ does not vary appreciably with frequency.

3.5 Frequency and temperature dependence of the dynamic modulus

3.5.1 Frequency dependence

Figure (3.5) shows the experimental data for test piece (2) (0.203 m long). Figure (3.11) shows the dynamic modulus obtained from the computer program using those data.

Similarly, Figure (3.6) gives the data for test piece (b) (0.373 m long) and fig. (3.12) gives the E* obtained for those data.

It can be seen that the modulus changes by a factor of 4 over the 900 Hz frequency range.

The temperature was not accurately measured during these tests so no direct comparison can be made.

In fig. (3.13) are the measured data for test pieces (a) and (b) at the same temperature.

Figure (3.14) gives the corresponding complex moduli. The values of E* obtained using the 'admittance method' are thus not dependent on specimen length. (Note that the rod must be long in comparison with the cross section to ensure the assumption that the stress is constant over the cross section is satisfied).

3.5.2 Temperature dependence

Figure (3.8) shows the measurements made at various temperatures between $-10^{\circ}C$ and $40^{\circ}C$.

Figures (3.15) and (3.16) give E_1 and E_2 resp. vs frequency for the various temperatures.

$|E^*|$ vs temperature at a constant frequency (1 000 Hz) is plotted in fig. (3.17). It may be seen that over the $50^{\circ}C$ temperature range the modulus changes by a factor of 40.

E_2/E_1 is plotted against temperature in fig. (3.18).

Note 1: It has been shown that

$$\xi = E_2/2E_1 \quad \text{(section 3.4.5)}$$

and by definition

$$Q = 1/2\xi$$

therefore $Q = E_1/E_2$

Experimentally determined values of ξ (using the relationship given in section 3.4.4) are given in fig. (3.19) with the graphs of $E_2/2E_1$ shown for comparison. Clearly the approximations of a single degree of freedom system made in 3.4.4 and 3.4.5 are acceptable, at least for the first 'resonance'.

3.5.3 Frequency-temperature superposition

The frequency-temperature superposition principle was applied (see section 1.2.11). The graphs of E* vs frequency for various temperatures were shifted along the x-axis to give a continuous curve for a reference temperature T_o. The amount each was shifted (α_T) was then plotted as log α_T vs T. (See fig. (3.20)). Ferry (reference (48)) gives this graph as convex and not concave so it was assumed that the results obtained at the extremes of temperature were not reliable. A straight line was drawn through the middle temperature range.

With these values of log α_T the composite graph of E^*T/T_o vs $\alpha_T f$ was plotted and is given in fig. (3.21).

$|E^*|$ at 1 000 Hz for various temperatures were calculated from this graph and are shown on fig. (3.17) for comparison with the measured values.

E* obtained from the frequency-temperature superposition was not very satisfactory at low frequencies; it was used to predict the response of the beam to forced transverse vibrations and was not very successful below 200 Hz. Further tests with more precise control on temperature would be necessary before any clear conclusions on the applicability of the superposition principle could be reached.

3.6 Comparison of predicted and measured response of the test piece to forced longitudinal vibrations

The experimental set-up was as described in section 3.3.

Two sets of measurements were made:

(i) with the accelerometer at the free end of the rod

(ii) with the accelerometer at the forced end of the rod

The first set of data was used to calculate E^* for the frequency range 100 Hz - 1 000 Hz; this was used to compute the response at the forced end ($x = l$) with the equation:

$$f(l,t) = \frac{F_o \omega^2 \left[AE^* \gamma \cos \gamma l - m_2 \omega^2 \sin \gamma l \right] e^{i\omega t}}{(A^2 E^{*2} \gamma^2 - m_1 m_2 \omega^4) \sin \gamma l + AE^* \gamma \omega^2 (m_1 + m_2) \cos \gamma l}$$

(from equation 3.2.(9) with $f(l,t) = \left[- \omega^2 u(x,t) \right]_{x=l}$)

The calculated response is shown in fig. (3.22) together with the measured response for comparison. The agreement is very good throughout the frequency range.

3.7 Comparison of predicted and measured response of the test piece to forced transverse vibrations

3.7.1 Experimental procedure

The same equipment was used as described in section 3.3. Transverse vibrations were excited by turning the vibrator through 90° and coupling the vibrator to the side of the mass bonded to the test piece (see fig.(3.23)).

Note that a piano wire connection was used, that is, a coupler which is stiff in tension/compression but very flexible in bending. This is to obviate the necessity of considering the flexural stiffness of the push rod as a restraining spring on the test piece.

The force was kept constant and acceleration and phase were measured at frequencies between 50 Hz and 1 000 Hz. Two sets of measurements were made:

(i) at the forced end - to give the point admittance

(ii) at the free end - to give the transfer admittance

Because of the doubt about the frequency-temperature superposition principle, as mentioned in section 3.5.3, the complex modulus was measured at the time of the experiment. It was measured before and after the transverse test and the average was used as that applying at the time of the test.

3.7.2 The calculated response

The theory was based on the Timoshenko equations for a beam in bending (see appendix (B)).

This gives:

$$\left.\begin{aligned} u(x,t) &= (B_1\cosh \alpha x + B_2\sinh \alpha x + B_3\cosh \beta x + B_4\sinh \beta x)e^{i\omega t} \\ \psi(x,t) &= (RB_2\cosh \alpha x + RB_1\sinh \alpha x + SB_4\cosh \beta x + SB_3\sinh \beta x)e^{i\omega t} \end{aligned}\right\} \quad 3.7.(1)$$

where $u(x,t)$ is the displacement of the neutral axis

and $\psi(x,t)$ is the slope of the neutral axis

and α, β, R and S are defined in Appendix B. (Equations B(17) - B(20))

B_1, B_2, B_3 and B_4 are the unknown coefficients which are found from the boundary conditions.

Boundary conditions:

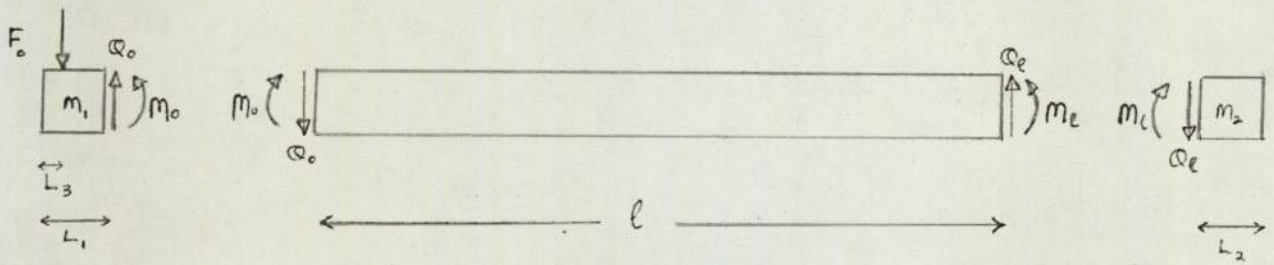

Let u_1, u_2 be the displacements at the C of G of masses m_1, m_2 respectively

ψ_1, ψ_2 be the slopes of the C of G of masses m_1, m_2 respectively

I, I_2 be the moments of inertia of masses m_1, m_2 respectively

L_1, L_2 be the lengths of inertia of masses m_1, m_2 respectively

L_3 be the distance between the point of application of F and the free edge.

Then considering the equilibrium of mass m_1:

$$F_o - Q_o = m_1 \ddot{u}_1 \qquad 3.7.(2)$$

$$M_o + F_o (L_1/2 - L_3) + Q_o L_1/2 = - I_1 \ddot{\psi}_1 \qquad 3.7.(3)$$

where $$Q_o = \left[Q(x,t) \right]_{x=o} = \left[-k'AG \left(\frac{\partial u}{\partial x} - \psi \right) \right]_{x=o}$$

and $$M_o = \left[M(x,t) \right]_{x=o} = \left[-EI \frac{\partial \psi}{\partial x} \right]_{x=o}$$

and $$\psi_o = \left[\psi (x,t) \right]_{x=o}$$

Similarly considering the equilibrium of mass m_2:

$$Q_1 = m_2 \ddot{u}_2 \qquad 3.7.(4)$$

$$M_1 - Q_1 L^2/2 = I_2 \ddot{\psi}_2 \qquad 3.7.(5)$$

where $Q_1 = Q(x,t)_{x=1}$

$M_1 = M(x,t)_{x=1}$

The four equations 3.7.(2) - 3.7.(5) were used to solve for the coefficients B_i, i=1,4

Now $u_1 = u(0,t) - L_1/2\psi(o,t)$, $\psi_1 = \psi(o,t)$

$u_2 = u(1,t) + L_2/2\psi(1,t)$, $\psi_2 = \psi(1,t)$

Substituting for M_o, Q_o, M_1, Q_1, u_1, ψ_1 and ψ_2 in equations 3.7.(2) - 3.7.(5) gives the equation $[A]\ \{B\} = \{C\}$

where $[A]$ =

$-m_1\omega^2$	$m_1\omega^2 \frac{L_1}{2} R - k'AG\,(\alpha-R)$	$m_1\omega^2$	$m_1\omega^2 \frac{L_1}{2} S - k'AG\,(\beta-S)$
$EIR\alpha$	$k'AG \frac{L_1}{2}(\alpha-R)$ $+ I_1\omega^2 R$	$EIS\beta$	$k'AG \frac{L_1}{2}(\beta-S)$ $+ I_1\omega^2 S$
$(-k'AG(\alpha-R)+ Rm_2\omega^2 \frac{L_2}{2})\sinh \alpha l$ $+ m_2\omega^2 \cosh \alpha l$	$(-k'AG(\alpha-R)+ Rm_2\omega^2 \frac{L_2}{2})\cosh \alpha l$ $+ m_2\omega^2 \sinh \alpha l$	$(-k'AG(\beta-S)+ Sm_2\omega^2 \frac{L_2}{2})\sinh \beta l$ $+ m_2\omega^2 \cosh \beta l$	$(-k'AG(\beta-S)+ Sm_2\omega^2 \frac{L_2}{2})\sinh \beta l$ $+ m_2\omega^2 \sinh \beta l$
$(k'AG \frac{L_2}{2}(\alpha-R)+ I_2\omega^2 R)\sinh \alpha l$ $- EIR\alpha \cosh \alpha l$	$(k'AG \frac{L_2}{2}(\alpha-R)+ I_2\omega^2 R)\cosh \alpha l$ $- EIR\alpha \sinh \alpha l$	$(k'AG \frac{L_2}{2}(\beta-S)+ I_2\omega^2 S)\sinh \beta l$ $- EIS\beta \cosh \beta l$	$(k'AG \frac{L_2}{2}(\beta-S)+ I_2\omega^2 S)\cosh \beta l$ $- EIS\beta \sinh \beta l$

$$\{B\} = \begin{bmatrix} B_1 \\ B_2 \\ B_3 \\ B_4 \end{bmatrix} \quad \text{and} \quad \{C\} = \begin{bmatrix} F_o \\ L_1/2 - F_o \\ 0 \\ 0 \end{bmatrix}$$

This equation is solved numerically using the Gauss elimination technique (see Appendix D).

Then B_i , $i = 1,4$ were substituted into equation 3.7.(1) to give $u(x,t)$ and $\psi(x,t)$.

The acceleration was measured at a distance d_1 from the bonded edge of mass m_1.

The acceleration was measured at a distance d_2 from the bonded edge of mass m_2.

Let the accelerations be P_1 and P_2 respectively

then $P_1 = -\omega^2(u(0,t) - d_1\psi(0,t))$

and $P_2 = -\omega^2(u(1,t) + d_2\psi(1,t))$

A computer program was written to calculate P_1 and P_2.

The input data were:

A	area (m^2)
ρ	density (kg/m^3)
l	length (m)
F_o	applied force (N)
I	second moment of area of the beam cross section (m^4)
k'	shape factor (see Cowper (22))
ν	Poisson's ratio
m_1	mass of block at forced end (kg)
m_2	mass of block at free end (kg)
L_1	length of mass m_1 (m)
L_2	length of mass m_2 (m)
L_3	distance between the point of application of the force and the free edge of mass m_1 (m)

I_1 moment of inertia of mass m_1 (kg m^2)

I_2 moment of inertia of mass m_2

d_1 distance of the accelerometer on mass m_1 from the bonded edge

d_2 distance of the accelerometer on mass m_2 from the bonded edge

P_1 and P_2 thus calculated, using the 'averaged' E^* is plotted in fig. (3.24) with the measured values shown for comparison. The agreement is very good throughout the frequency range.

3.8 Comparison of predicted and measured response of the full scale sample to forced transverse vibrations

The preliminary trials reported in section 2.3 were used to further check the validity of the modulus measuring method.

The ambient temperature at the time of the experiments was approximately 18°C so the dynamic modulus measured at that temperature was used. The computer program referred to in the previous section was employed to calculate the response; it was amended slightly to compute the response at points along the length of the beam and not just at the end masses. The force was applied directly to the propellant at a distance of 3 cm from the bonded edge, it was considered reasonably accurate to assume that it was applied to the bonded edge.

At low frequencies the measured and calculated responses were very close (see fig. (3.25)). The modal shapes agreed well for the first six bending modes. At higher frequencies the measured response had a large sustained peak over the range 500 Hz - 1 000 Hz which was not predicted by the Timoshenko beam theory.

It was thought that the peak could be due to resonances in the cross section - radial, longitudinal, torsional etc. - coupled with the bending modes. Armenakas (Reference (60)) tabulated the resonant frequencies of an infinite solid cylinder based on exact three dimensional analysis. The results were based on a Poisson's ratio of 0.3 whereas that of propellant was assumed to be 0.5; the tabulated values were for elastic materials with a constant real modulus so the tables were not exactly applicable to the present problem but it was hoped that they would give an indication.

With a modulus of 100 MN/m^2, all the resonances up to 1 000 Hz were extracted from the tables (see fig. (3.26)). Also shown are the resonant frequencies in bending as given by the Timoshenko theory. (They do not correspond exactly because the end conditions were considered in the

latter whereas the frequencies in reference (60) were based on an infinite cylinder. It may be seen that there were many resonances other than bending in the region of the unexplained peak but only three (torsional) resonances at lower frequencies.

As there was good agreement between measurements and calculations for the region where the Timoshenko theory was sufficiently accurate then it was considered as evidence that the modulus measurements were valid for the large scale sample.

Note: It will be seen (section 4.3) that when considering a cartridge loaded motor and the likelihood that the propellant will impact on the case, the important variable is "displacement", (if the relative displacement of the propellant to the case is greater than the gap between them, then impacting will occur). The maximum gap between the case and the propellant is 2 mm, displacements of that order only occur for frequencies below 100 Hz and as the Timoshenko beam theory is adequate for those frequencies it was not thought necessary to do an exact three dimensional analysis. It may be seen in fig. (3.27) that the measured and calculated displacements agree well over the region where they are large enough to cause problems.

3.9 The measurement of the complex modulus of a sample of natural rubber

The test piece was of square cross section 0.025 m x 0.025 m, it was 0.15 m long and m_1 and m_2 were equal to 0.0274 kg and 0.0108 kg respectively. The procedure and equipment were as reported in section 3.3. The measured acceleration and phase are shown in fig. (3.28) for frequencies between 100 Hz and 1 000 Hz. It should be noted that the rubber had much less damping than propellant No. 1, the first resonance was much lower and the first five modes were excited within the frequency range.

From the frequency of maximum acceleration (160 Hz) the modulus was estimated as described in section 3.4.3:

The density of the rubber was 999.5 kg/m^3

therefore $\rho Al = 0.0933$ kg

therefore $M = 0.294$, $N = 0.116$

From fig. (3.10), $\bar{b} = 2.28$

therefore from equation 3.4.(4),

$$|E^*| \simeq 4\pi^2 \; 160^2 \; 0.15^2 \; 999.5 / 2.28^2 = 4.37 \; 10^6 \; N/m^2$$

Using $p = 0.5$ gave $f_1 = 150$,

since $f_m = 160$, then $\Omega = 0.9375$

therefore from 3.4.(6)

$\xi = 0.04$

then from 3.4.(7)

$E_1 = 4.36$, $E_2 = 0.35$

$$b_o = 2\pi 160 \; 0.15 \sqrt{999.5 / (4.36 + i\, 0.35)} = 2.28 - i\, 0.09 \quad \text{(at 160 Hz)}$$

This was used as the starting value for 160 Hz, the program automatically generated b_o for succeeding frequencies as discussed in 3.4.3. The output from the program is shown in fig. (3.28). The dynamic modulus of the natural rubber was also measured using a "Rheovibron" for four frequencies: 3.5 Hz, 11 Hz, 110 Hz, these are also shown in fig. (3.29), they compare well with the results obtained from the present metho

It should be noted that at higher frequencies the modulus decreases with frequency; this is an unlikely occurrence although it has been reported before (Coote (44)), who also cites three other references where similar phenomena were noted). However, the rod was in the fifth mode of vibration at 1 000 Hz so the wave length was of the same order as the cross section which would invalidate the assumption that the stress was constant over the cross section.

This conjecture could easily be verified by reducing the dimensions of the cross section to 0.01 m x 0.01 m say. Since the resonant frequency is independent of the area, the rod would still be in the fifth mode at 1 000 Hz but then the wave length would be approximately twice the cross sectional dimension.

Table 3.1 Measurements made on test piece (a) and resulting complex modulus $E^* (= E_1 + i E_2)$

Frequency (Hz)	Acceleration (g)	Phase (radians)	E_1 (MN/m^2)	E_2 (MN/m^2)
1 000	3.95	-3.30	143.55	94.18
980	4.02	-3.22	144.37	94.19
960	4.10	-3.22	139.76	89.05
940	4.18	-3.17	138.54	87.12
920	4.22	-3.13	135.96	85.29
900	4.26	-3.09	133.31	83.50
880	4.37	-3.03	132.92	82.00
860	4.42	-2.96	132.10	82.18
840	4.52	-2.90	131.19	81.07
820	4.60	-2.83	130.33	81.00
800	4.66	-2.77	128.31	80.49
780	4.77	-2.70	127.31	80.05
760	4.86	-2.63	125.71	79.77
740	4.98	-2.56	124.21	79.07
720	5.10	-2.49	122.42	78.24
700	5.23	-2.42	120.45	77.15
680	5.32	-2.34	118.22	76.81
660	5.47	-2.26	116.41	75.70
640	5.57	-2.18	113.86	74.72
620	5.66	-2.10	111.07	73.51
600	5.75	-2.02	108.15	72.01
580	5.84	-1.92	106.02	71.11
560	5.85	-1.81	103.70	70.83
540	5.84	-1.71	100.85	69.86
520	5.75	-1.60	98.06	69.54
500	5.65	-1.50	94.89	68.59

480	5.55	-1.39	92.42	67.64
460	5.30	-1.28	89.35	67.90
440	5.10	-1.16	87.54	67.78
420	4.80	-1.05	84.98	68.60
400	4.60	-0.96	82.04	67.51
380	4.37	-0.87	79.26	66.97
360	4.20	-0.80	75.57	64.89
340	4.00	-0.71	73.74	64.00
320	3.86	-0.68	67.09	60.43
300	3.73	-0.62	63.39	57.39
280	3.60	-0.56	59.90	54.36
260	3.50	-0.52	54.78	50.14
240	3.35	-0.49	48.54	47.20
220	3.21	-0.42	46.48	44.99
200	3.08	-0.40	39.44	41.54
180	2.96	-0.34	36.80	38.91
160	2.84	-0.30	32.11	35.98
140	2.69	-0.28	24.59	33.67
120	2.54	-0.22	20.93	34.07
100	2.45	-0.19	14.77	29.77
80	2.41	-0.12	16.45	27.42
60	2.44	-0.04	24.97	12.21

Table 3.2 Measurements made on test piece (b) and resulting complex modulus $E^* (= E_1 + i E_2)$

Frequency (Hz)	Acceleration (g)	Phase (radians)	E_1 (MN/m^2)	E_2 (MN/m^2)
1 000	2.21	-6.28	140.47	90.23
980	2.26	-6.20	138.13	88.39
960	2.31	-6.11	136.04	86.86
940	2.37	-6.00	134.66	85.82
920	2.42	-5.90	132.74	84.59
900	2.47	-5.76	132.01	84.59
880	2.53	-5.65	130.36	83.50
860	2.56	-5.52	128.89	83.36
840	2.65	-5.41	127.42	81.82
820	2.69	-5.27	126.22	81.73
800	2.72	-5.13	124.85	81.67
780	2.76	-4.97	124.21	82.01
760	2.80	-4.85	122.24	81.00
740	2.83	-4.73	120.14	80.01
720	2.84	-4.57	119.22	80.37
700	2.86	-4.43	117.77	79.91
680	2.89	-4.31	115.75	78.63
660	2.90	-4.19	113.55	77.54
640	2.90	-4.05	112.08	77.17
620	2.90	-3.93	109.88	76.16
600	2.92	-3.79	108.79	75.55
580	2.94	-3.67	106.91	74.32
560	2.95	-3.56	104.48	72.94
540	2.97	-3.44	102.56	71.86
520	3.04	-3.28	103.08	71.80
500	3.11	-3.19	100.24	69.02
480	3.19	-3.07	98.71	67.50

460	3.30	-2.95	97.26	65.70
440	3.40	-2.79	96.92	66.00
420	3.55	-2.67	94.95	63.80
400	3.80	-2.51	95.07	62.24
380	3.87	-2.32	93.44	63.35
360	3.92	-2.15	90.41	62.97
340	3.95	-1.94	88.52	63.34
320	3.90	-1.75	85.20	62.72
300	3.88	-1.55	82.81	61.05
280	3.78	-1.31	82.25	60.11
260	3.47	-1.12	78.85	60.01
240	3.16	-0.96	74.62	59.38
220	2.89	-0.80	71.66	58.23
200	2.56	-0.66	68.05	59.49
180	2.32	-0.58	60.17	58.26
160	2.07	-0.45	57.91	61.26
140	1.94	-0.38	50.63	57.28
120	1.77	-0.35	35.72	54.86
100	1.66	-0.24	33.98	56.45
80	1.52	-0.17	17.12	62.23
60	1.46	-0.17	1.32	36.98
40	1.46	-0.18	0.58	15.52

Table 3.3 Measurements made on test piece (a) for various temperatures

Temperature(°C)	Frequency (Hz)	Acceleration (g)	Phase (radians)
-9	1 822	10.9	-2.02
	1 710	11.28	-1.73
	1 635	11.15	-1.52
	1 526	10.46	-1.17
	1 428	9.06	-0.91
-6	1 819	9.51	-2.2
	1 708	10.14	-1.99
	1 642	10.39	-1.82
	1 582	10.77	-1.66
	1 542	10.58	-1.54
	1 440	10.16	-1.22
-4	1 806	8.43	-2.48
	1 726	8.59	-2.30
	1 665	8.87	-2.18
	1 556	9.87	-1.90
	1 493	10.14	-1.75
	1 450	10.08	-1.50
+1	1 523	7.22	-2.41
	1 475	7.29	-2.30
	1 377	7.98	-2.09
	1 289	8.56	-1.78
	1 193	8.75	-1.43
	1 060	7.29	-0.91
	997	6.46	-0.87
	901	5.32	-0.68
	819	4.44	-0.54
	715	3.80	-0.42

+4	1 800	6.78	-3.16
	1 663	6.59	-2.97
	1 543	6.34	-2.78
	1 500	6.34	-2.67
	1 392	6.57	-2.44
	1 287	7.20	-2.18
	1 210	7.77	-1.95
	1 140	8.11	-1.73
	1 094	8.05	-1.55
	1 045	7.96	-1.41
	991	7.48	-1.22
+6	1 811	6.59	-3.40
	1 697	6.34	-3.25
	1 563	6.08	-3.05
	1 405	5.83	-2.74
	1 300	6.08	-2.51
	1 188	6.82	-2.18
	1 096	7.33	-1.85
	1 050	7.67	-1.71
	983	7.58	-1.48
	943	7.33	-1.34
	885	6.84	-1.17
+9	1 410	5.58	-3.04
	1 287	5.39	-2.72
	1 239	5.55	-2.64
	1 178	5.70	-2.48
	1 103	6.08	-2.29
	1 040	6.53	-2.09
	980	6.91	-1.88
	920	7.12	-1.73
	904	7.10	-1.64
	883	7.10	-1.55
	832	6.89	-1.38

11	1 200	5.32	-2.90
	1 112	5.51	-2.67
	1 045	5.77	-2.50
	980	6.08	-2.32
	920	6.46	-2.13
	820	7.12	-1.76
	793	7.12	-1.66
	760	7.12	-1.54
	690	6.64	-1.31
14	1 234	5.20	-3.23
	1 107	5.07	-2.90
	1 005	5.30	-2.62
	900	5.82	-2.32
	800	6.44	-1.99
	750	6.69	-1.80
	720	6.82	-1.68
	700	6.75	-1.61
	650	6.57	-1.41
	609	6.10	-1.22
	501	4.69	-0.77
	402	3.56	-0.37
	308	2.94	-0.19
	197	2.69	-0.0
	115	2.47	0
	73	2.38	0
19	1 100	3.80	-3.70
	1 000	3.80	-3.40
	900	3.83	-2.97
	800	4.18	-2.64
	700	4.63	-2.34

	600	5.30	-2.08
	550	5.56	-1.78
	520	5.58	-1.62
	500	5.45	-1.52
	400	4.56	-0.91
	300	3.36	-0.40
	200	2.66	-0.16
	100	2.18	0
22	1 000	3.31	-4.05
	900	3.52	-3.61
	800	3.66	-3.30
	700	3.95	-2.95
	600	4.33	-2.55
	500	5.17	-2.11
	400	5.27	-1.40
	300	4.06	-0.84
	200	2.99	-0.35
	100	2.51	-0.14
28	1 000	2.04	-5.39
	900	2.29	-4.94
	800	2.60	-4.43
	700	2.85	-3.86
	600	3.16	-3.35
	500	3.56	-2.86
	400	4.33	-2.39
	300	4.83	-1.57
	200	3.78	-0.77
	100	2.53	-0.31

34	1 000	0.80	-7.33
	900	1.00	-6.72
	800	1.27	-6.07
	700	1.58	-5.43
	600	2.02	-4.78
	500	2.50	-4.03
	400	3.03	-3.32
	300	3.92	-2.51
	200	4.87	-1.57
	100	3.35	-0.35
39	1 000	0.34	-8.90
	900	0.48	-8.34
	800	0.68	-7.59
	700	0.91	-6.98
	600	1.25	-6.00
	500	1.76	-5.10
	400	2.32	-4.10
	300	2.98	-3.14
	200	4.33	-1.99
	100	3.56	-0.44

Table 3.4 Variation of measurements and E* with time caused by increase in temperature due to energy dissipation

Time (hours)	Acceleration (g)	Phase (radians)	E_1 (MN/m^2)	E_2 (MN/m^2)
0	7.63	-1.73	95.03	48.28
0.25	7.49	-1.76	93.46	48.24
0.62	7.34	-1.85	89.73	46.65
0.83	7.16	-1.92	86.71	45.59
1.42	7.29	-2.02	84.07	42.26
1.57	7.11	-2.04	82.76	42.44
1.68	7.11	-2.06	82.17	41.87

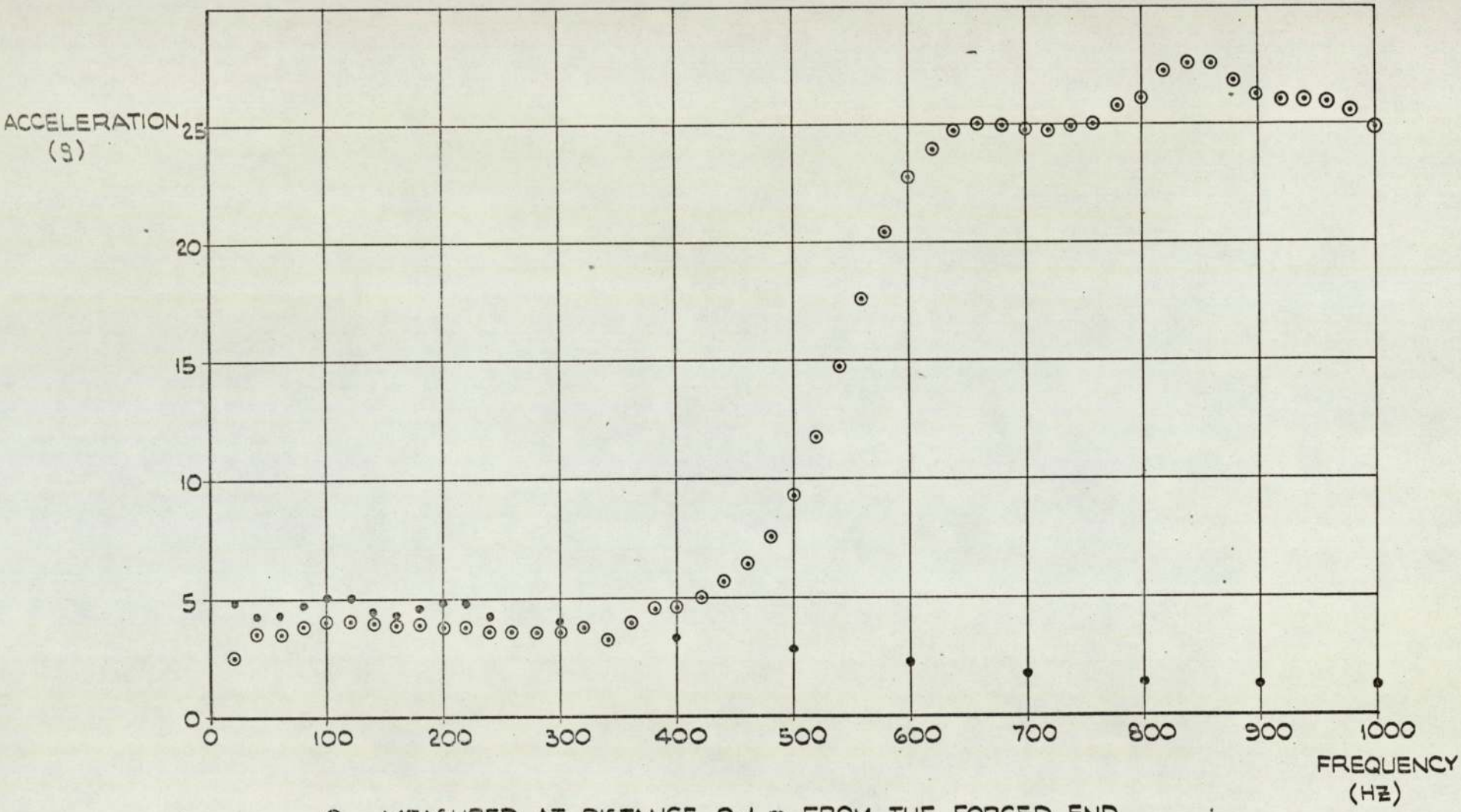

⊙ MEASURED AT DISTANCE 0·1 m FROM THE FORCED END.

• CALCULATED USING EULER-BERNOULLI EQUATIONS AND COMPLEX MODULUS OBTAINED FROM THE TRANSFORMATION OF THE RELAXATION MODULUS.

FIG. 3.1

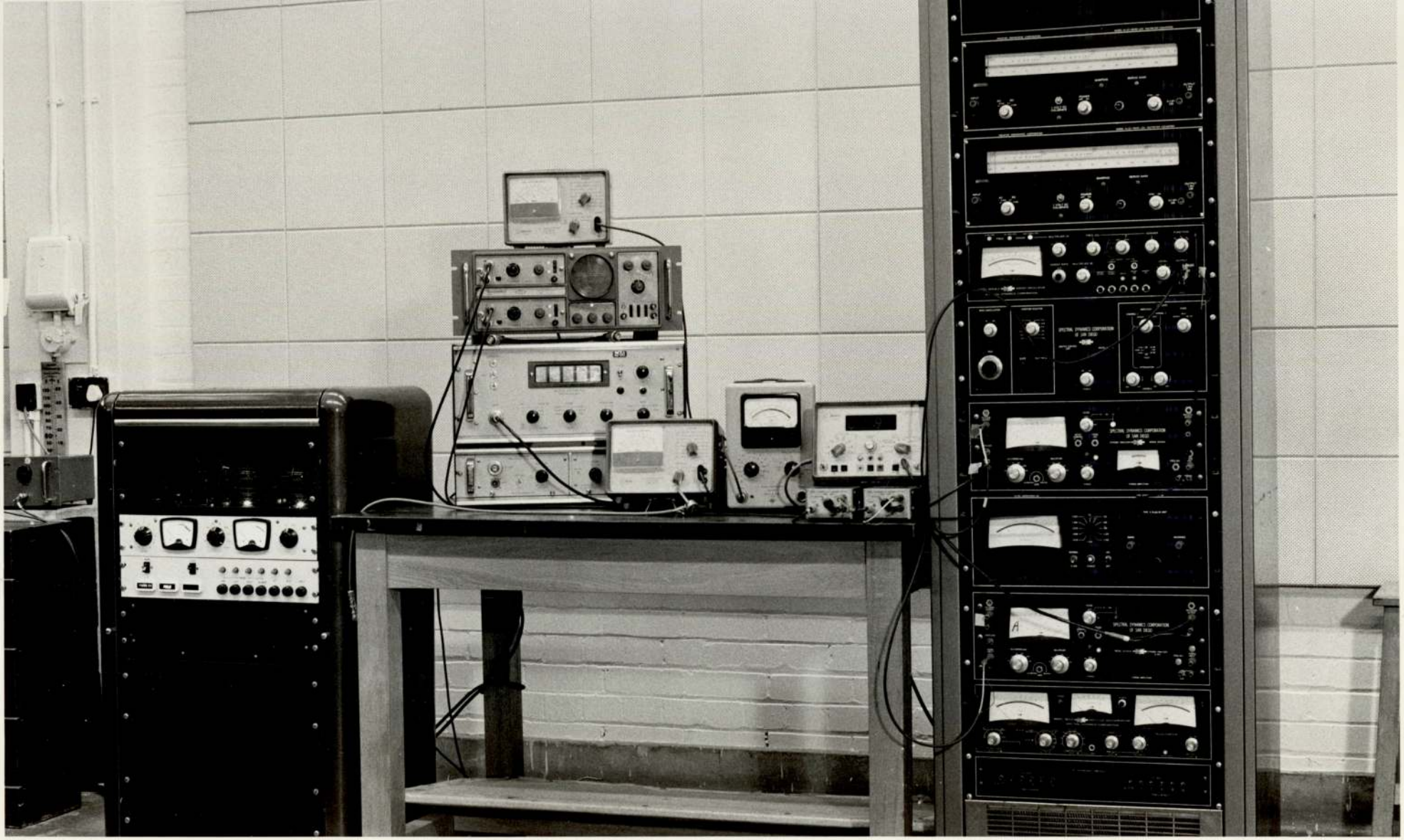

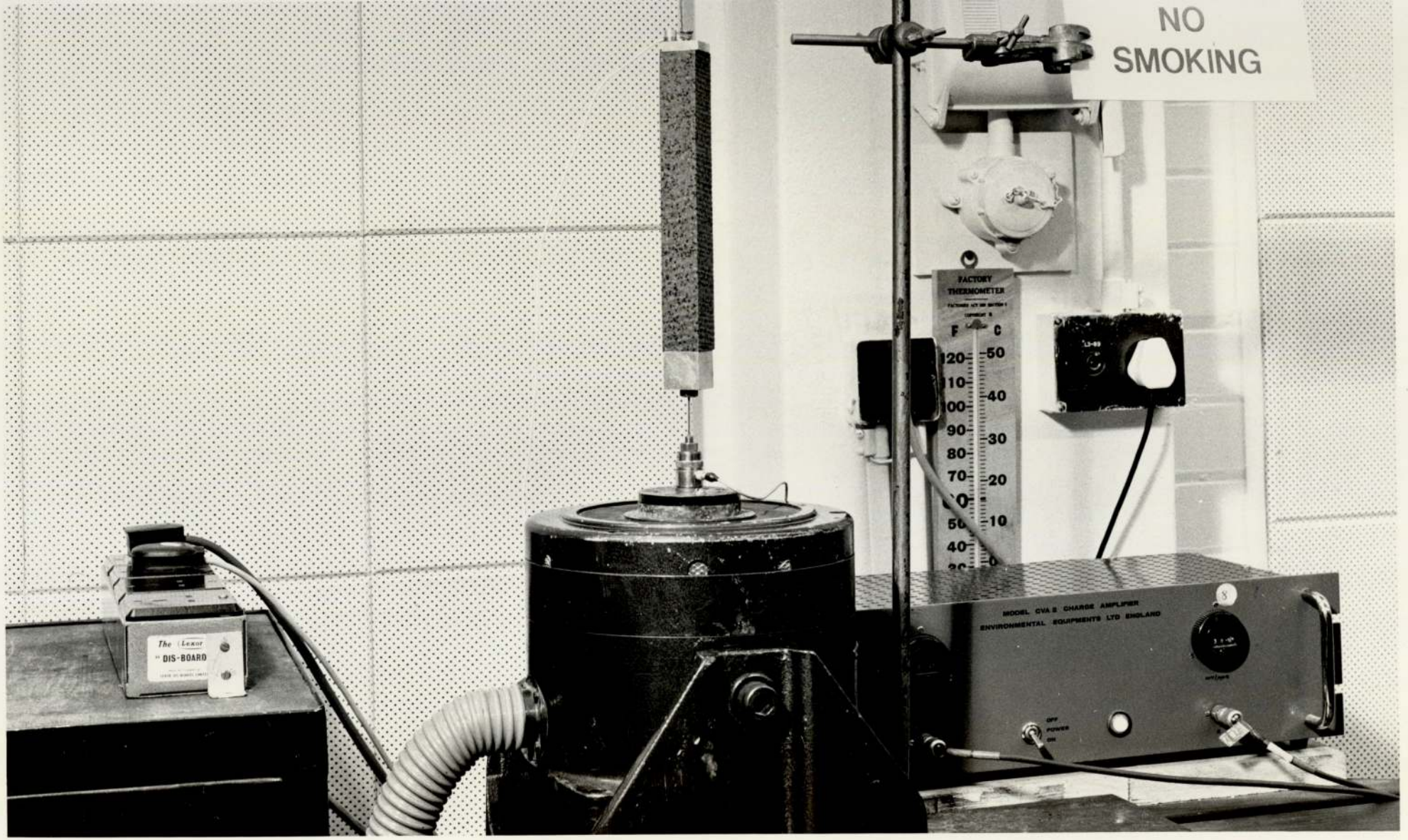
NO
SMOKING
FACTORY
THERMOMETER
F C
120 50
110
100 40
90 30
80
70 20
0
10
MODEL CVA 2 CHARGE AMPLIFIER
ENVIRONMENTAL EQUIPMENTS LTD ENGLAND
OFF
POWER
ON
The Lexor
DIS-BOARD

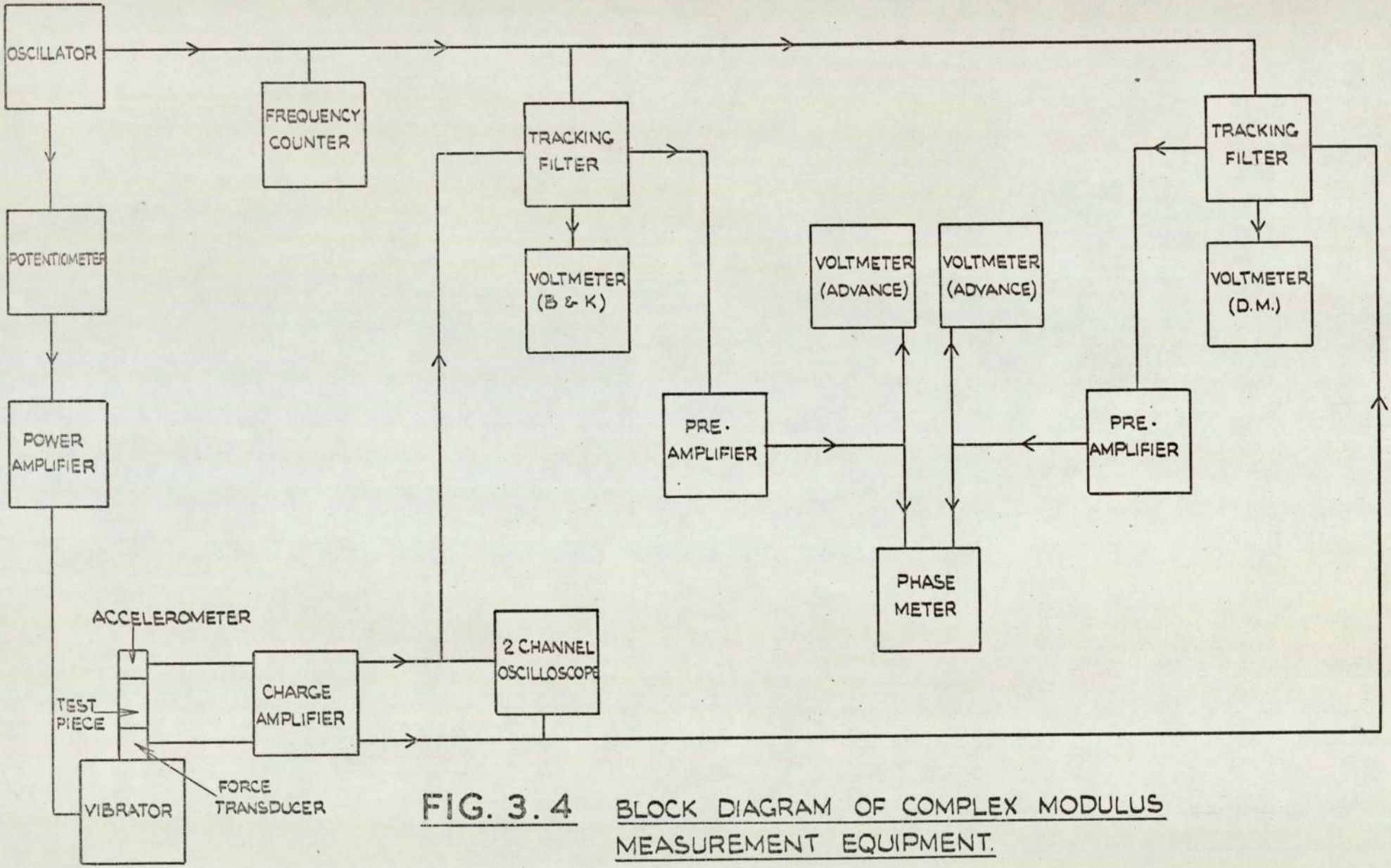

FIG. 3.4 BLOCK DIAGRAM OF COMPLEX MODULUS MEASUREMENT EQUIPMENT.

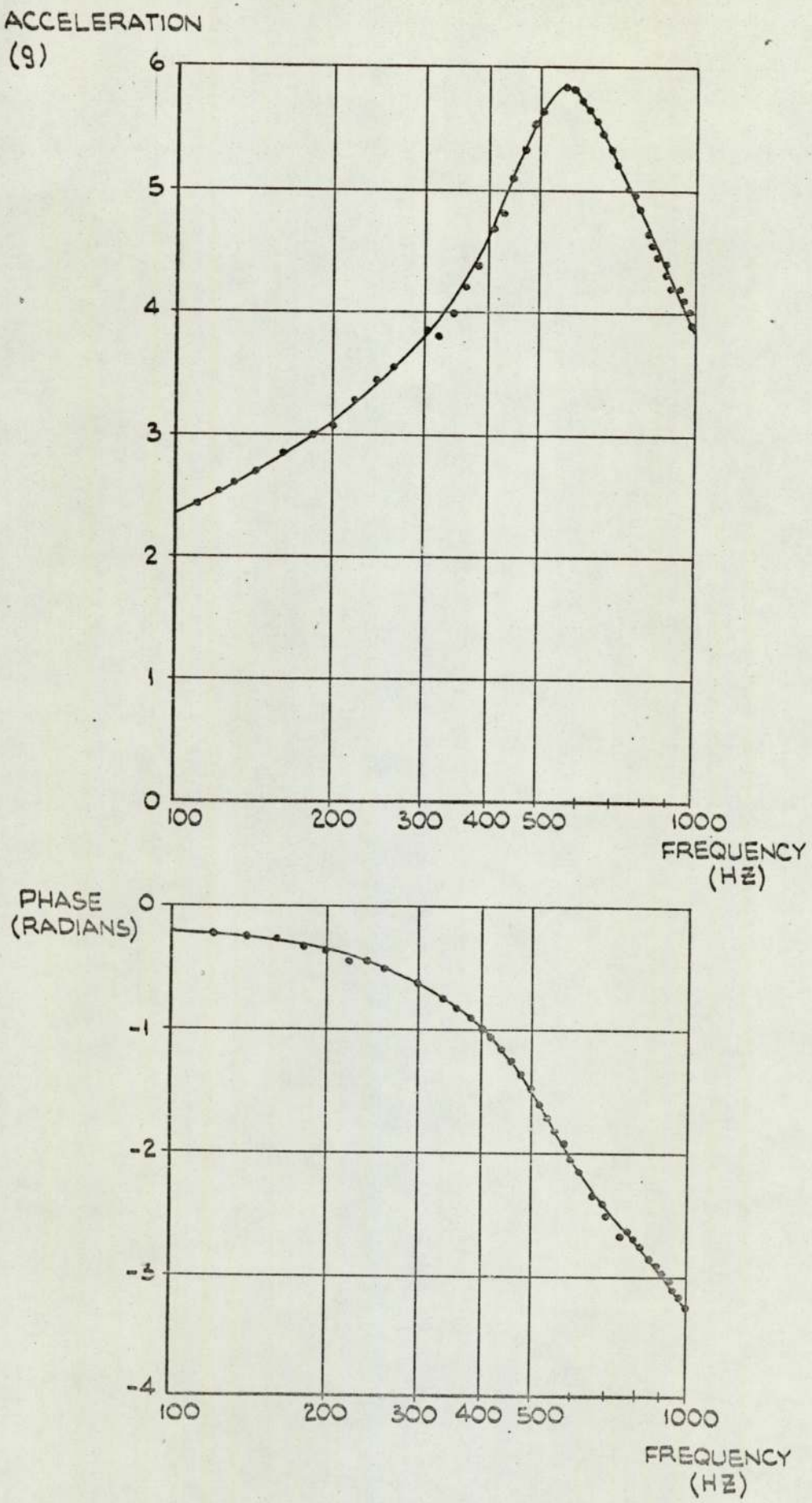

FIG. 3.5 MEASUREMENTS MADE ON TEST PIECE (a)

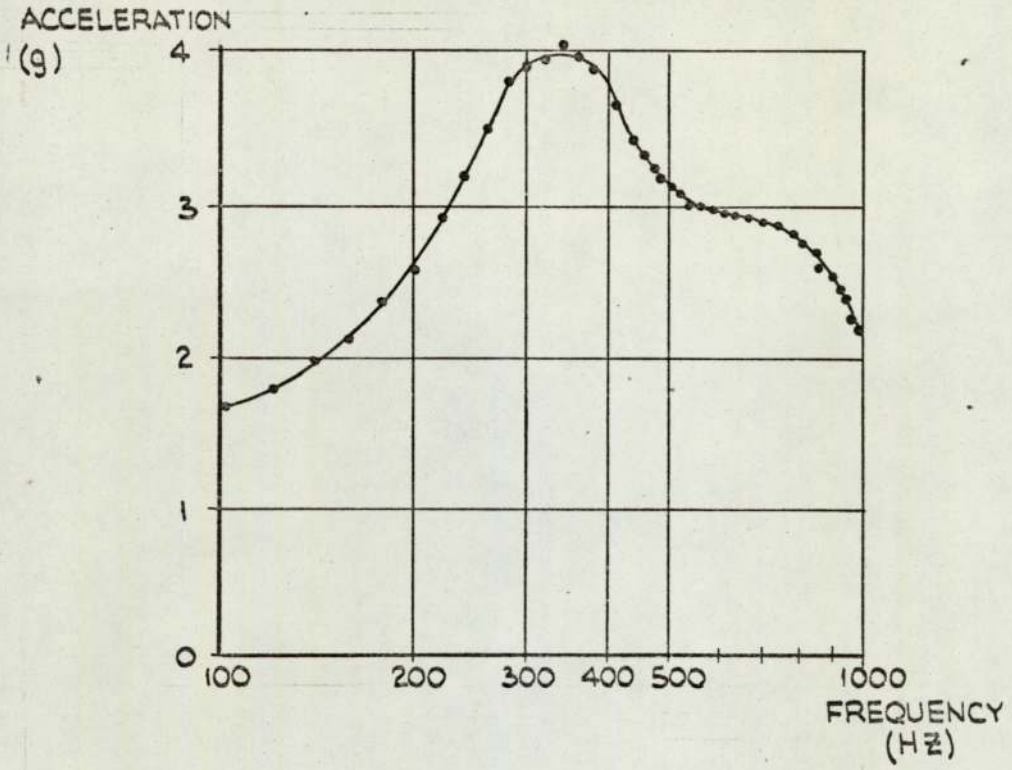

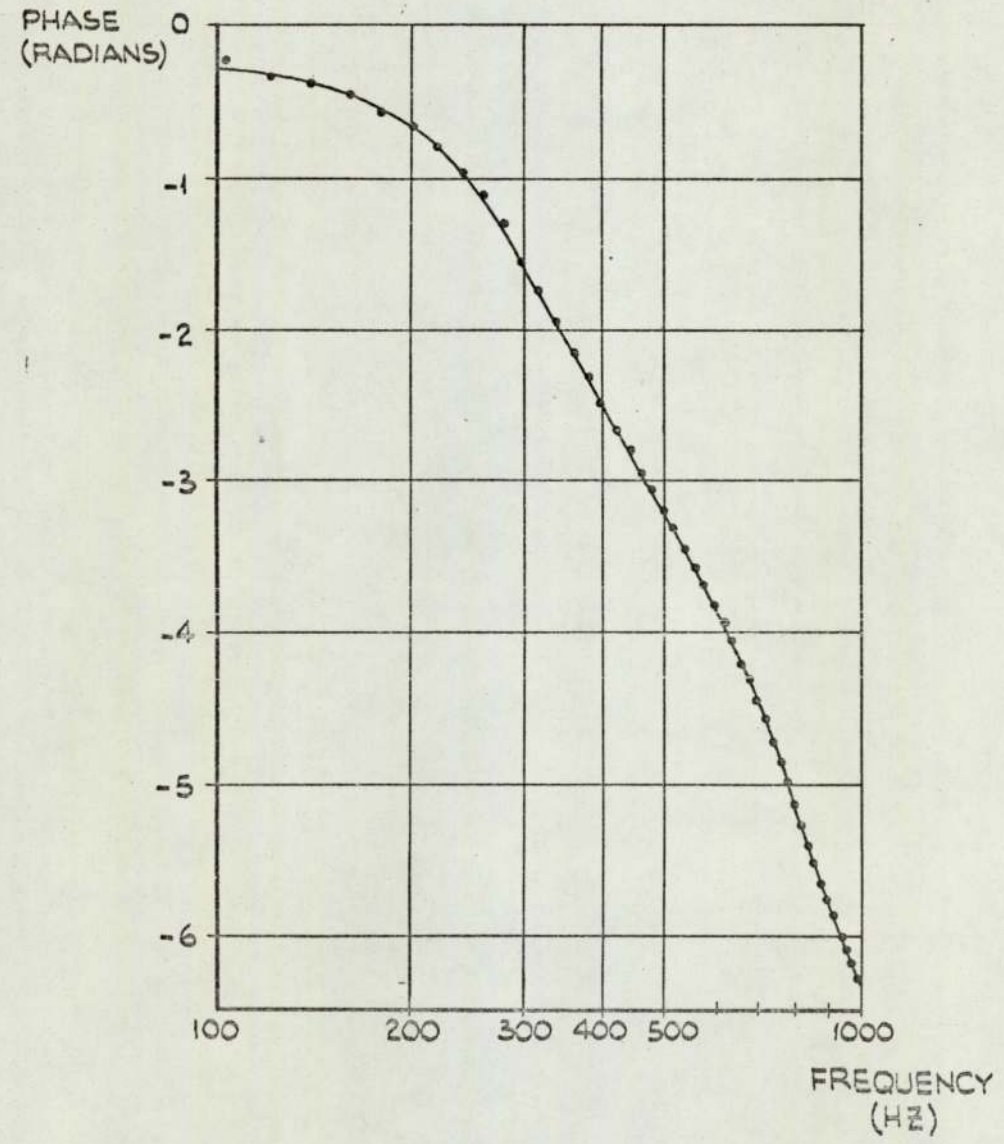

FIG. 3.6 MEASUREMENTS MADE ON TEST PIECE (b)


SATCHWELL

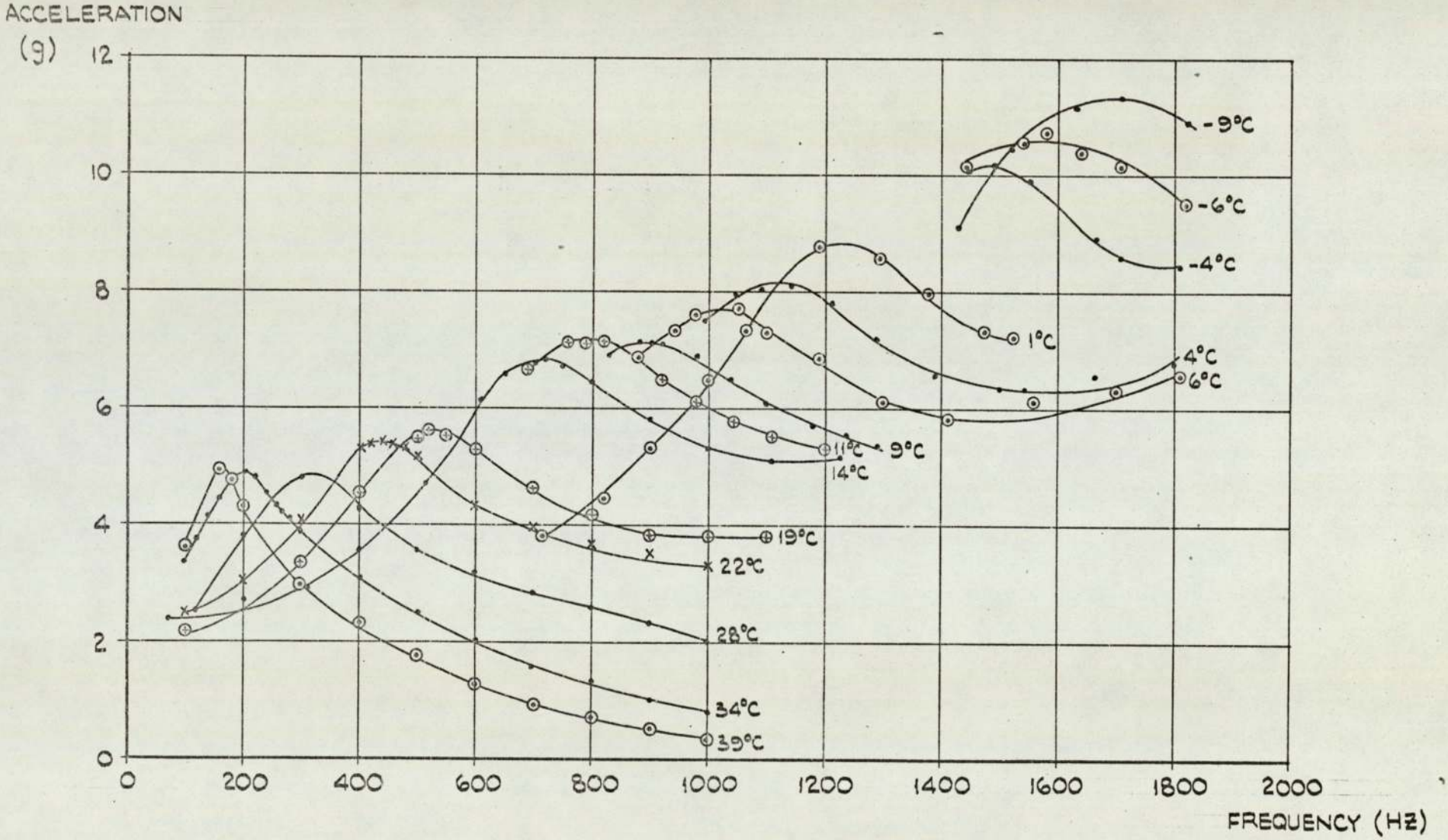

FIG. 3.8(a) ACCELERATION VS. FREQUENCY FOR VARIOUS TEMPERATURES.

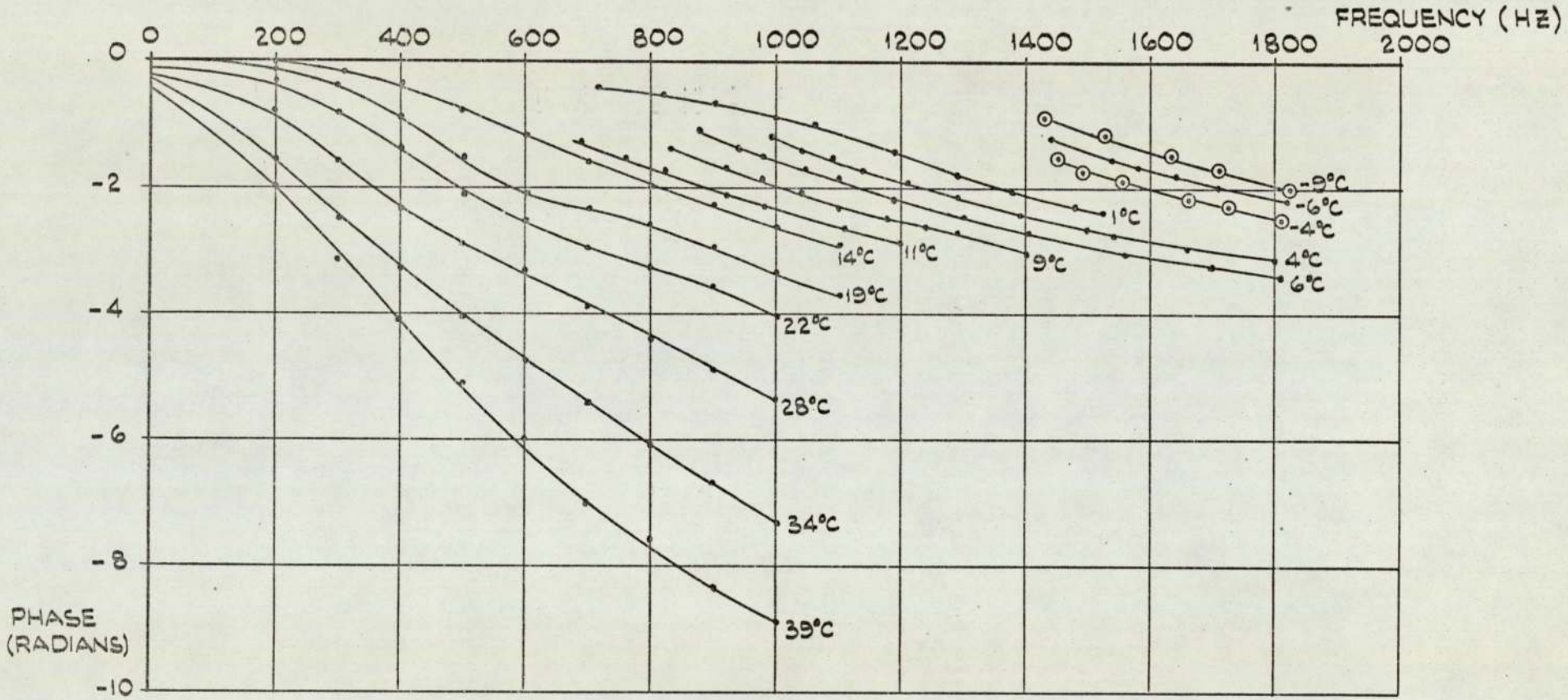

FIG. 3.8(b) PHASE VS. FREQUENCY FOR VARIOUS TEMPERATURES.

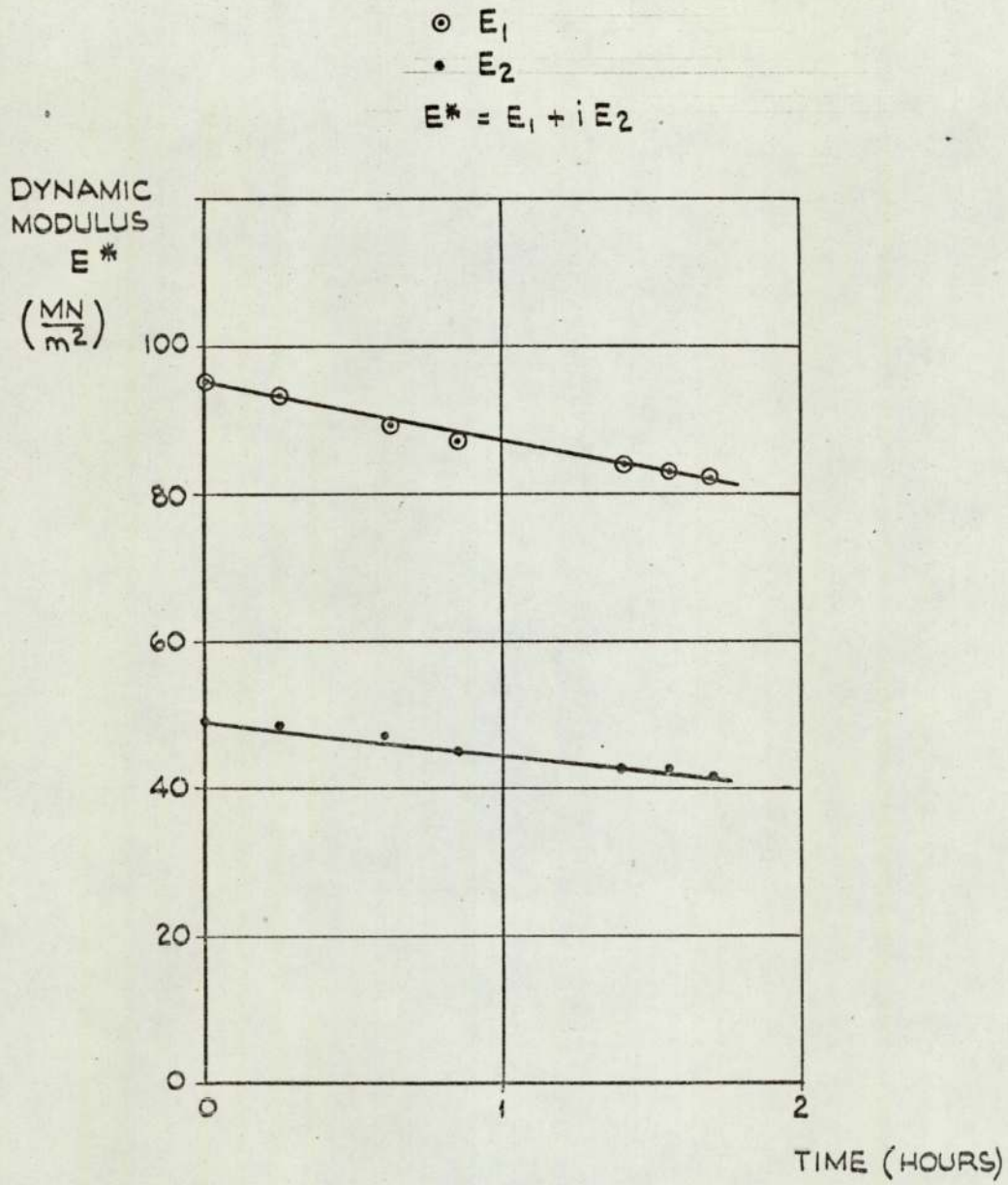

FIG. 3.9 VARIATION OF DYNAMIC MODULUS WITH TIME. THE TEMPERATURE OF THE MATERIAL INCREASES THUS CAUSING A DECREASE IN MODULUS.

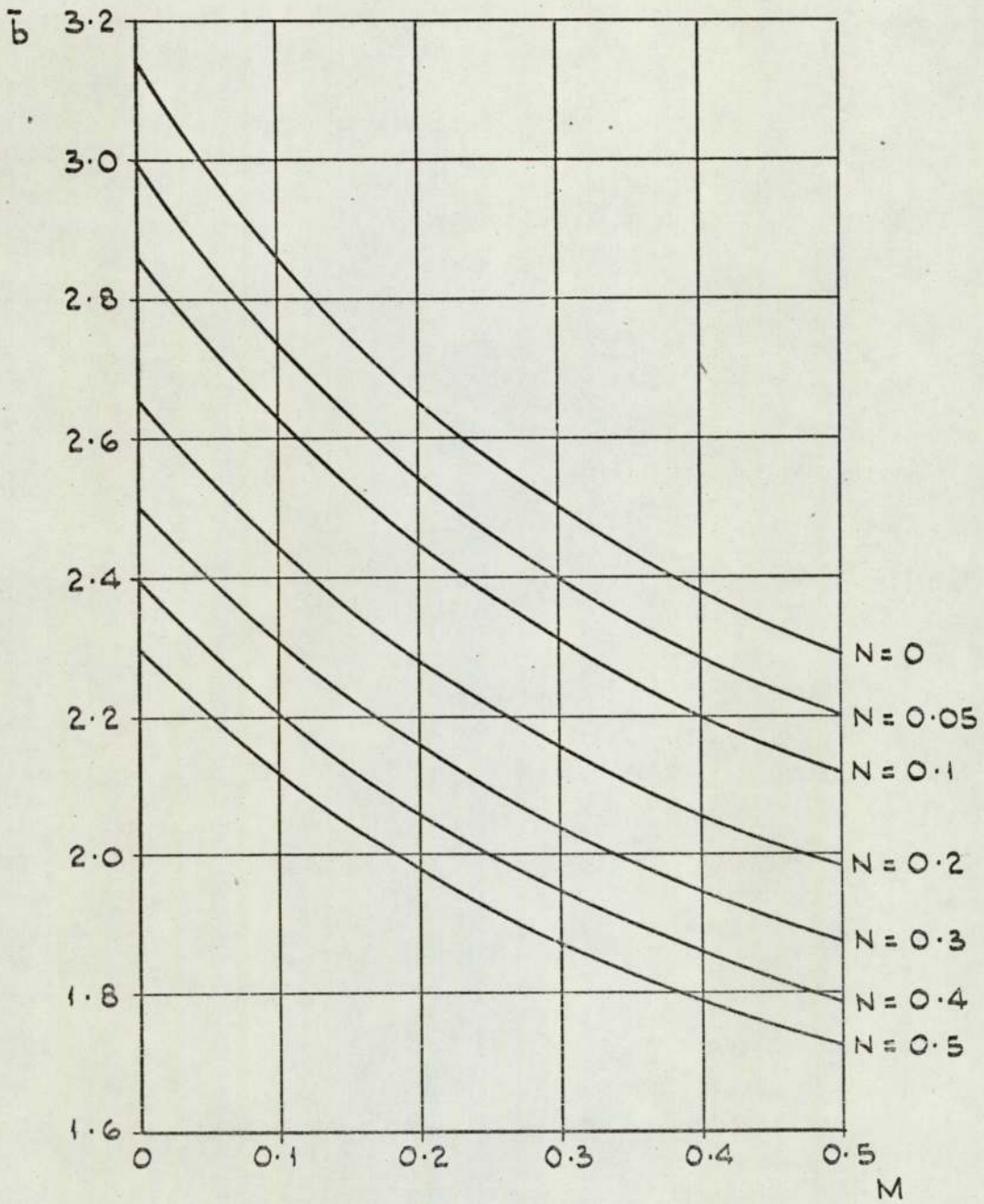

FIG. 3.10 $\bar{b}$ VS. m FOR VARIOUS VALUES OF N.

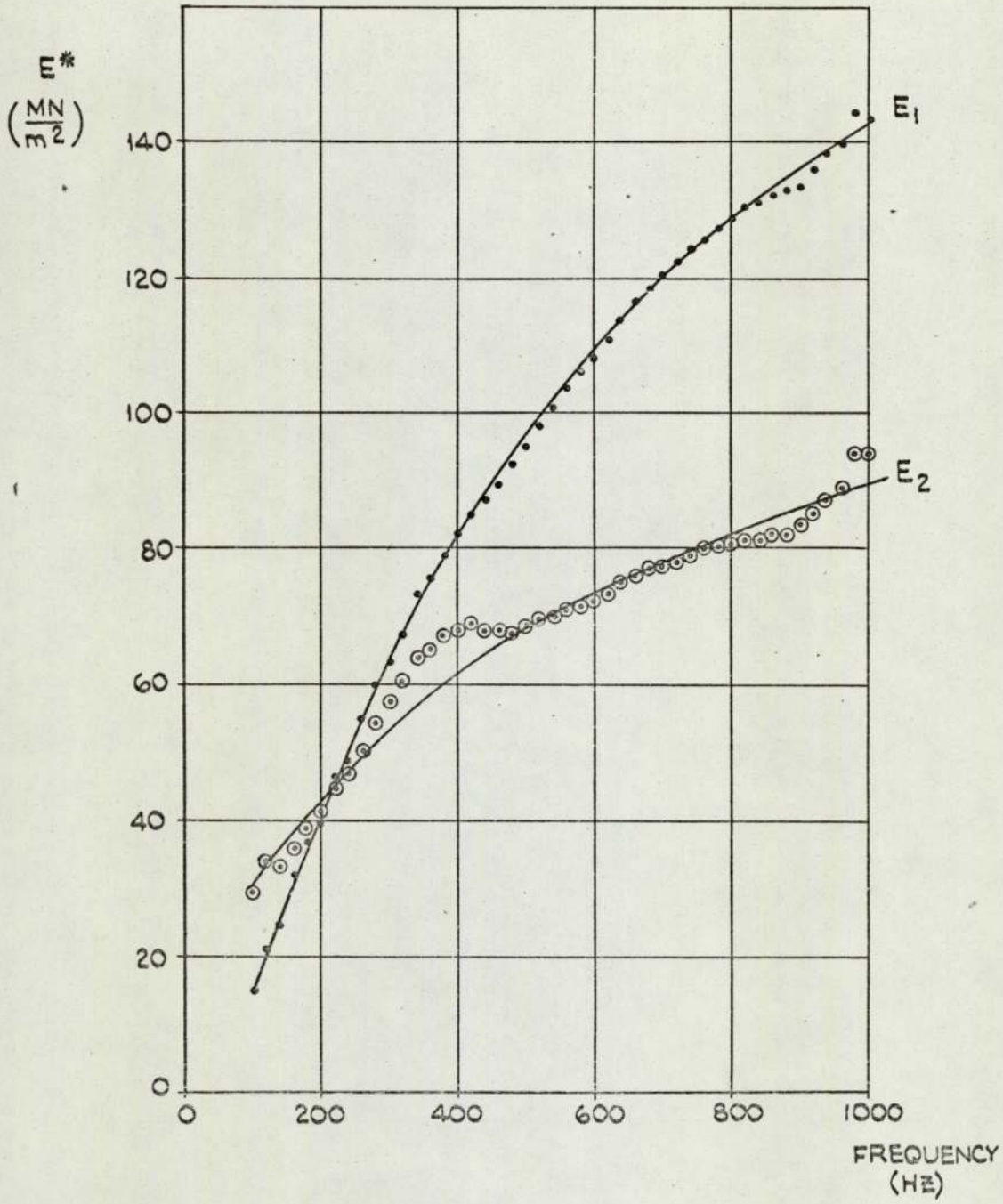

FIG. 3.11 DYNAMIC MODULUS E^* OBTAINED FROM THE MEASUREMENTS ON TEST PIECE (a) (FIG. 3.5)

$E^* = E_1 + i E_2$

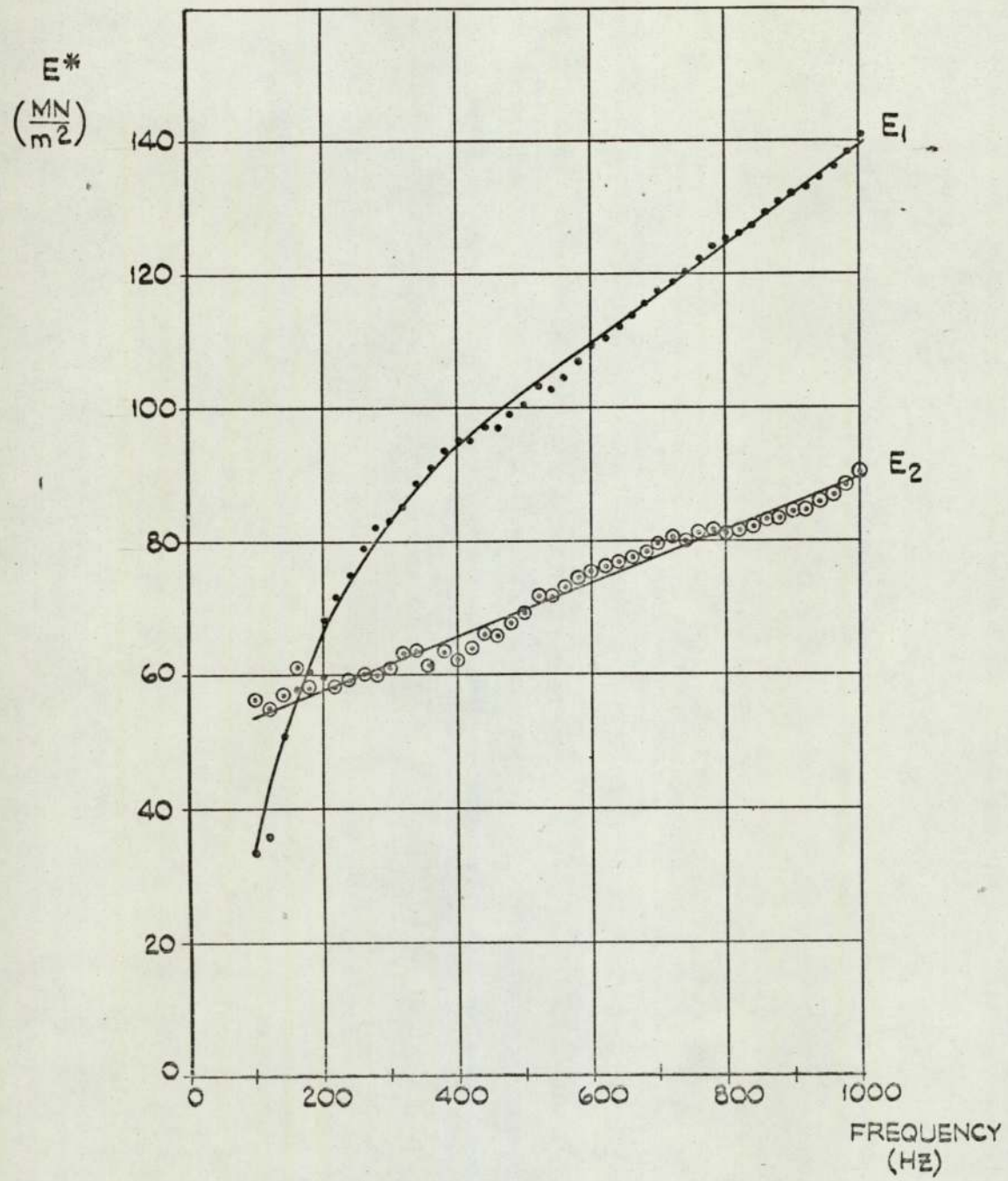

FIG. 3.12 DYNAMIC MODULUS E^* OBTAINED FROM THE MEASUREMENTS ON TEST PIECE (b) (FIG. 3.6)

$E^* = E_1 + i E_2$

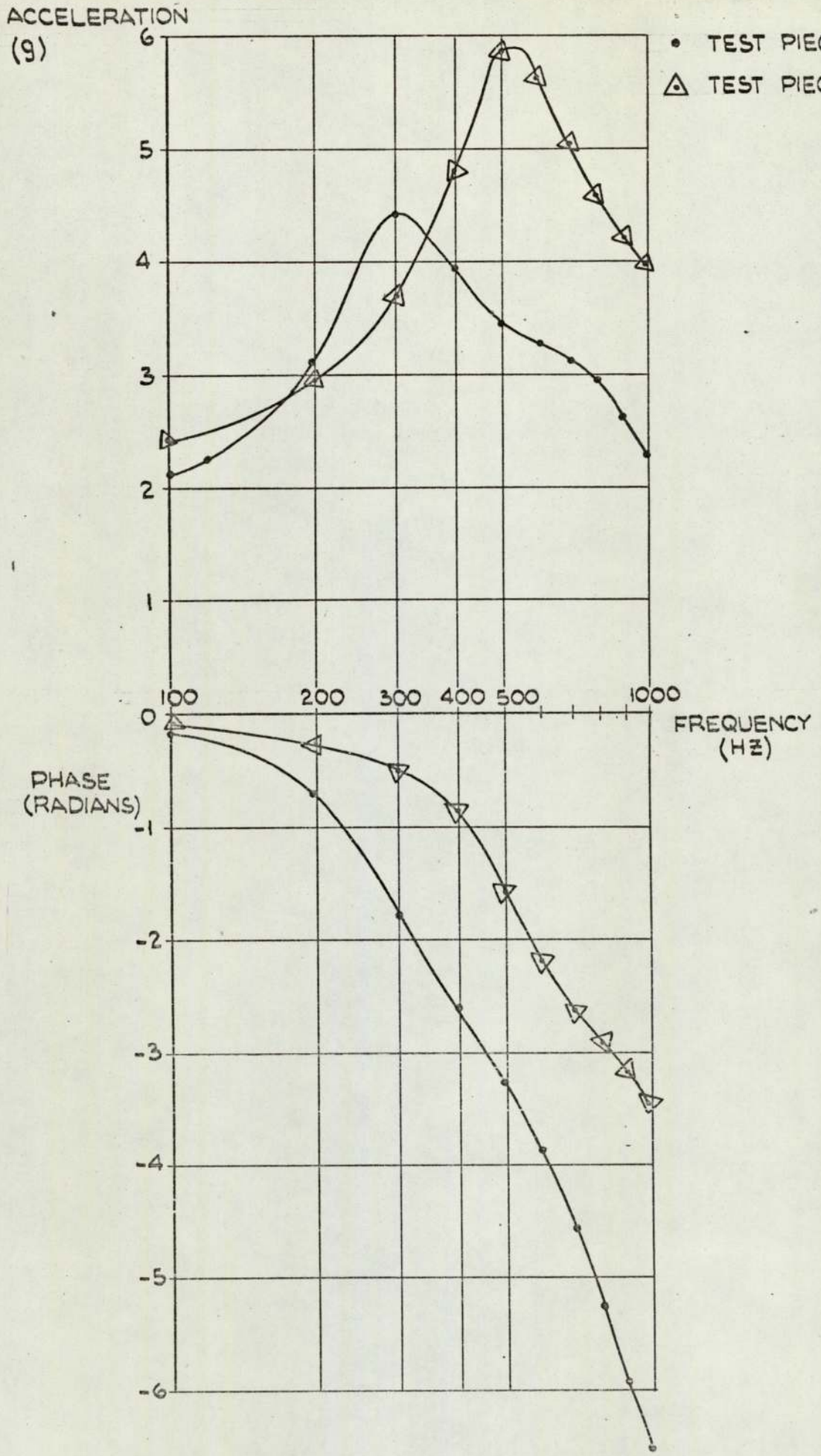

FIG. 3. 13 MEASUREMENTS MADE ON TEST PIECES (a) AND (b) AT THE SAME TEMPERATURE.

TEST PIECE (a) - ⊙ E_1 ⊕ E_2
TEST PIECE (b) - • E_1 + E_2
$E^* = E_1 + i E_2$

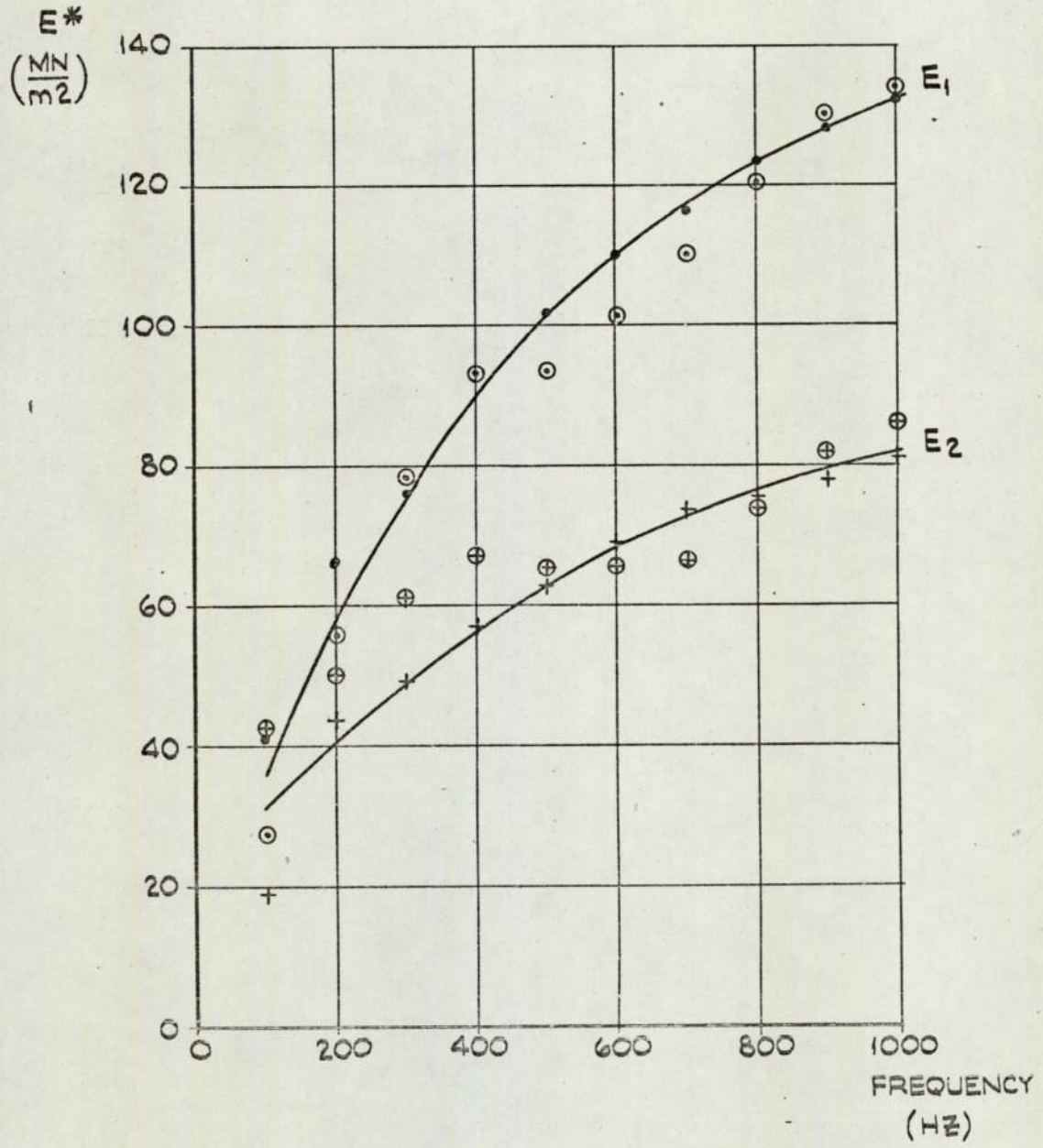

FIG. 3.14 DYNAMIC MODULUS E^* OBTAINED FROM THE MEASUREMENTS ON TEST PIECES (a) AND (b) AT THE SAME TEMPERATURE. (FIG. 3.13)

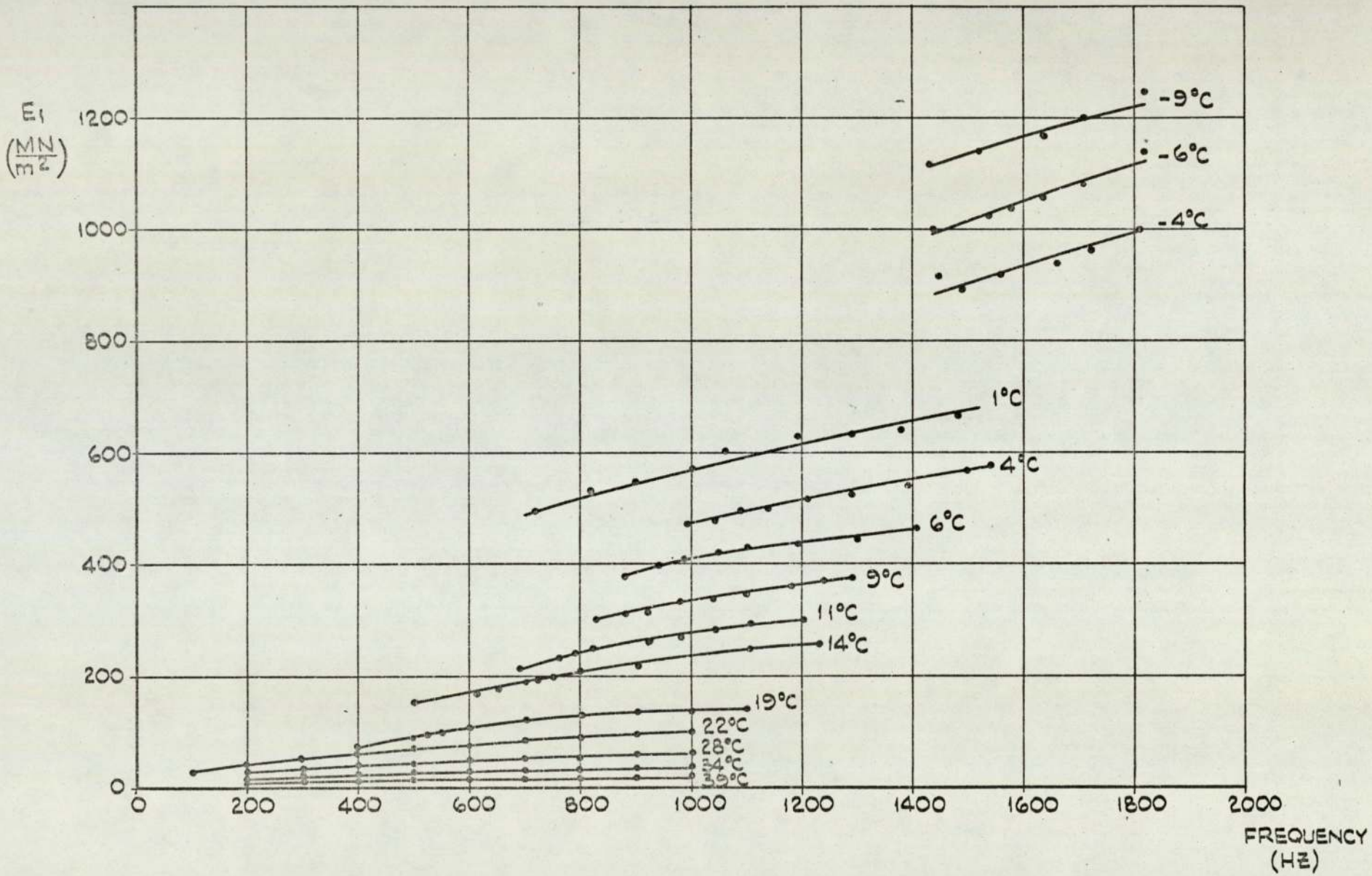

FIG. 3.15 REAL PART OF DYNAMIC MODULUS VS. FREQUENCY FOR VARIOUS TEMPERATUES.

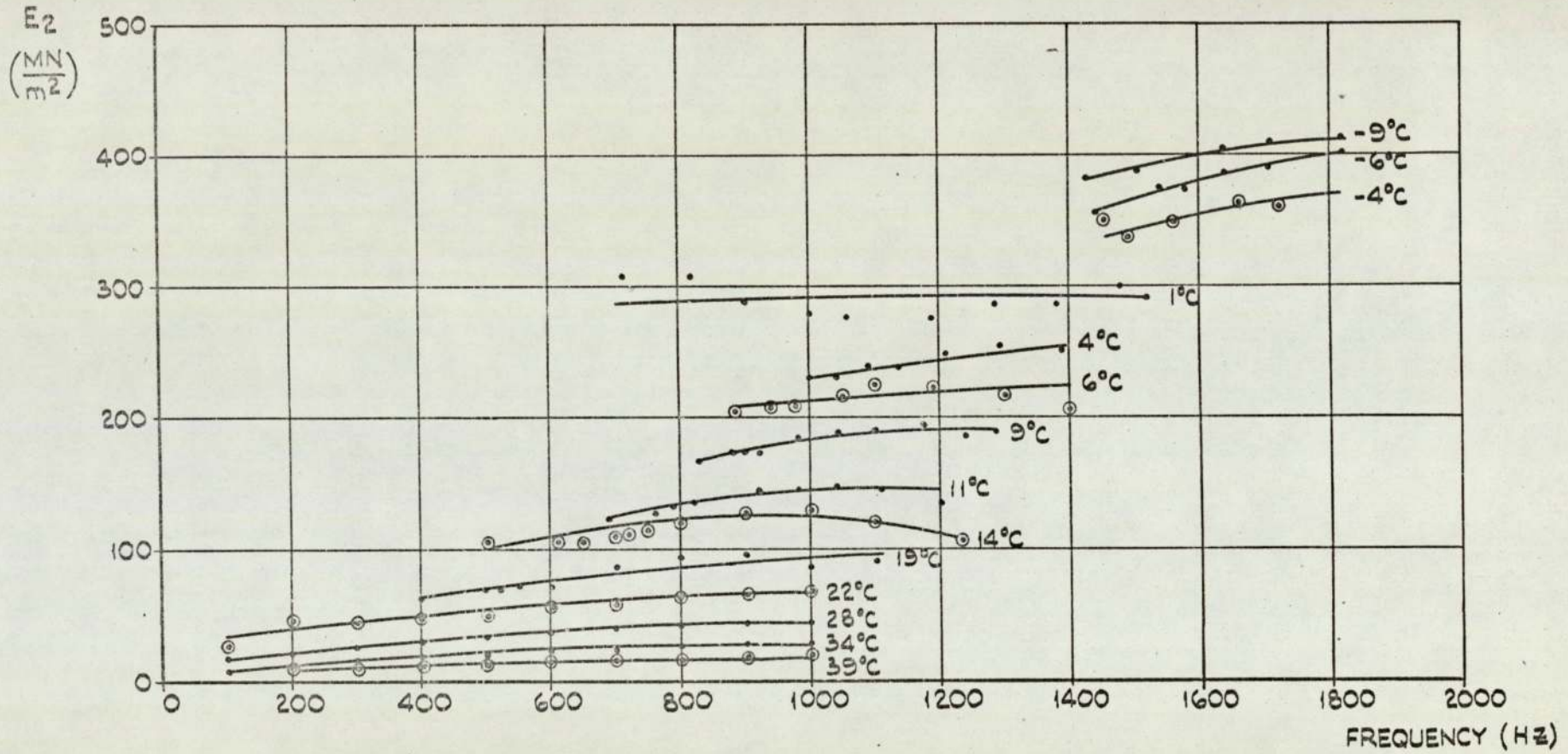

FIG. 3.16 IMAGINARY PART OF DYNAMIC MODULUS VS. FREQUENCY FOR VARIOUS TEMPERATUES.

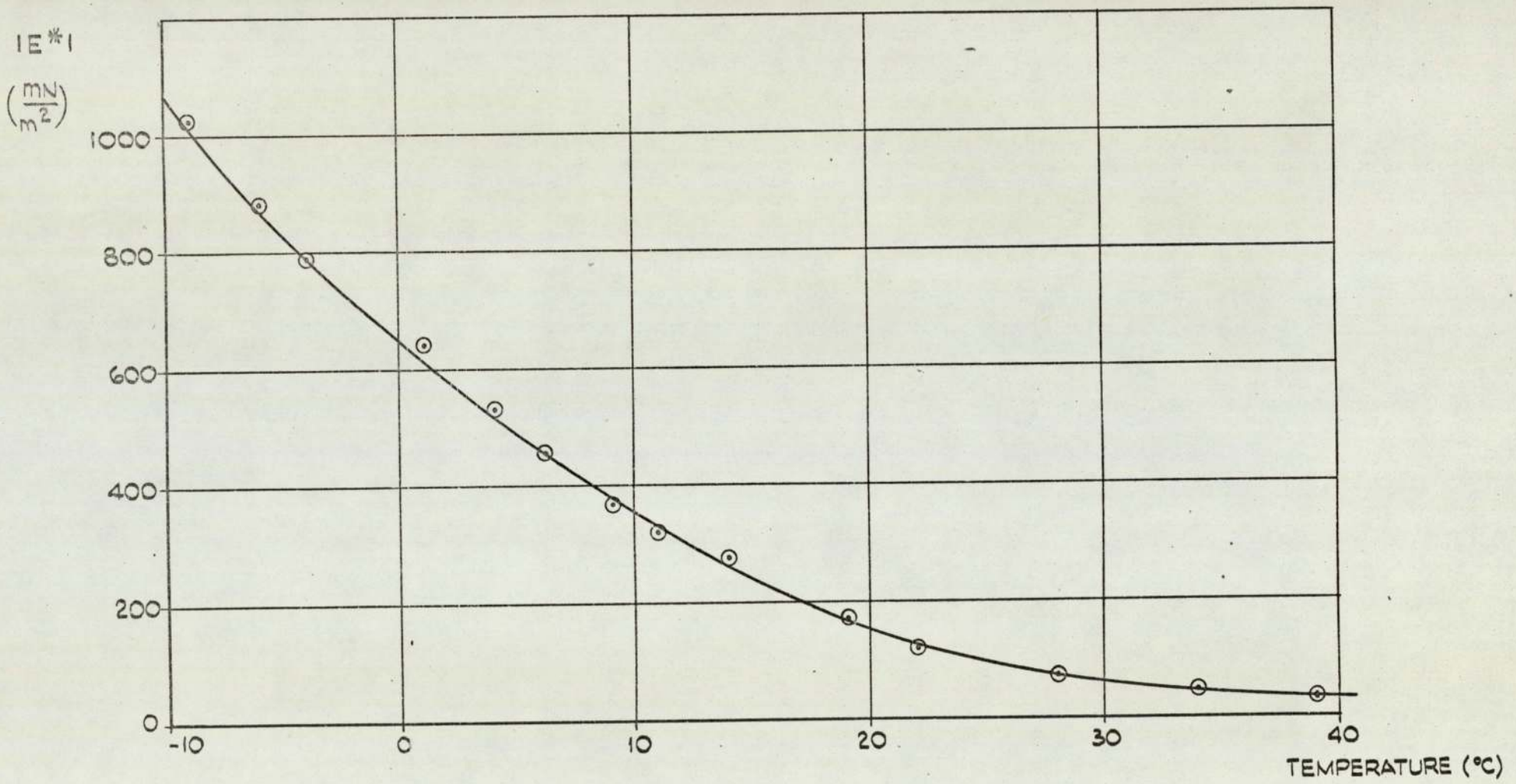

FIG. 3.17 |E*| VS TEMPERATURE FOR CONSTANT FREQUENCY (1000 HZ)

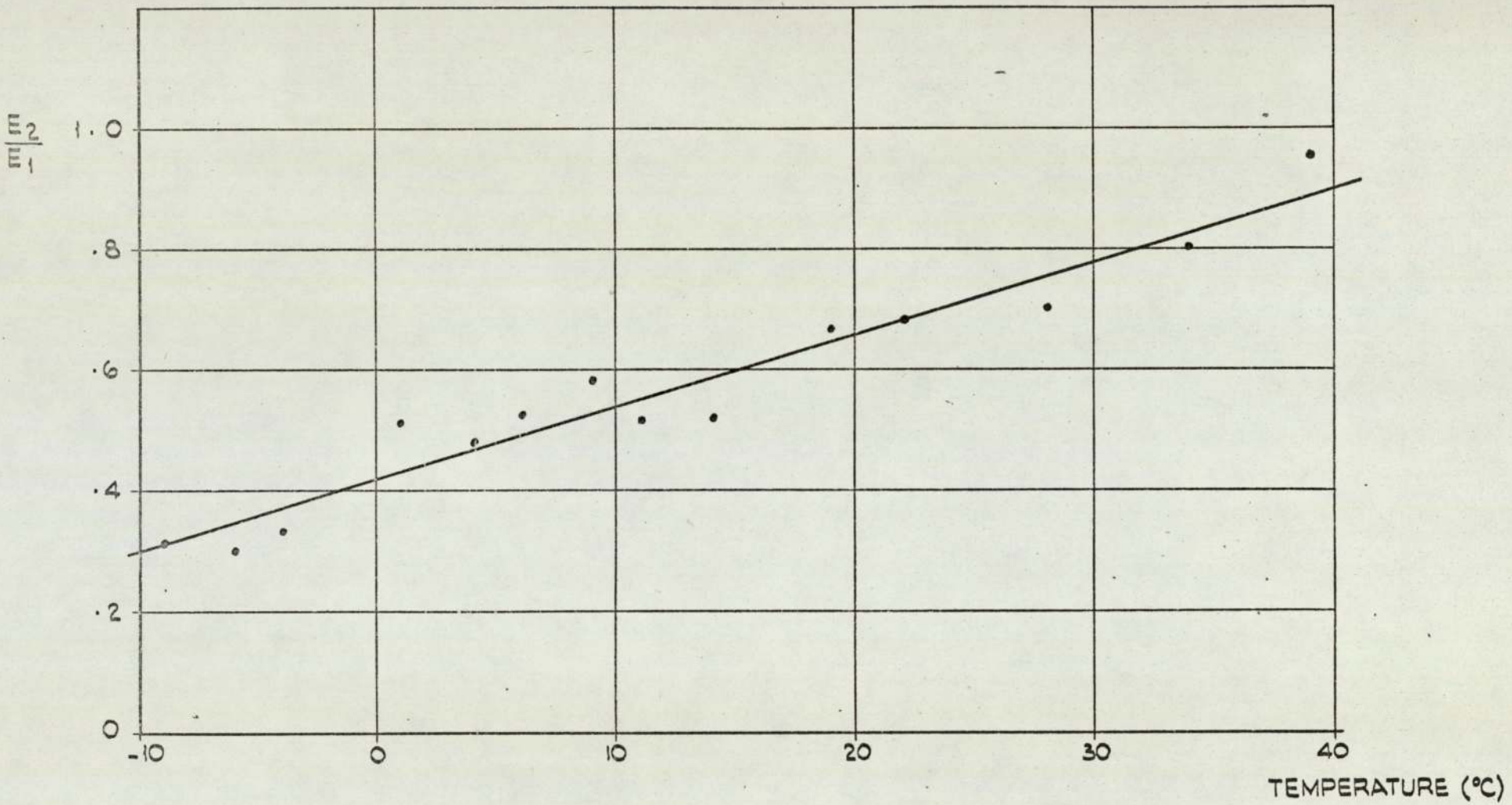

FIG. 3.18 E_2 / E_1 VS. TEMPERATURE FOR CONSTANT FREQUENCY (1000 HZ)

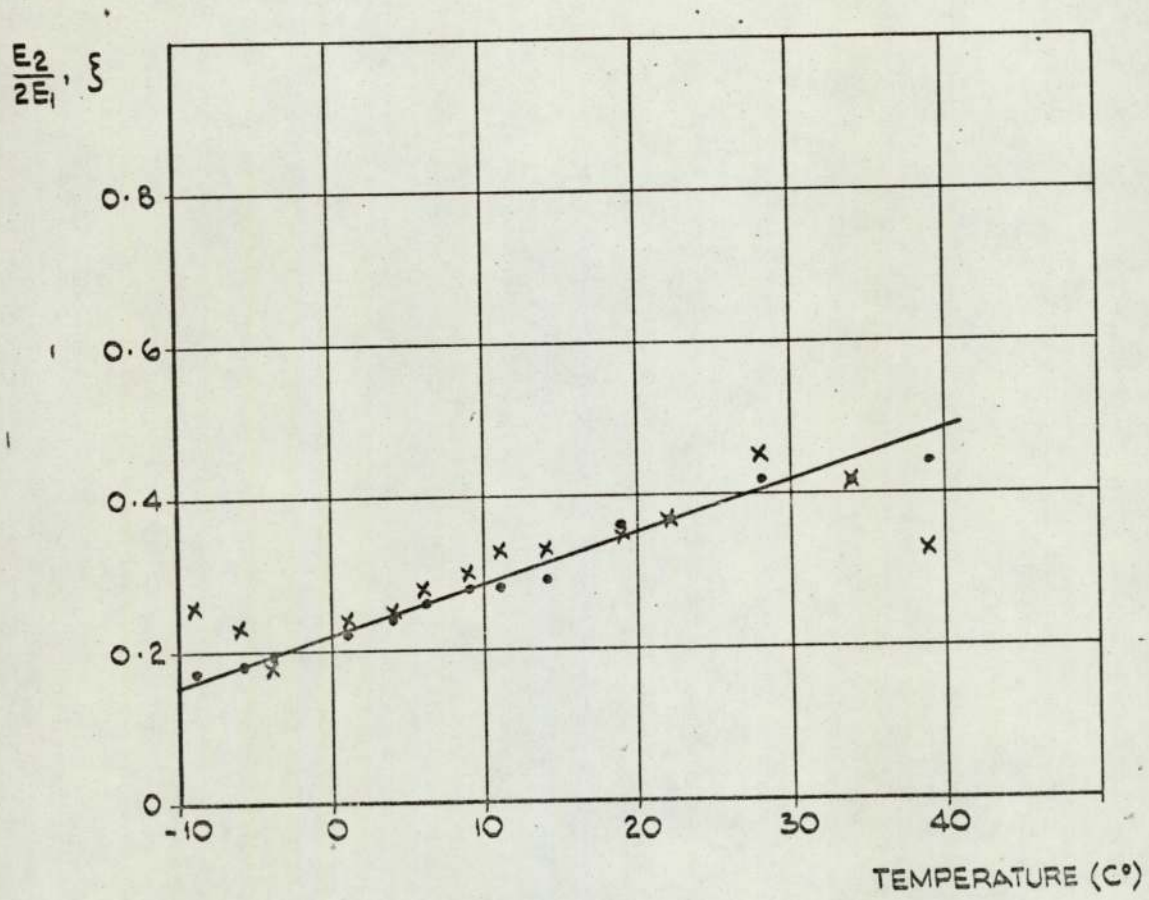

• $\frac{E_2}{2E_1}$ AT FREQUENCY f_m

× ζ AT FREQUENCY f_m

FIG. 3.19 COMPARISON OF $E_2/2E_1$ AND ζ PLOTTED VS. TEMPERATURE.

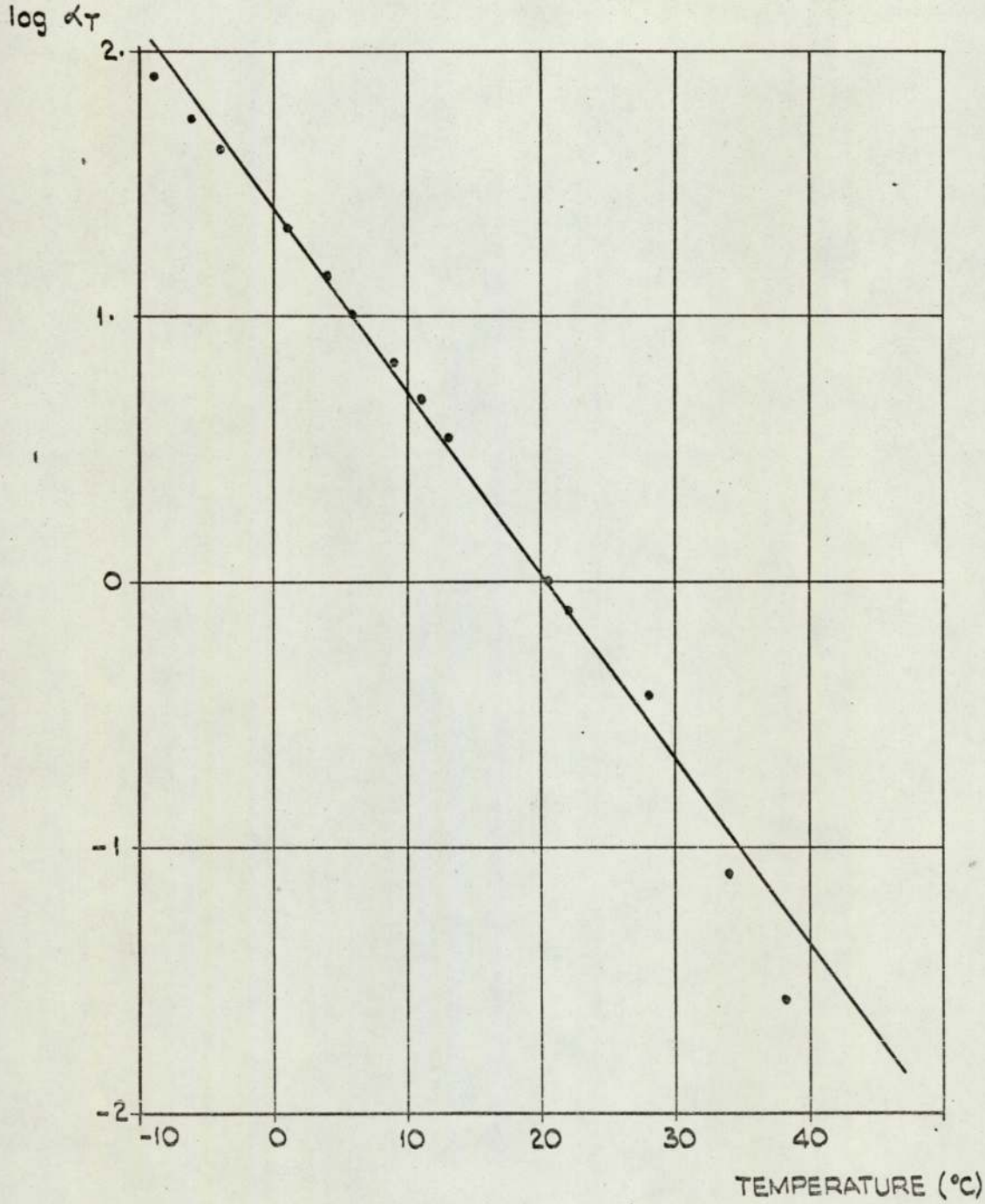

FIG. 3. 20 SHIFT FACTOR (α_T) VS. TEMPERATURE.

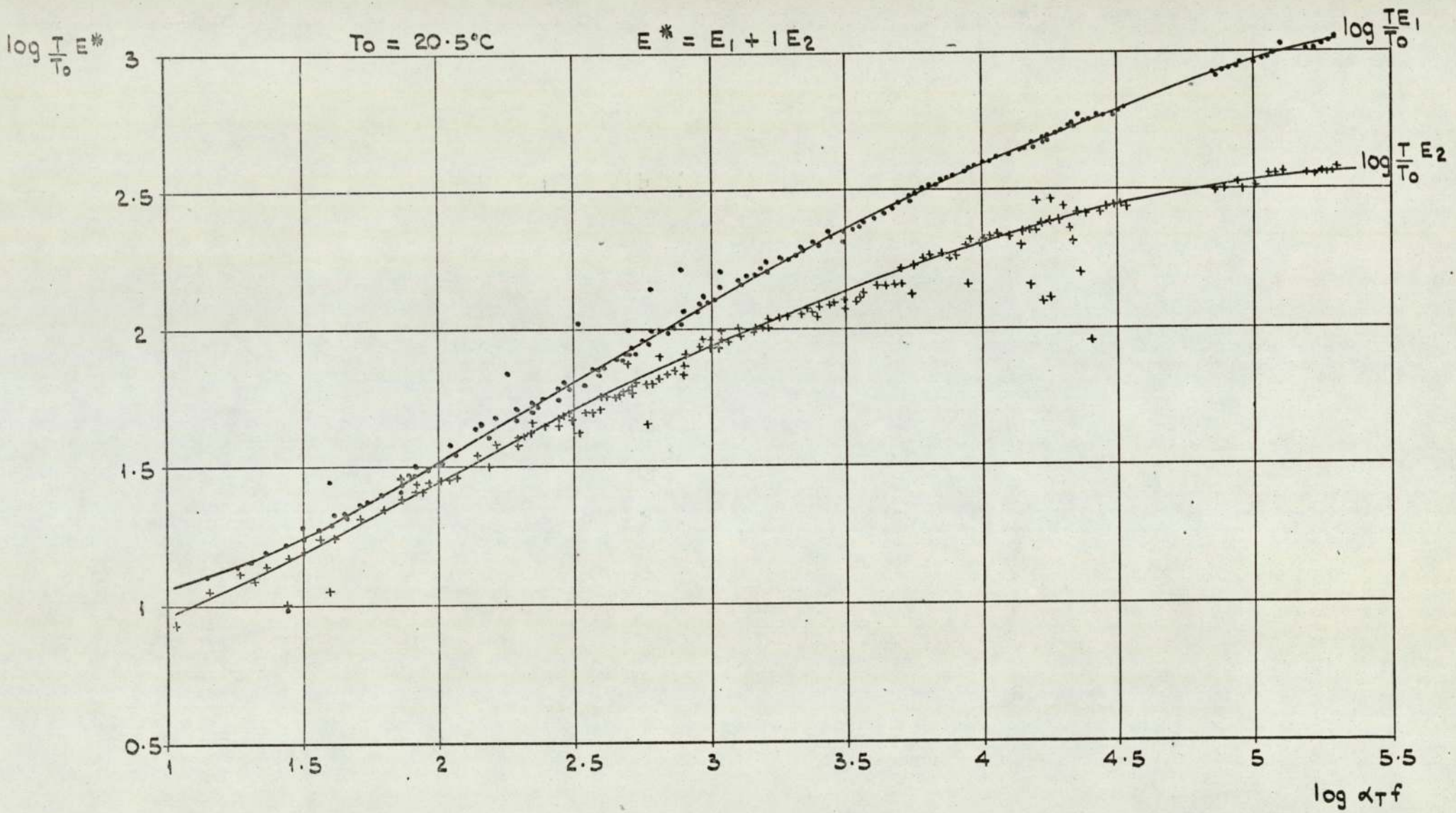

FIG. 3.21 $E^* \frac{T}{T_0}$ VS $\alpha_T f$. RESULT OF TEMPERATURE - FREQUENCY SUPERPOSITION.

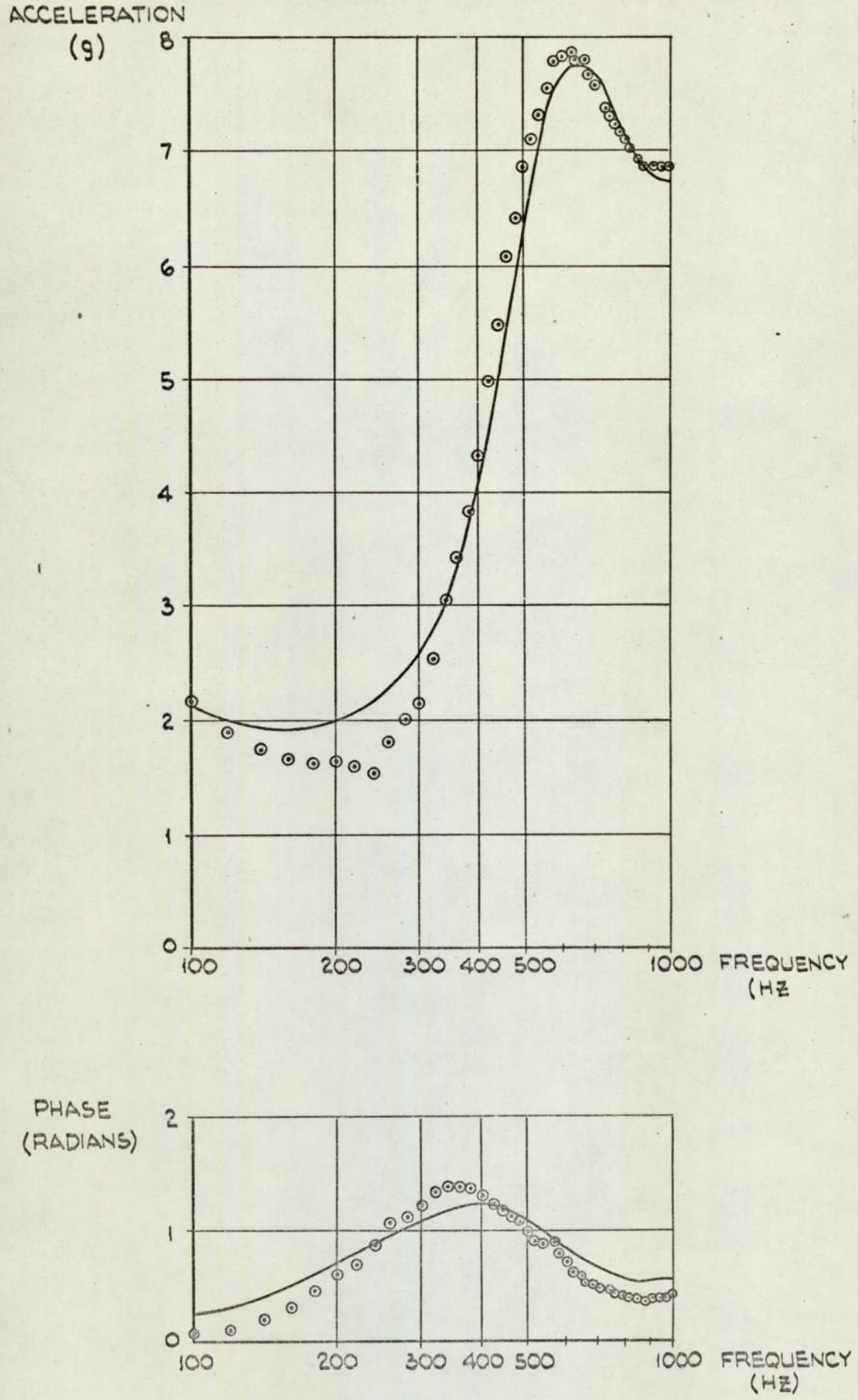

FIG. 3.22 LONGITUDINAL VIBRATIONS - FORCED END COMPARISON OF MEASURED AND CALCULATED RESPONSE.

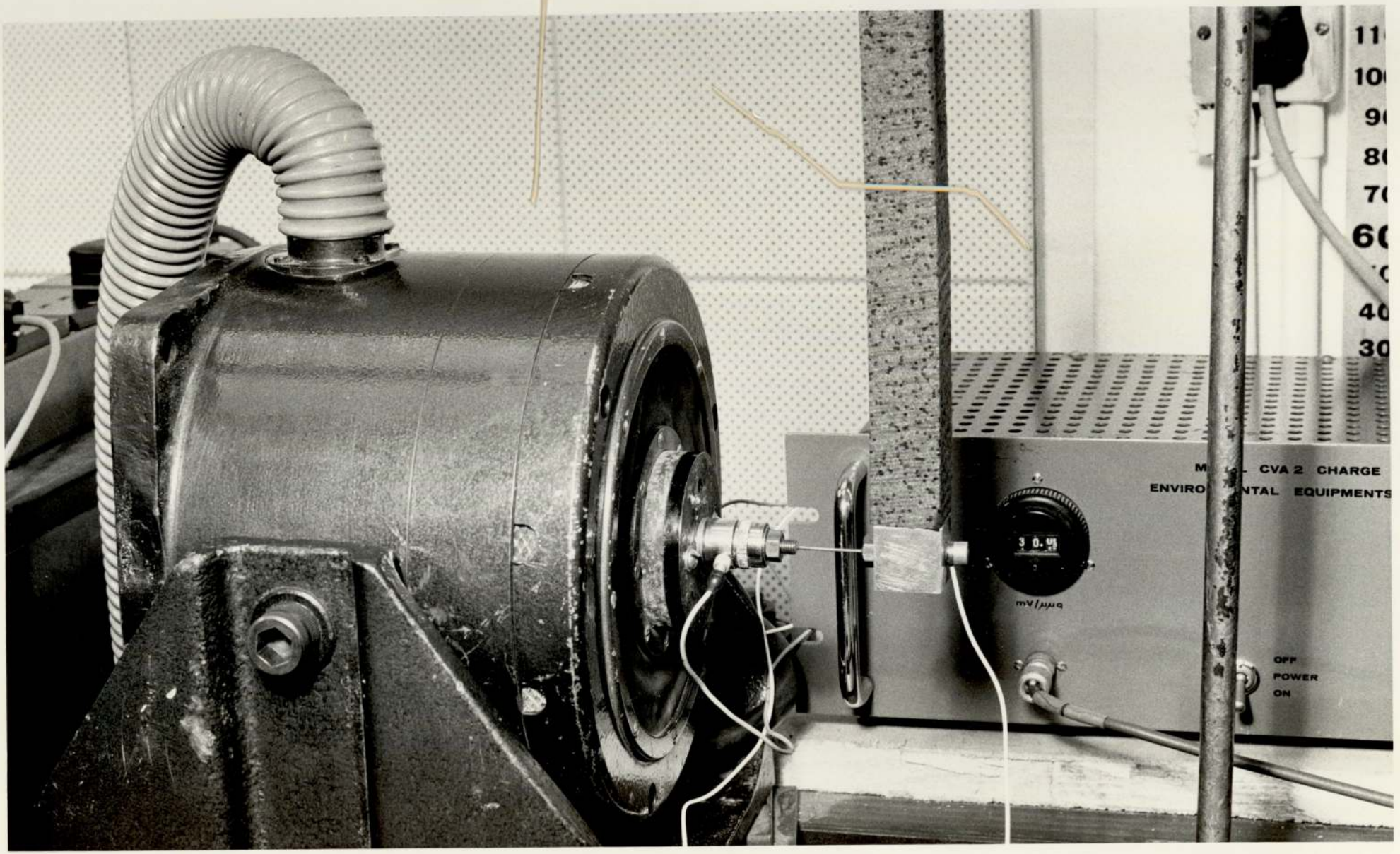
CVA 2 CHARGE
ENVIRO NTAL EQUIPMENTS
OFF
POWER
ON

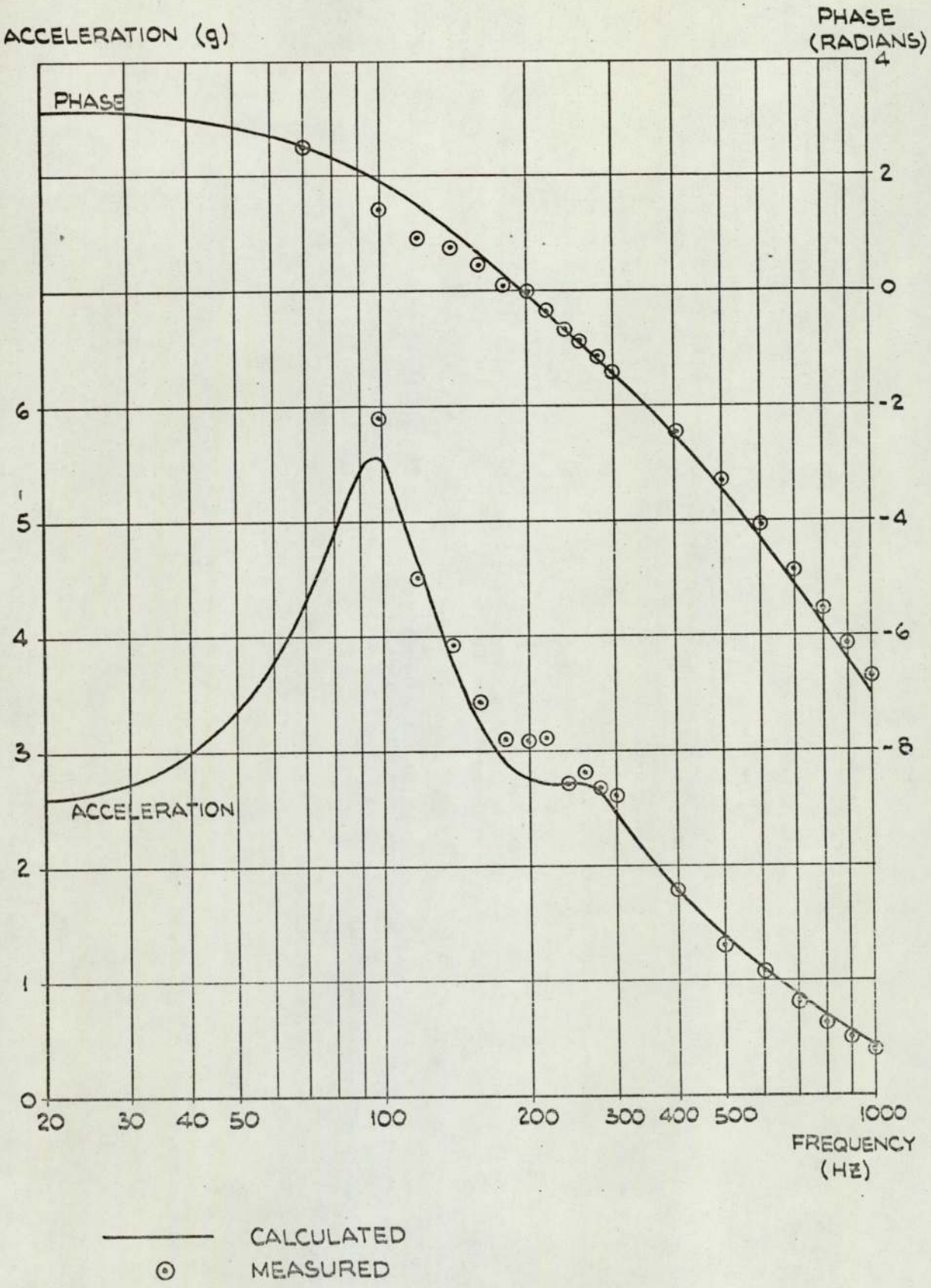

FIG. 3. 24(a) TRANSVERSE VIBRATIONS - FREE END COMPARISON OF MEASURED AND CALCULATED RESPONSE.

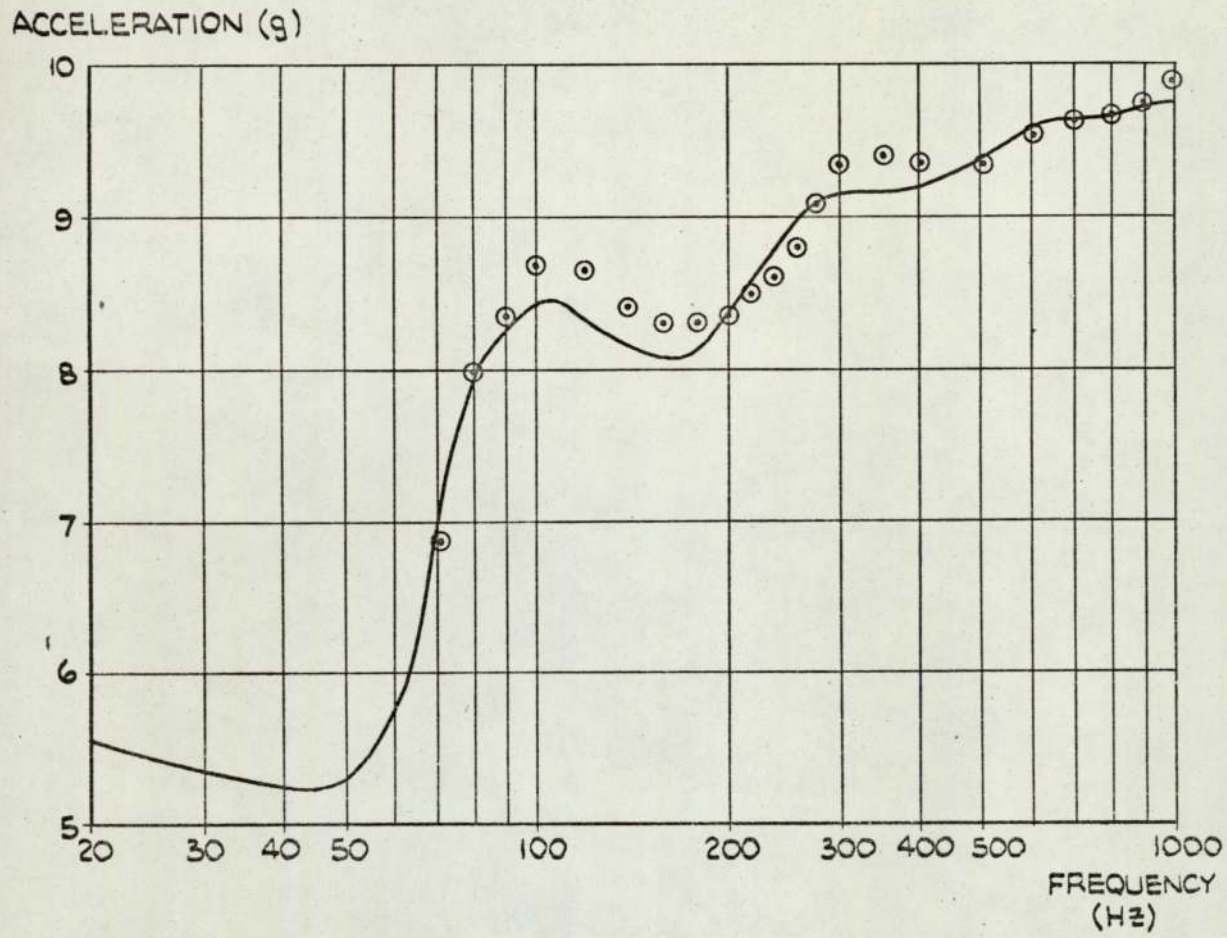

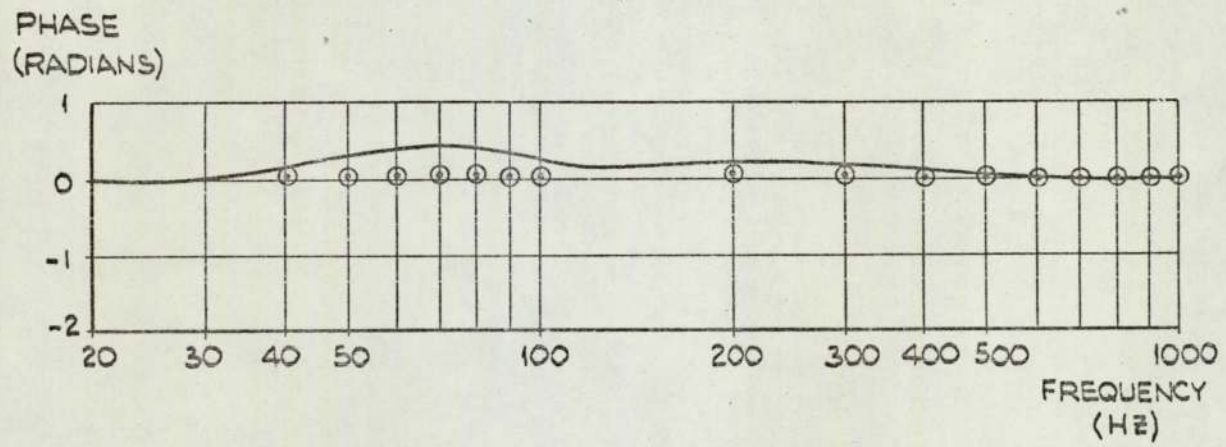

CALCULATED

MEASURED

FIG. 3.24(b) TRANSVERSE VIBRATIONS - FORCED END COMPARISON OF MEASURED AND CALCULATED RESPONSE.

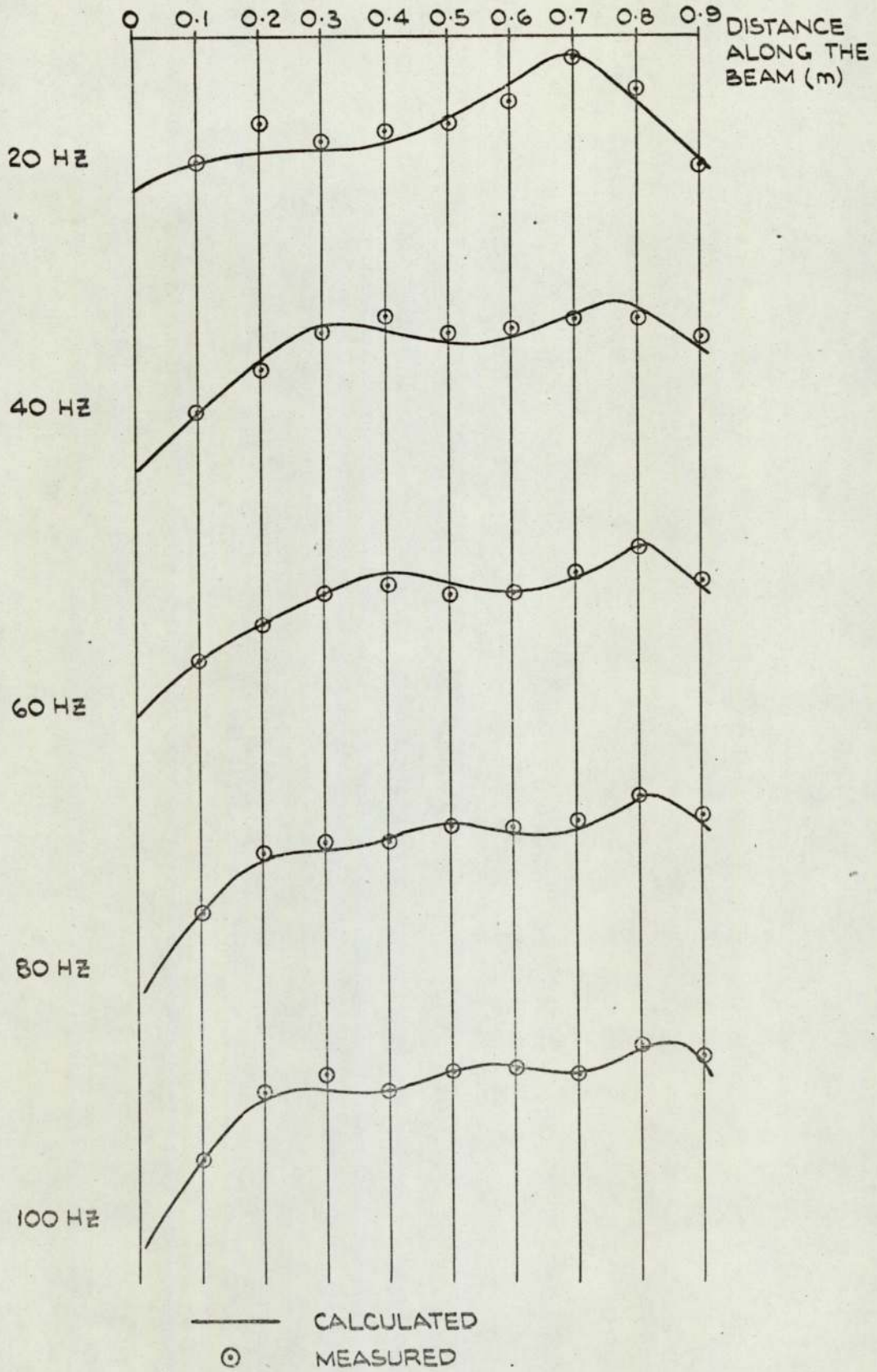

FIG. 3. 25 COMPARISON OF MEASURED AND CALCULATED RESPONSE OF LARGE SCALE SAMPLE.

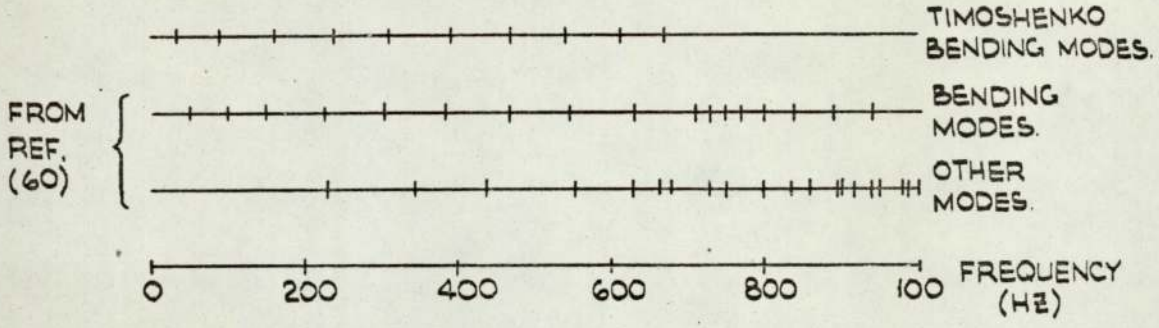

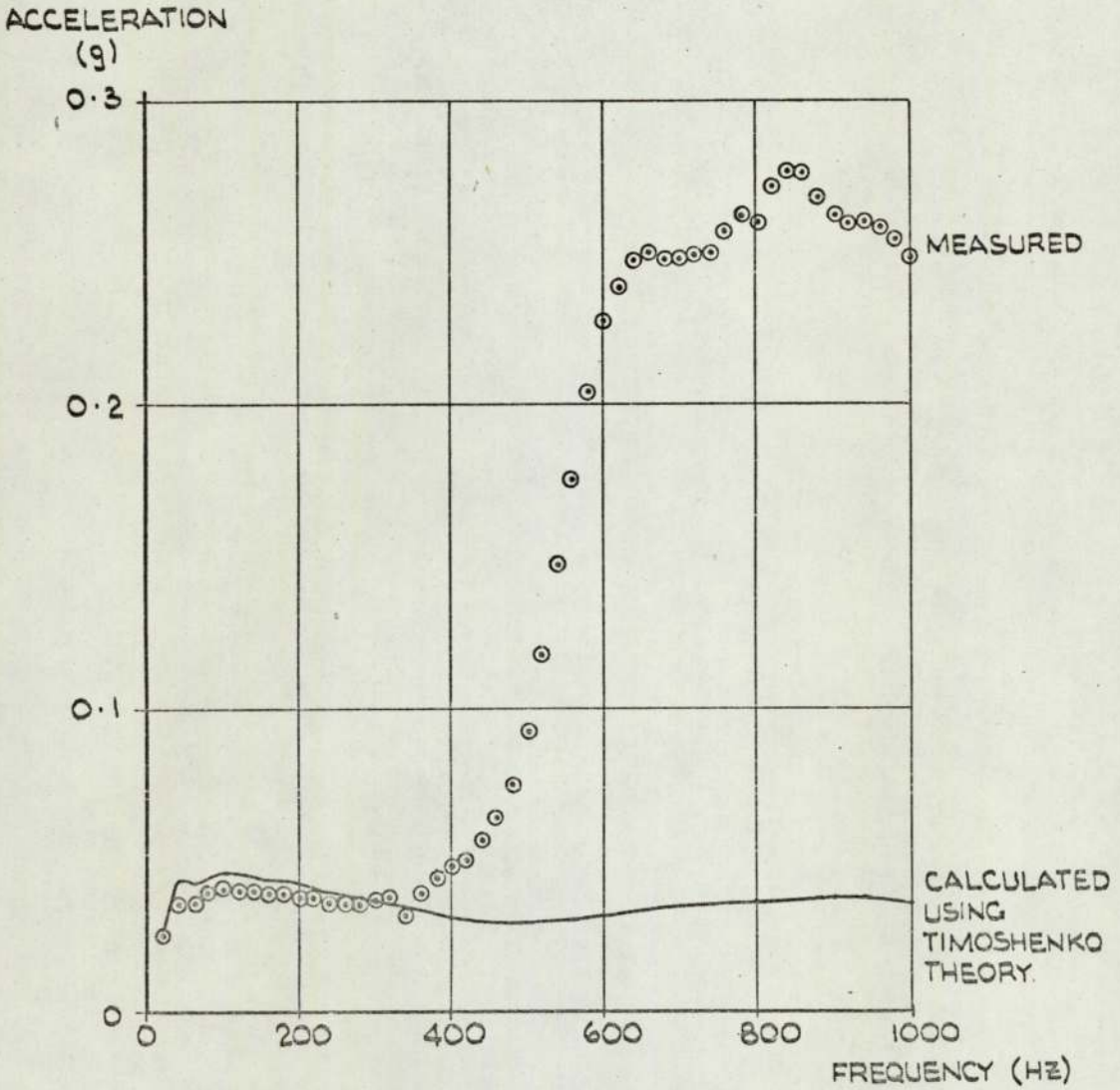

FIG. 3.26 RESONANCES FROM ARMENÀKAS (REFERENCE (60)) FROM 3 - DIMENSIONAL THEORY.

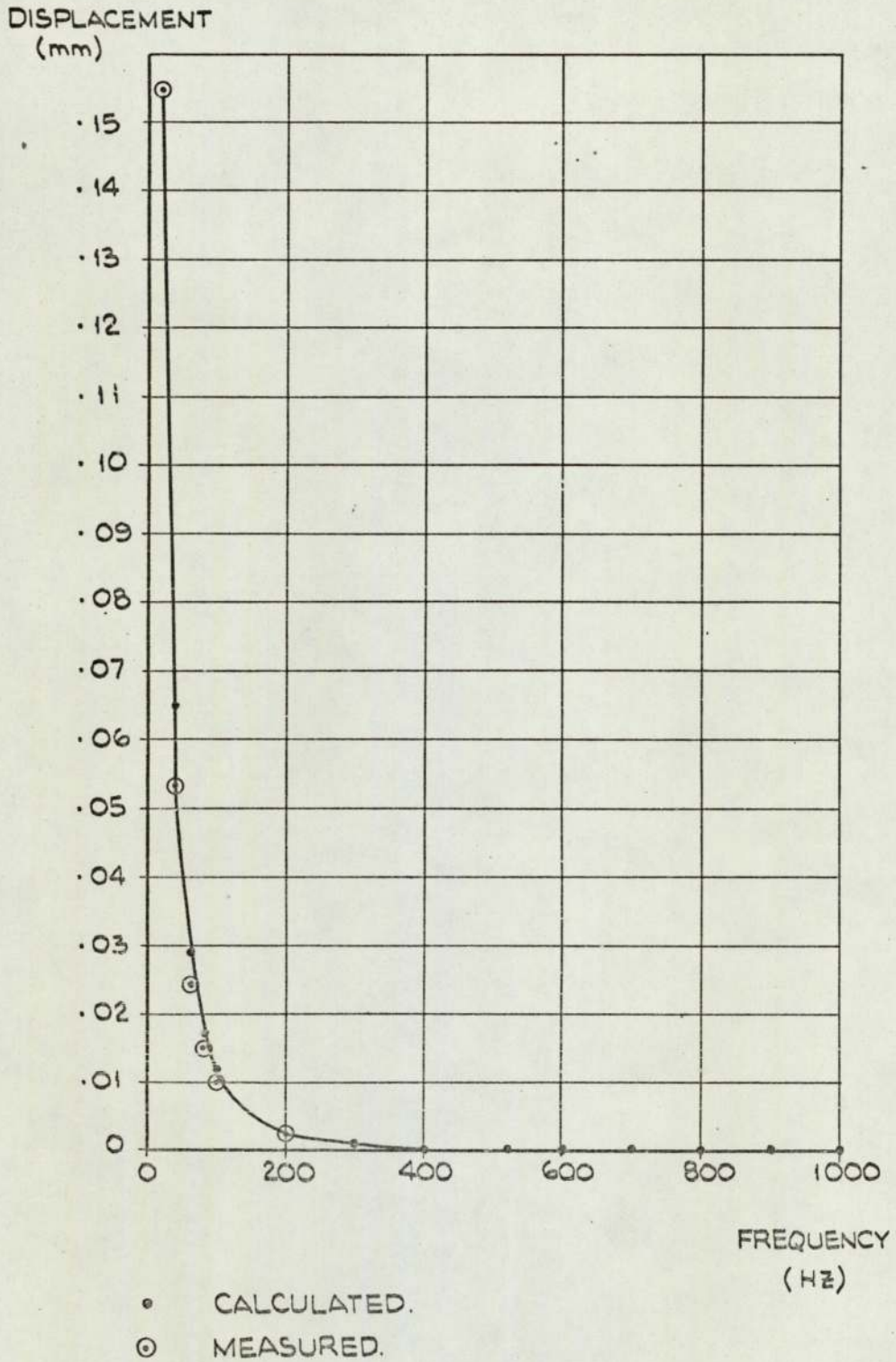

FIG. 3. 27 DISPLACEMENT VS. FREQUENCY FOR LARGE SCALE SAMPLE.

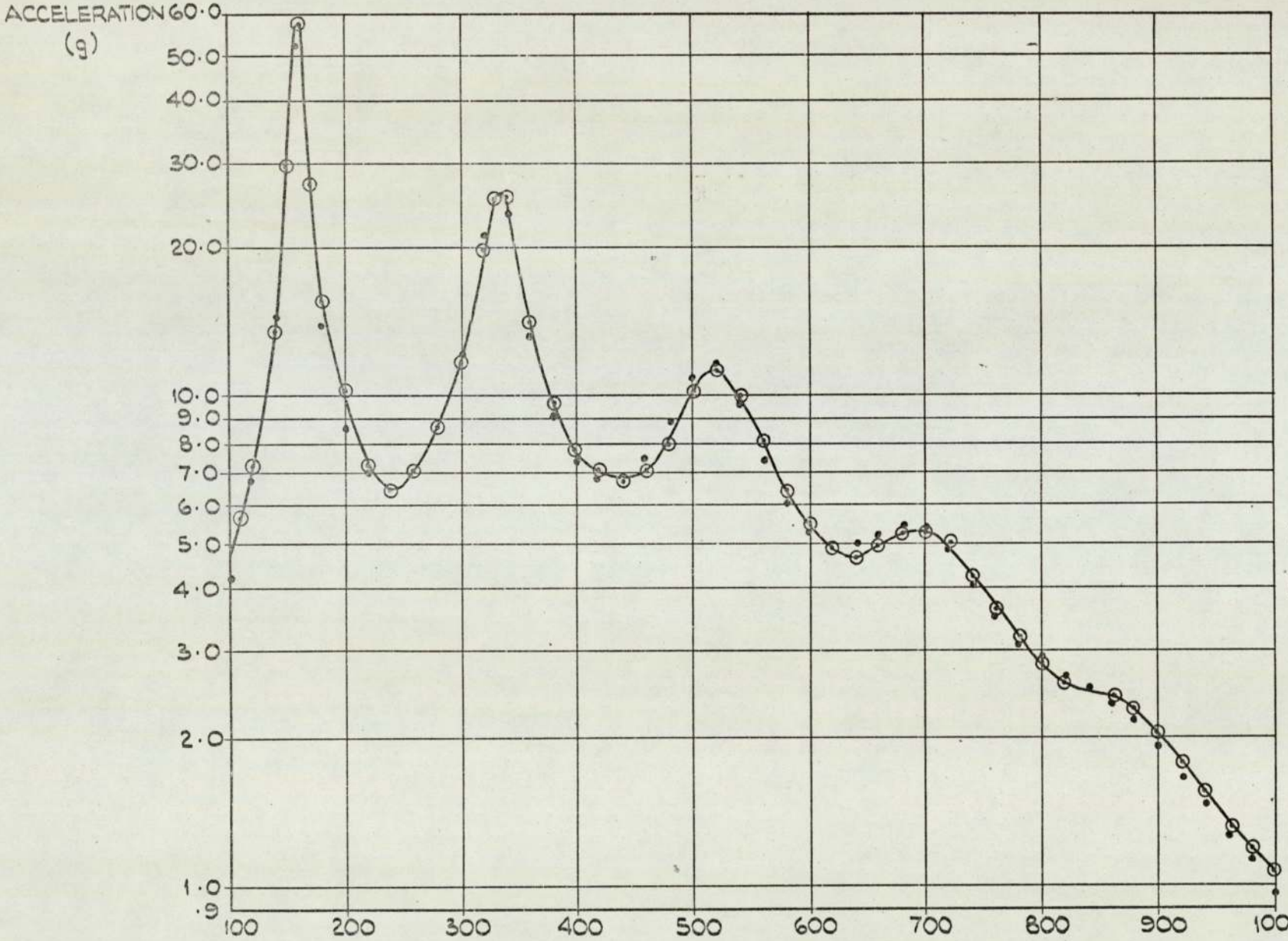

⊙ MEASURED

• CALCULATED FROM THE CURVE SHOWN IN FIGURE 3.29.

FIG. 3. 28(a)

ACCELERATION VS. FREQUENCY MEASUREMENTS FOR NATURAL RUBBER.

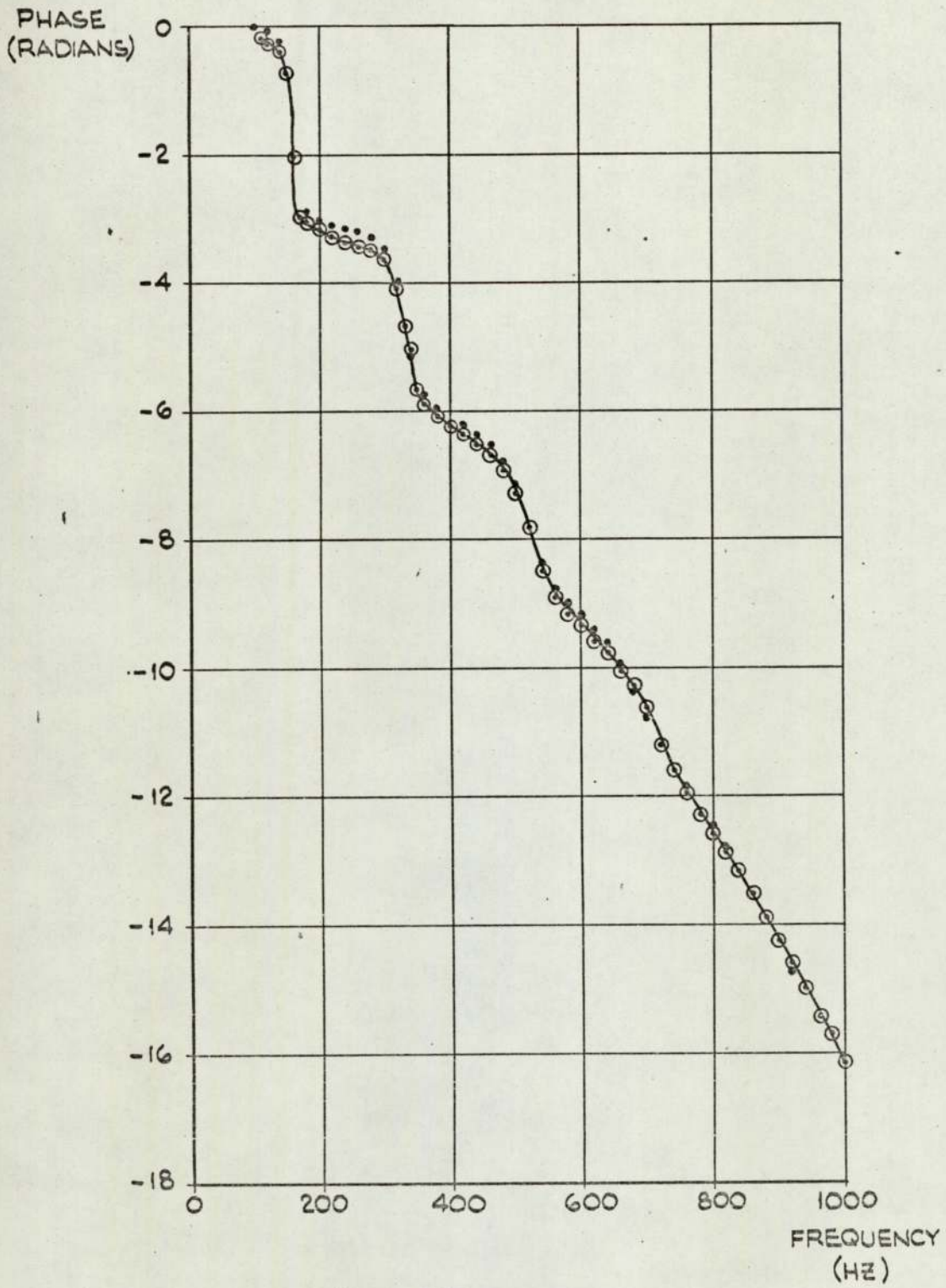

FIG. 3.28(b) PHASE VS. FREQUENCY MEASUREMENTS FOR NATURAL RUBBER.

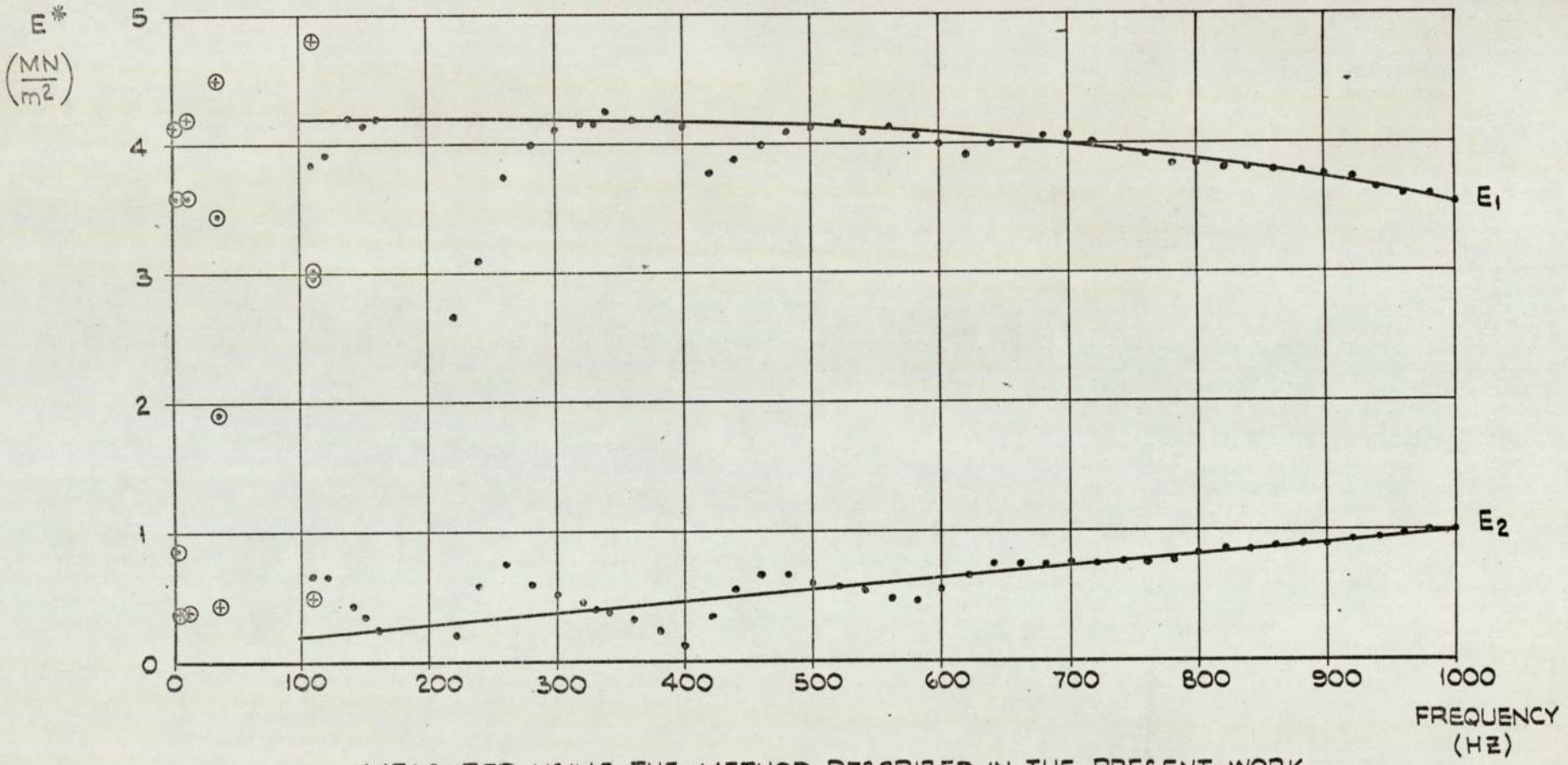

FIG. 3.29. DYNAMIC MODULUS OF NATURAL RUBBER.

Chapter 4

DYNAMIC RESPONSE OF SOLID FUEL ROCKET MOTORS

4.1 Introduction and literature survey

It was observed in section 1.1 that there were two types of solid fuel rocket motor design - case bonded and cartridge loaded. No literature pertaining to cartridge loaded motors has been found but analyses of case bonded motors have been reported. A long viscoelastic cylinder bonded to a thin elastic case was considered in references (12), (14), (15), (16), (18), (21), (35).

The analyses dealt with the cross sectional modes of vibration which are excited during firing. In the references given above it was assumed that the cylinder was long enough so that displacements along the length could be disregarded and only radial and tangential displacements within a cross section were considered.

These methods were not suitable for the present research since it is concerned with environmental vibrations when the motor must be considered as a beam vibrating in flexural and longitudinal modes.

Sowers (reference (29)) suggested a lumped parameter approach for the analysis of missile vibrations which was equally applicable to rocket motors. However, as noted in section 1.3, the difficulties were the representation of the material properties and the solution of the equations. (The equations with a general damping matrix were given in (29), but not solved).

The motors were therefore analysed in the present research as continuous structures. Since a method for measuring the complex modulus had been developed and as forced vibrations were under consideration, it was possible to analyse the assembly as an elastic material then apply the second form of the correspondence principle (see section 1.2.7) and replace E with E^* for the viscoelastic condition.

In the present work only flexural vibrations were considered but the approach for the analysis of longitudinal vibrations is suggested.

4.2 Case bonded motors

4.2.1 This analysis applies to all types of case bonded motor, irrespectiv of charge geometry. The slotted-radial charge design is typical and is exemplified in fig. (4.1), which shows the general arrangement of a case bonded motor. The mathematical model is given in fig. (4.2) i.e. two rigidly connected uniform beams - the main motor body and the blast tube or nozzle.

The motor is generally secured to the missile at two points; when the motor undergoes the environmental vibration trials it is attached to the vibrator at the same places. It was assumed that the motor was excited by two sinusoidally varying forces $F_1 e^{i\omega t}$ and $F_2 e^{i\omega t}$ at those two points.

Since the 'direct method' ** was used to find the response, the applied forces had to be at the end of a beam - hence the main motor body was subdivided at the forcing positions as shown in fig. (4.2).

** The 'direct method' applies in the case of sinusoidally varying applied forces. If the force is $F_o e^{i\omega t}$ then it is assumed that the displacement $u(x,t) = u_o(x)e^{i\omega t}$. The applied force is considered as an end condition - thus the need to subdivide the main motor body at the forcing positions. An alternative method which applies for all types of applied forces (step functions, moving loads, etc.) is 'modal analysis'. Here it is assumed that

$$u(x,t) = \sum_{n=1}^{\infty} X_n \phi_n$$

where $\{X_n\}$ are the normal modes of free vibration

and $\{\phi_n\}$ are the generalised coordinates (dependent on the applied force)

Appendix C shows that the two methods give the same solution when the applied force varies sinusoidally with time.

The 'direct method' has been used throughout, see sections 3.2 and 3.7 for the analysis of longitudinal and transverse vibrations resp. of beams; the boundary conditions were obtained by considering the equilibrium of the end masses, the applied force being one of the forces acting on one end mass. **

4.2.2 The solution when the applied forces F_1, F_2 are known

The Timoshenko equations were solved (see Appendix (B)) for each of the four beams shown in fig. (4.2).

The displacement of the neutral axis of beam i is given by

$$u_i(x,t)$$

and the slope of the neutral axis of beam i is given by

$$\psi_i(x,t)$$

Then for beam 1,

$$\left.\begin{aligned} u_1 &= (B_1\cosh \alpha_1 x + B_2\sinh \alpha_1 x + B_3\cosh \beta_1 x + B_4\sinh \beta_1 x)e^{i\omega t} \\ \psi_1 &= (R_1B_2\cosh \alpha_1 x + R_1B_1\sinh \alpha_1 x + S_1B_4\cosh \beta_1 x + S_1B_3\sinh \beta_1 x)e^{i\omega t} \end{aligned}\right\}$$

For beam 2,

$$\left.\begin{aligned} u_2 &= (B_5\cosh \alpha_2 x + B_6\sinh \alpha_2 x + B_7\cosh \beta_2 x + B_8\sinh \beta_2 x)e^{i\omega t} \\ \psi_2 &= (R_2B_6\cosh \alpha_2 x + R_2B_5\sinh \alpha_2 x + S_2B_8\cosh \beta_2 x + S_2B_7\sinh \beta_2 x)e^{i\omega t} \end{aligned}\right\} \quad 4.2.(1$$

Similarly for beam 3: u_3 and ψ_3 and for beam 4: u_4 and ψ_4

where B_j, $j = 1,16$ are the unknown coefficients and α, β, R and S are defined in Appendix (B), (Equations B(17) - B(20)).

Boundary conditions:

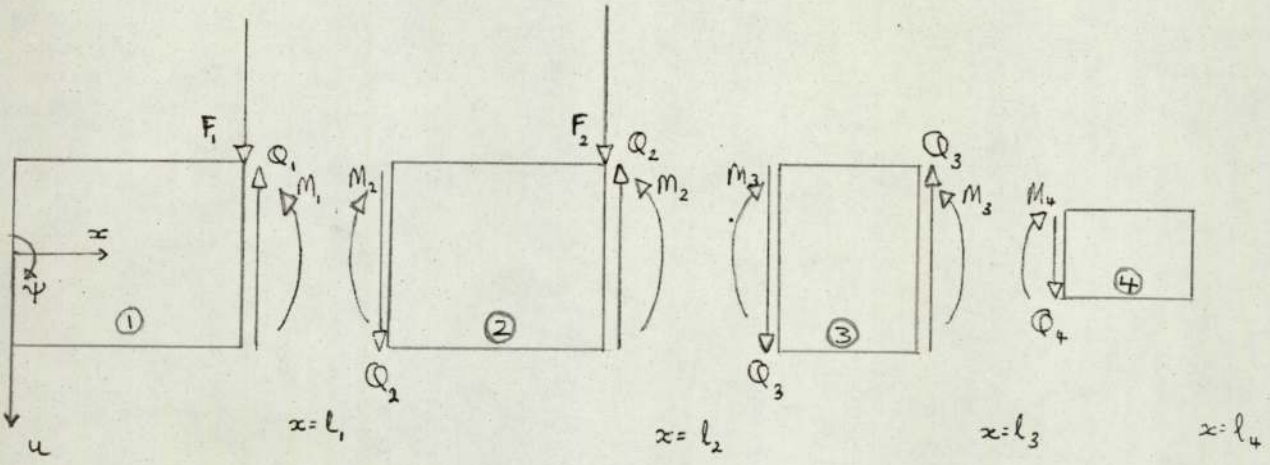

Figure (a)

Figure (a) shows the interactive forces and moments between the four beams, the beams were assumed to be continuous and rigidly connected therefore the following conditions must be satisfied:

at $x = 0$, $\quad M_1 = 0,\ Q_1 = 0.$

at $x = l_1$, $\quad u_1 = u_2,\ \psi_1 = \psi_2,\ M_1 = M_2,\ Q_1 + F_1 = Q_2.$

at $x = l_2$, $\quad u_2 = u_3,\ \psi_2 = \psi_3,\ M_2 = M_3,\ Q_2 + F_2 = Q_3.$

at $x = l_3$, $\quad u_3 = u_4,\ \psi_3 = \psi_4,\ M_3 = M_4,\ Q_3 = Q_4.$

at $x = l_4$, $\quad M_4 = 0,\ Q_4 = 0$

where $\quad M_i = -E_i I_i \left(\dfrac{\partial \psi_i}{\partial x} \right)$ is the bending moment of beam i

$$Q_i = -k'_i A_i G_i \left(\frac{\partial u_i}{\partial x} - \psi_i \right)$$ is the shear force of beam i.

Then there were 16 equations to solve for B_j, $j = 1, 16$.

Substituting for u_i, ψ_i $\quad i = 1,4$ (from equations 4.2.(1)) into equations 4.2.(2) gave a matrix equation $[A]\ \{B\} = \{C\}$ which was solved numerically using the Gauss elimination technique (see Appendix (D)) to give $\{B\}$. The matrix equation is as follows:

0	$\alpha_1 - R_1$	0	$\beta_1 - S_1$	0	0	0	0	0	0	0	0	0	0	0	0	B_2	0
$\cosh \alpha_1 l_1$	$\sinh \alpha_1 l_1$	$\cos \beta_1 l_1$	$\sinh \beta_1 l_1$	$-\cosh \alpha_2 l_1$	$-\sinh \alpha_2 l_1$	$-\cosh \beta_2 l_1$	$-\sinh \beta_2 l_1$	0	0	0	0	0	0	0	0	B_3	0
R_1 $\sinh \alpha_1 l_1$	R_1 $\cosh \alpha_1 l_1$	S_1 $\sinh \beta_1 l_1$	S_1 $\cosh \beta_1 l_1$	$-R_2$ $\sinh \alpha_2 l_1$	$-R_2$ $\cosh \alpha_2 l_1$	$-S_2$ $\sinh \beta_2 l_1$	$-S_2$ $\cosh \beta_2 l_1$	0	0	0	0	0	0	0	0	B_4	0
$\alpha_1 R_1 E_1 I_1$ $\cosh \alpha_1 l_1$	$\alpha_1 R_1 E_1 I_1$ $\sinh \alpha_1 l_1$	$\beta_1 S_1 E_1 I_1$ $\cosh \beta_1 l_1$	$\beta_1 S_1 E_1 I_1$ $\sinh \beta_1 l_1$	$-\alpha_2 R_2 E_2 I_2$ $\cosh \alpha_2 l_1$	$-\alpha_2 R_2 E_2 I_2$ $\sinh \alpha_2 l_1$	$-\beta_2 S_2 E_2 I_2$ $\cosh \beta_2 l_1$	$-\beta_2 S_2 E_2 I_2$ $\sinh \beta_2 l_1$	0	0	0	0	0	0	0	0	B_5	0
$k_1 A_1 G_1$ $(\alpha_1 - R_1)$ $\sinh \alpha_1 l_1$	$k_1 A_1 G_1$ $(\alpha_1 - R_1)$ $\cosh \alpha_1 l_1$	$k_1 A_1 G_1$ $(\beta_1 - S_1)$ $\sinh \beta_1 l_1$	$k_1 A_1 G_1$ $(\beta_1 - S_1)$ $\cosh \beta_1 l_1$	$-k_2 A_2 G_2$ $(\alpha_2 - R_2)$ $\sinh \alpha_2 l_1$	$-k_2 A_2 G_2$ $(\alpha_2 - R_2)$ $\cosh \alpha_2 l_1$	$-k_2 A_2 G_2$ $(\beta_2 - S_2)$ $\sinh \beta_2 l_1$	$-k_2 A_2 G_2$ $(\beta_2 - S_2)$ $\cosh \beta_2 l_1$	0	0	0	0	0	0	0	0	B_6	F_1
0	0	0	0	$\cosh \alpha_2 l_2$	$\sinh \alpha_2 l_2$	$\cosh \beta_2 l_2$	$\sinh \beta_2 l_2$	$-\cosh \alpha_3 l_2$	$-\sinh \alpha_3 l_2$	$-\cosh \beta_3 l_2$	$-\sinh \beta_3 l_2$	0	0	0	0	B_7	0
0	0	0	0	R_2 $\sinh \alpha_2 l_2$	R_2 $\cosh \alpha_2 l_2$	S_2 $\sinh \beta_2 l_2$	S_2 $\cosh \beta_2 l_2$	$-R_3$ $\sinh \alpha_3 l_2$	$-R_3$ $\cosh \alpha_3 l_2$	$-S_3$ $\sinh \beta_3 l_2$	$-S_3$ $\cosh \beta_3 l_2$	0	0	0	0	B_8	0
0	0	0	0	$E_2 I_2 \alpha_2 R_2$ $\cosh \alpha_2 l_2$	$E_2 I_2 \alpha_2 R_2$ $\sinh \alpha_2 l_2$	$E_2 I_2 \beta_2 S_2$ $\cosh \beta_2 l_2$	$E_2 I_2 \beta_2 S_2$ $\sinh \beta_2 l_2$	$-E_3 I_3 \alpha_3 R_3$ $\cosh \alpha_3 l_2$	$-E_3 I_3 \alpha_3 R_3$ $\sinh \alpha_3 l_2$	$-E_3 I_3 \beta_3 S_3$ $\cosh \beta_3 l_2$	$-E_3 I_3 \beta_3 S_3$ $\sinh \beta_3 l_2$	0	0	0	0	B_9	0
0	0	0	0	$k_2 A_2 G_2$ $(\alpha_2 - R_2)$ $\sinh \alpha_2 l_2$	$k_2 A_2 G_2$ $(\alpha_2 - R_2)$ $\cosh \alpha_2 l_2$	$k_2 A_2 G_2$ $(\beta_2 - S_2)$ $\sinh \beta_2 l_2$	$k_2 A_2 G_2$ $(\beta_2 - S_2)$ $\cosh \beta_2 l_2$	$-k_3 A_3 G_3$ $(\alpha_3 - R_3)$ $\sinh \alpha_3 l_2$	$-k_3 A_3 G_3$ $(\alpha_3 - R_3)$ $\cosh \alpha_3 l_2$	$-k_3 A_3 G_3$ $(\beta_3 - S_3)$ $\sinh \beta_3 l_2$	$-k_3 A_3 G_3$ $(\beta_3 - S_3)$ $\cosh \beta_3 l_2$	0	0	0	0	B_{10}	F_2
0	0	0	0	0	0	0	0	$\cosh \alpha_3 l_3$	$\sinh \alpha_3 l_3$	$\cosh \beta_3 l_3$	$\sinh \beta_3 l_3$	$-\cosh \alpha_4 l_3$	$-\sinh \alpha_4 l_3$	$-\cosh \beta_4 l_3$	$-\sinh \beta_4 l_3$	B_{11}	0
0	0	0	0	0	0	0	0	R_3 $\sinh \alpha_3 l_3$	R_3 $\cosh \alpha_3 l_3$	S_3 $\sinh \beta_3 l_3$	S_3 $\cosh \beta_3 l_3$	$-R_4$ $\sinh \alpha_4 l_3$	$-R_4$ $\cosh \alpha_4 l_3$	$-S_4$ $\sinh \beta_4 l_3$	$-S_4$ $\cosh \beta_4 l_3$	B_{12}	0
0	0	0	0	0	0	0	0	$-E_3 I_3 \alpha_3 R_3$ $\cosh \alpha_3 l_3$	$-E_3 I_3 \alpha_3 R_3$ $\sinh \alpha_3 l_3$	$-E_3 I_3 \beta_3 S_3$ $\cosh \beta_3 l_3$	$-E_3 I_3 \beta_3 S_3$ $\sinh \beta_3 l_3$	$E_4 I_4 \alpha_4 R_4$ $\cosh \alpha_4 l_3$	$E_4 I_4 \alpha_4 R_4$ $\sinh \alpha_4 l_3$	$E_4 I_4 \beta_4 S_4$ $\cosh \beta_4 l_3$	$E_4 I_4 \beta_4 S_4$ $\sinh \beta_4 l_3$	B_{13}	0
0	0	0	0	0	0	0	0	$-k_3 A_3 G_3$ $(\alpha_3 - R_3)$ $\sinh \alpha_3 l_3$	$-k_3 A_3 G_3$ $(\alpha_3 - R_3)$ $\cosh \alpha_3 l_3$	$-k_3 A_3 G_3$ $(\beta_3 - S_3)$ $\sinh \beta_3 l_3$	$-k_3 A_3 G_3$ $(\beta_3 - S_3)$ $\cosh \beta_3 l_3$	$k_4 A_4 G_4$ $(\alpha_4 - R_4)$ $\sinh \alpha_4 l_3$	$k_4 A_4 G_4$ $(\alpha_4 - R_4)$ $\cosh \alpha_4 l_3$	$k_4 A_4 G_4$ $(\beta_4 - S_4)$ $\sinh \beta_4 l_3$	$k_4 A_4 G_4$ $(\beta_4 - S_4)$ $\cosh \beta_4 l_3$	B_{14}	0
0	0	0	0	0	0	0	0	0	0	0	0	$\alpha_4 R_4$ $\cosh \alpha_4 l_4$	$\alpha_4 R_4$ $\sinh \alpha_4 l_4$	$\beta_4 S_4$ $\cosh \beta_4 l_4$	$\beta_4 S_4$ $\sinh \beta_4 l_4$	B_{15}	0
0	0	0	0	0	0	0	0	0	0	0	0	$(\alpha_4 - R_4)$ $\sinh \alpha_4 l_4$	$(\alpha_4 - R_4)$ $\cosh \alpha_4 l_4$	$(\beta_4 - S_4)$ $\sinh \beta_4 l_4$	$(\beta_4 - S_4)$ $\cosh \beta_4 l_4$	B_{16}	0

Then the displacement and slope of any position (X) on the motor could be evaluated by substitution of the appropriate B_j's into the appropriate equation of 4.2.(1):

For $0 \leq X \leq l_1$ $\quad u_1(X,t)$, $\psi_1(X,t)$ were evaluated

$l_1 \leq X \leq l_2$ $\quad u_2(X,t)$, $\psi_2(X,t)$ were evaluated

$l_2 \leq X \leq l_3$ $\quad u_3(X,t)$, $\psi_3(X,t)$ were evaluated

$l_3 \leq X \leq l_4$ $\quad u_4(X,t)$, $\psi_4(X,t)$ were evaluated

A computer program was written to evaluate the response of a case bonded motor.

The data required were:

F_1, F_2,

A_i, ρ_i, l_i, I_i, k'_i, ν_i, E^*_i for $i = 1,4$

Note: $A_1 = A_2 = A_3$, $\rho_1 = \rho_2 = \rho_3$, etc. since they all refer to the main motor body.

A_4, ρ_4, l_4 etc. refer to the blast tube or nozzle.

For values of k', see Cowper (22).

The main motor body was a composite elastic/viscoelastic beam and the parameters were evaluated as follows (where the subscript c refers to the case and p refers to the propellant):

$$A_i = A_c + A_p$$

$$\rho_i = (A_c\rho_c + A_p\rho_p \frac{l_p}{l_c}) / (A_c + A_p).$$

$$I_i = I_c + E_p / E_c I_p$$

(Since for the motors considered, $(EI)_c \simeq 250\ (EI)_p$ it was assumed that

the propellant did not add stiffness to the structure i.e. $I_i = I_c$)

$l_i = l_c$

k'_i was based on the shape of the propellant + case

$\nu_i = 0.5$

$E^*_i = E_c (1 + i \eta_p)$

where the dynamic modulus of the propellant $E^*_p = E_p(1 + i \eta_p)$

Note: since η_p varied with frequency, $E^*_1 (= E^*_2 = E^*_3)$ was input for the various frequencies required.

4.2.3 The solution when the accelerations at the forcing points are known

Let the acceleration at l_1 be a_1

and the acceleration at l_2 be a_2

The Timoshenko equations were solved for the four beams as before (equations 4.2.(1)).

The boundary conditions were given by:

$$\left.\begin{array}{llll} \text{at } x = 0, & M_1 = 0, \quad Q_1 = 0. & & \\ \text{at } x = l_1 & u_1 = -a_1/\omega^2, \; u_2 = -a_1/\omega^2, & \psi_1 = \psi_2, & M_1 = M_2. \\ \text{at } x = l_2 & u_2 = -a_2/\omega^2, \; u_3 = -a_2/\omega^2, & \psi_1 = \psi_2, & M_2 = M_3. \\ \text{at } x = l_3 & u_3 = u_4, \quad \psi_3 = \psi_4, & M_3 = M_4, & Q_3 = Q_4. \\ \text{at } x = l_4 & M_4 = 0, \quad Q_4 = 0 . & & \end{array}\right\} \qquad 4.2.(3)$$

where $$M_i = -E_i I_i \left(\frac{\partial \psi_i}{\partial x} \right)$$

and $$Q_i = -k'_i A_i G_i \left(\frac{\partial u_i}{\partial x} - \psi_i \right)$$

Then substituting 4.2.(1) into 4.2.(3) gave the following matrix equation which was solved as above with the Gauss elimination technique.

$\alpha_1 R_1$	0	$\beta_1 S_1$	0	0	0	0	0	0	0	0	0	0	0	0	0	B_1	$= 0$
0	$\alpha_1 - R_1$	0	$\beta_1 - S_1$	0	0	0	0	0	0	0	0	0	0	0	0	B_2	0
$\cosh \alpha_1 l_1$	$\sinh \alpha_1 l_1$	$\cosh \beta_1 l_1$	$\sinh \beta_1 l_1$	0	0	0	0	0	0	0	0	0	0	0	0	B_3	$-a_1/\omega^2$
0	0	0	0	$\cosh \alpha_2 l_1$	$\sinh \alpha_2 l_1$	$\cosh \beta_2 l_1$	$\sinh \beta_2 l_1$	0	0	0	0	0	0	0	0	B_4	$-a_1/\omega^2$
$R_1 \sinh \alpha_1 l_1$	$R_1 \cosh \alpha_1 l_1$	$S_1 \sinh \beta_1 l_1$	$S_1 \cosh \beta_1 l_1$	$-R_2 \sinh \alpha_2 l_1$	$-R_2 \cosh \alpha_2 l_1$	$-S_2 \sinh \beta_2 l_1$	$-S_2 \cosh \beta_2 l_1$	0	0	0	0	0	0	0	0	B_5	0
$\alpha_1 R_1 \cosh \alpha_1 l_1$	$\alpha_1 R_1 \sinh \alpha_1 l_1$	$\beta_1 S_1 \cosh \beta_1 l_1$	$\beta_1 S_1 \sinh \beta_1 l_1$	$-\alpha_2 R_2 \cosh \alpha_2 l_1$	$-\alpha_2 R_2 \sinh \alpha_2 l_1$	$-\beta_2 S_2 \cosh \beta_2 l_1$	$-\beta_2 S_2 \sinh \beta_2 l_1$	0	0	0	0	0	0	0	0	B_6	0
0	0	0	0	$\cosh \alpha_2 l_2$	$\sinh \alpha_2 l_2$	$\cosh \beta_2 l_2$	$\sinh \beta_2 l_2$	0	0	0	0	0	0	0	0	B_7	$-a_2/\omega^2$
0	0	0	0	0	0	0	0	$\cosh \alpha_3 l_2$	$\sinh \alpha_3 l_2$	$\cosh \beta_3 l_2$	$\sinh \beta_3 l_2$	0	0	0	0	B_8	$-a_2/\omega^2$
0	0	0	0	$R_2 \sinh \alpha_2 l_2$	$R_2 \cosh \alpha_2 l_2$	$S_2 \sinh \beta_2 l_2$	$S_2 \cosh \beta_2 l_2$	$R_3 \sinh \alpha_3 l_2$	$R_3 \cosh \alpha_3 l_2$	$S_3 \sinh \beta_3 l_2$	$S_3 \cosh \beta_3 l_2$	0	0	0	0	B_9	0
0	0	0	0	$\alpha_2 R_2 \cosh \alpha_2 l_2$	$\alpha_2 R_2 \sinh \alpha_2 l_2$	$\beta_2 S_2 \cosh \beta_2 l_2$	$\beta_2 S_2 \sinh \beta_2 l_2$	$-\alpha_3 R_3 \cosh \alpha_3 l_2$	$-\alpha_3 R_3 \sinh \alpha_3 l_2$	$-\beta_3 S_3 \cosh \beta_3 l_2$	$-\beta_3 S_3 \sinh \beta_3 l_2$	0	0	0	0	B_{10}	0
0	0	0	0	0	0	0	0	$\cosh \alpha_3 l_3$	$\sinh \alpha_3 l_3$	$\cosh \beta_3 l_3$	$\sinh \beta_3 l_3$	$-\cosh \alpha_4 l_3$	$-\sinh \alpha_4 l_3$	$-\cosh \beta_4 l_3$	$-\sinh \beta_4 l_3$	B_{11}	0
0	0	0	0	0	0	0	0	$R_3 \sinh \alpha_3 l_3$	$R_3 \cosh \alpha_3 l_3$	$S_3 \sinh \beta_3 l_3$	$S_3 \cosh \beta_3 l_3$	$-R_4 \sinh \alpha_4 l_3$	$-R_4 \cosh \alpha_4 l_3$	$-S_4 \sinh \beta_4 l_3$	$-S_4 \cosh \beta_4 l_3$	B_{12}	0
0	0	0	0	0	0	0	0	$-E_3 I_3 \alpha_3 R_3 \cosh \alpha_3 l_3$	$-E_3 I_3 \alpha_3 R_3 \sinh \alpha_3 l_3$	$-E_3 I_3 \beta_3 S_3 \cosh \beta_3 l_3$	$-E_3 I_3 \beta_3 S_3 \sinh \beta_3 l_3$	$E_4 I_4 \alpha_4 R_4 \cosh \alpha_4 l_3$	$E_4 I_4 \alpha_4 R_4 \sinh \alpha_4 l_3$	$E_4 I_4 \beta_4 S_4 \cosh \beta_4 l_3$	$E_4 I_4 \beta_4 S_4 \sinh \beta_4 l_3$	B_{13}	0
0	0	0	0	0	0	0	0	$-k_3 A_3 G_3 (\alpha_3 - R_3) \sinh \alpha_3 l_3$	$-k_3 A_3 G_3 (\alpha_3 - R_3) \cosh \alpha_3 l_3$	$-k_3 A_3 G_3 (\beta_3 - S_3) \sinh \beta_3 l_3$	$-k_3 A_3 G_3 (\beta_3 - S_3) \cosh \beta_3 l_3$	$k_4 A_4 G_4 (\alpha_4 - R_4) \sinh \alpha_4 l_3$	$k_4 A_4 G_4 (\alpha_4 - R_4) \cosh \alpha_4 l_3$	$k_4 A_4 G_4 (\beta_4 - S_4) \sinh \beta_4 l_3$	$k_4 A_4 G_4 (\beta_4 - S_4) \cosh \beta_4 l_3$	B_{14}	0
0	0	0	0	0	0	0	0	0	0	0	0	$\alpha_4 R_4 \cosh \alpha_4 l_4$	$\alpha_4 R_4 \sinh \alpha_4 l_4$	$\beta_4 S_4 \cosh \beta_4 l_4$	$\beta_4 S_4 \sinh \beta_4 l_4$	B_{15}	0
0	0	0	0	0	0	0	0	0	0	0	0	$(\alpha_4 - R_4) \sinh \alpha_4 l_4$	$(\alpha_4 - R_4) \cosh \alpha_4 l_4$	$(\beta_4 - S_4) \sinh \beta_4 l_4$	$(\beta_4 - S_4) \cosh \beta_4 l_4$	B_{16}	0

Note: The Gauss elimination is only applicable if there is a non-zero element at every position along the leading diagonal i.e. $A_{jj} \neq 0$ for $j = 1,16$; for that reason rows 4 and 5 were interchanged and rows 8 and 9 were interchanged.

4.2.4 Longitudinal vibrations of a case bonded motor

The mathematical model is given by:

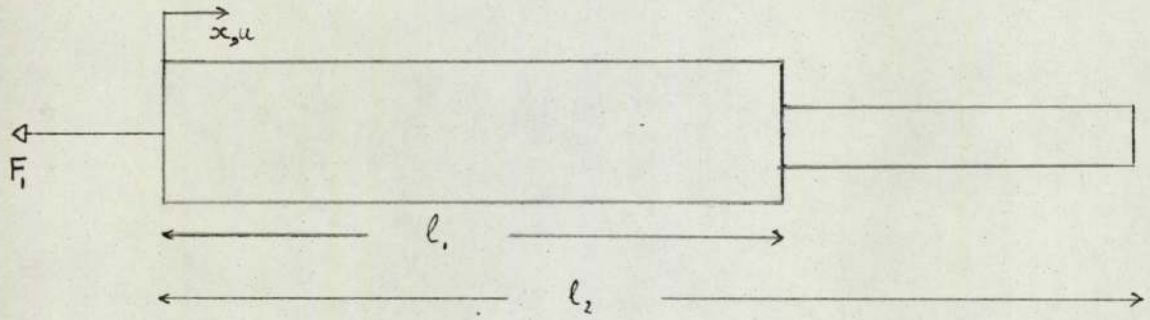

The solution of the equation for longitudinal vibrations of a long thin beam is given by (see reference (59)):

$$u = (B \cos \alpha x + C \sin \alpha x)e^{i\omega t}$$

where $$\alpha^2 = \frac{\omega^2 \rho}{E}$$

Hence the response of beam i is given by:

$$u_i = (B_i \cos \alpha_i x + C_i \sin \alpha_1 x)\, e^{i\omega t}$$

where $$\alpha_i^2 = \frac{\omega^2 \rho_i}{E_i}$$

The end conditions are:

$$\text{at } x = 0, \quad \sigma_1 A_1 = -F_1 \ .$$

$$\text{at } x = l_1, \quad \sigma_1 A_1 = \sigma_2 A_2 , \quad u_1 = u_2 \ .$$

$$\text{at } x = l_2, \quad \sigma_2 = 0 \ .$$

where $$\sigma_i = E_i \frac{\partial u_i}{\partial x}$$

Thus four equations to solve for the four unknown coefficients B_1, B_2, C_1, C_2.

Since a sinusoidal applied force is considered then the correspondence principle may be applied. Beam 1 is a viscoelastic/elastic composite, therefore E_1 is replaced by E^*_1

and $$\alpha_1 = \omega \sqrt{\frac{\rho}{E^*_1}}$$

and $$\sigma_1 = E^*_1 \frac{\partial u_1}{\partial x}$$

Note: $$E^*_1 = E_c (1 + i \eta_p)$$

where E_c is the modulus of the case

and $E_p (1 + i\eta_p)$ is the modulus of the propellant.

If the acceleration at the forcing point is known, let it be a_1 then the boundary condition at $x = 0$ is given by:

$$u_1 = -a_1 / \omega^2$$

the other boundary conditions remain the same.

4.2.5 Results of computer analysis and comparison with measurement

Motor A

The general arrangement of motor A is shown in fig. (4.1). Figure (4.5) gives the mounting position during the transverse vibration trials. The motor was clamped to the vibrator at each end of the main motor body. A control accelerometer was connected to each clamp and a reference accelerometer was positioned at the centre of gravity of the motor.

The specification stated that the motor must be subjected to a constant amplitude vibration of 1.2 mm (peak-to-peak) from 5 Hz to 35 Hz and to a constant acceleration of 4 g from 35 Hz to 200 Hz.

The program used was the one which calculates the response when the accelerations at the control points are known (described in section 4.2.3). Acceleration levels of 4 g were specified at the forcing points, the response of the centre of gravity was computed and is plotted against frequency in fig. (4.6). The maximum value is 45 g which occurs at 124 Hz.

The program which calculates the response when the applied forces are given (section 4.2.2) was also used with these data. The forces were adjusted to give responses of 4 g at the control points; this program predicted the maximum response as 17.4 g at 117 Hz.

The programs gave differing results because the phase relations between the forces and accelerations were dissimilar:

In the first case the control accelerations were specified as 4 g and thus were exactly in phase.

In the second case the applied forces were specified as 1 000 N and 1 050 N, hence they were exactly in phase, the control accelerations were both 4 g but with a phase difference of about 30°.

As the phase lag between the control acceleration signals was not measured it was not possible to calculate the response any more accurately.

Thirty-five sets of measurements were made on motors of design A, the maximum response and the associated frequency for each is given in Table 4.1. It may be seen that there are considerable variations within the data, the averages are shown in the last line of the table 24.6 g and 117 Hz. The root mean square scatter of the maximum response is 7.5 g and of the frequency is 11.3 Hz. It is thought that the variations were due to the clamping arrangement. If the clamps were loose then the motor would behave as a free-free beam; if the clamps held the motor so that no vertical movement was possible but allowed twisting then it would act as a simply supported beam.

Thus the computer analysis was in good agreement with measurements within the bounds caused by uncertainties regarding phase differences and clamping arrangements.

Motor B

The specification states that the motor must be subjected to a constant acceleration of 0.5 g (the average of the signals from the two control points) for frequencies between 20 and 500 Hz. The response of the centre of gravity was also to be measured. The trials were to be carried out at +20°C and -10°C.

The program was run with the motor B data prior to the vibration trials, the predicted and measured responses of the centre of gravity are shown in fig. (4.7). It may be seen that the agreement is very good.

Note: The complex moduli used in these analyses were those obtained from the relaxation modulus and then modified by a 'correction factor' q_T found empirically for propellant No. 1 at various temperatures.

$$q_T = \left(\frac{E_{1m}}{E_{1R}} + i \frac{E_{2m}}{E_{2R}} \right)_T$$

where suffix m indicates a measured value

and suffix R indicates a value obtained from the relaxation modulus

and T indicates a particular temperature

4.3 Cartridge loaded motors

4.3.1 This analysis applies to cartridge loaded motors where the propellant is rigidly connected to the case at the forward end. The motors where the propellant is located on spigots or just loosely inserted have not been studied.

The general arrangement of a cartridge loaded motor is shown in fig. (4.3), the mathematical model is given in fig. (4.4) i.e. three rigidly connected uniform beams - the motor case, the blast tube and the propellant.

The motor is generally attached to the vibrator at two points; it was assumed that the motor was excited by two sinusoidally varying forces at those positions. For the reasons discussed in section 4.2.1 (note**), the case is subdivided at the forcing points to give a total of five beams; where 1,2,3 were the case, 4 was the blast tube, and 5 was the propellant.

4.3.2 The solution when the applied forces F_1, F_2 are known

The Timoshenko equations were solved (see Appendix (B)) for each of the five beams.

The displacement of the neutral axis of beam i is given by

$$u_i(x,t)$$

The slope of the neutral axis of beam i is given by

$$\psi_i(x,t)$$

Then for beam 1:

$$\left.\begin{aligned} u_1 &= (B_1\cosh \alpha_1 x + B_2\sinh \alpha_1 x + B_3\cosh \beta_1 x + B_4\sinh \beta_1 x)e^{i\omega t} \\ \psi_1 &= (R_1B_2\cosh \alpha_1 x + R_1B_1\sinh \alpha_1 x + S_1B_4\cosh \beta_1 x + S_1B_3\sinh \beta_1 x)e^{i\omega t} \end{aligned}\right\} \quad 4.3.(1)$$

For beam 2:

$$u_2 = (B_5 \cosh \alpha_2 x + B_6 \sinh \alpha_2 x + B_7 \cosh \beta_2 x + B_8 \sinh \beta_2 x) e^{i\omega t}$$

$$\psi_2 = (R_2 B_6 \cosh \alpha_2 x + R_2 B_5 \sinh \alpha_2 x + S_2 B_8 \cosh \beta_2 x + S_2 B_7 \sinh \beta_2 x) e^{i\omega t}$$

and similarly for beams 3, 4 and 5.

B_j, $j = 1,20$ are the unknown coefficients,

α, β, R and S are defined in Appendix (B), (Equations B(17) - B(20)).

Boundary conditions:

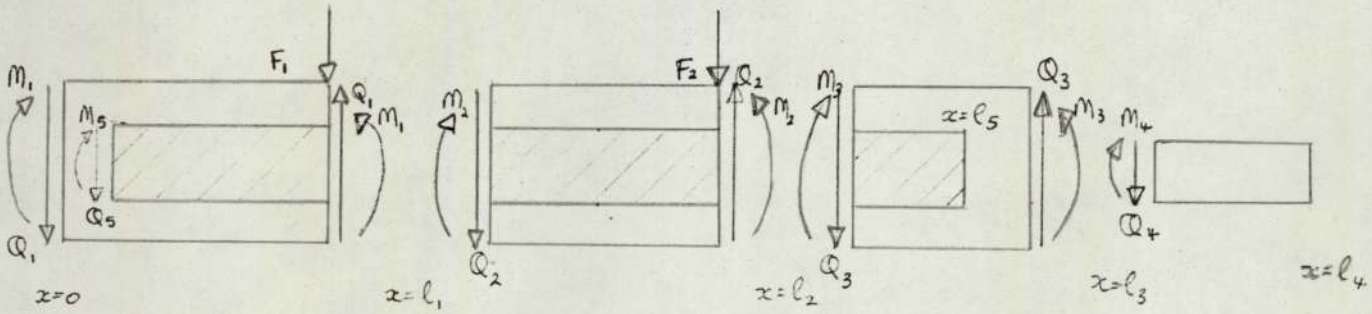

$$\begin{aligned}
&\text{at } x = 0, \quad u_1 = u_5, \quad \psi_1 = \psi_5, \quad M_1 + M_5 = 0, \quad Q_1 + Q_5 = 0 . \\
&\text{at } x = l_1, \quad u_1 = u_2, \quad \psi_1 = \psi_2, \quad M_1 = M_2, \quad Q_1 + F_1 = Q_2 . \\
&\text{at } x = l_2, \quad u_2 = u_3, \quad \psi_2 = \psi_3, \quad M_2 = M_3, \quad Q_2 + F_2 = Q_3 , \\
&\text{at } x = l_3, \quad u_3 = u_4, \quad \psi_3 = \psi_4, \quad M_3 = M_4, \quad Q_3 = Q_4 . \\
&\text{at } x = l_4, \quad M_4 = 0, \quad Q_4 = 0 . \\
&\text{at } x = l_5, \quad M_5 = 0, \quad Q_5 = 0 .
\end{aligned} \qquad 4.3.(2)$$

where

$$M_i = -E_i I_i \left(\frac{\partial \psi_i}{\partial x} \right) \text{ is the bending moment of beam i,}$$

$$Q_i = -k'_i A_i G_i \left(\frac{\partial u_i}{\partial x} - \psi_i \right) \text{ is the shear force of beam i.}$$

Substituting for u_i and ψ_i for $i = 1,5$ from equations 4.3.(1) into equations 4.3.(2) gave 20 equations which were solved numerically to give B_j, $j = 1,20$, using the Gauss elimination technique. (see Appendix (D)). The matrix equation is as follows:

0	R_1	0	S_1	0	0	0	0	0	0	0	0	0	0	0	0	$-R_5$	0	$-S_5$	B_2
$-E_1I_1$ $R_1\alpha_1$	0	$-E_1I_1$ $S_1\beta_1$	0	0	0	0	0	0	0	0	0	0	0	0	$-E_5I_5$ $R_5\alpha_5$	0	$-E_5I_5$ $S_5\beta_5$	0	B_3
0	$-k_1'A_1G_1$ $(\alpha_1 - R_1)$	0	$-k_1'A_1G_1$ $(\beta_1 - S_1)$	0	0	0	0	0	0	0	0	0	0	0	0	$-k_5'A_5G_5$ $(\alpha_5 - R_5)$	0	$-k_5'A_5G_5$ $(\beta_5 - S_5)$	B_4
$\cosh\alpha_1 l_1$	$\sinh\alpha_1 l_1$	$\cosh\beta_1 l_1$	$\sinh\beta_1 l_1$	$-\cosh\alpha_2 l_1$	$-\sinh\alpha_2 l_1$	$-\cosh\beta_2 l_1$	$-\sinh\beta_2 l_1$	0	0	0	0	0	0	0	0	0	0	0	B_5
R_1 $\sinh\alpha_1 l_1$	R_1 $\cosh\alpha_1 l_1$	S_1 $\sinh\beta_1 l_1$	S_1 $\cosh\beta_1 l_1$	$-R_2$ $\sinh\alpha_2 l_1$	$-R_2$ $\cosh\alpha_2 l_1$	$-S_2$ $\sinh\beta_2 l_1$	$-S_2$ $\cosh\beta_2 l_1$	0	0	0	0	0	0	0	0	0	0	0	B_6
$E_1I_1\alpha_1R_1$ $\cosh\alpha_1 l_1$	$E_1I_1\alpha_1R_1$ $\sinh\alpha_1 l_1$	$E_1I_1\beta_1S_1$ $\cosh\beta_1 l_1$	$E_1I_1\beta_1S_1$ $\sinh\beta_1 l_1$	$-E_2I_2\alpha_2R_2$ $\cosh\alpha_2 l_1$	$-E_2I_2\alpha_2R_2$ $\sinh\alpha_2 l_1$	$-E_2I_2\beta_2S_2$ $\cosh\beta_2 l_1$	$-E_2I_2\beta_2S_2$ $\sinh\beta_2 l_1$	0	0	0	0	0	0	0	0	0	0	0	B_7
$k_1'A_1G_1$ $(\alpha_1 - R_1)$ $\sinh\alpha_1 l_1$	$k_1'A_1G_1$ $(\alpha_1 - R_1)$ $\cosh\alpha_1 l_1$	$k_1'A_1G_1$ $(\beta_1 - S_1)$ $\sinh\beta_1 l_1$	$k_1'A_1G_1$ $(\beta_1 - S_1)$ $\cosh\beta_1 l_1$	$-k_2'A_2G_2$ $(\alpha_2 - R_2)$ $\sinh\alpha_2 l_1$	$-k_2'A_2G_2$ $(\alpha_2 - R_2)$ $\cosh\alpha_2 l_1$	$-k_2'A_2G_2$ $(\beta_2 - S_2)$ $\sinh\beta_2 l_1$	$-k_2'A_2G_2$ $(\beta_2 - S_2)$ $\cosh\beta_2 l_1$	0	0	0	0	0	0	0	0	0	0	0	B_8 F_1
0	0	0	0	$\cosh\alpha_2 l_2$	$\sinh\alpha_2 l_2$	$\cosh\beta_2 l_2$	$\sinh\beta_2 l_2$	$-\cosh\alpha_3 l_2$	$-\sinh\alpha_3 l_2$	$-\cosh\beta_3 l_2$	$-\sinh\beta_3 l_2$	0	0	0	0	0	0	0	B_9
0	0	0	0	R_2 $\sinh\alpha_2 l_2$	R_2 $\cosh\alpha_2 l_2$	S_2 $\sinh\beta_2 l_2$	S_2 $\cosh\beta_2 l_2$	$-R_3$ $\sinh\alpha_3 l_2$	$-R_3$ $\cosh\alpha_3 l_2$	$-S_3$ $\sinh\beta_3 l_2$	$-S_3$ $\cosh\beta_3 l_2$	0	0	0	0	0	0	0	B_{10}
0	0	0	0	$E_2I_2\alpha_2R_2$ $\cosh\alpha_2 l_2$	$E_2I_2\alpha_2R_2$ $\sinh\alpha_2 l_2$	$E_2I_2\beta_2S_2$ $\cosh\beta_2 l_2$	$E_2I_2\beta_2S_2$ $\sinh\beta_2 l_2$	$-E_3I_3\alpha_3R_3$ $\cosh\alpha_3 l_2$	$-E_3I_3\alpha_3R_3$ $\sinh\alpha_3 l_2$	$-E_3I_3\beta_3S_3$ $\cosh\beta_3 l_2$	$-E_3I_3\beta_3S_3$ $\sinh\beta_3 l_2$	0	0	0	0	0	0	0	B_{11}
0	0	0	0	$k_2'A_2G_2$ $(\alpha_2 - R_2)$ $\sinh\alpha_2 l_2$	$k_2'A_2G_2$ $(\alpha_2 - R_2)$ $\cosh\alpha_2 l_2$	$k_2'A_2G_2$ $(\beta_2 - S_2)$ $\sinh\beta_2 l_2$	$k_2'A_2G_2$ $(\beta_2 - S_2)$ $\cosh\beta_2 l_2$	$-k_3'A_3G_3$ $(\alpha_3 - R_3)$ $\sinh\alpha_3 l_2$	$-k_3'A_3G_3$ $(\alpha_3 - R_3)$ $\cosh\alpha_3 l_2$	$-k_3'A_3G_3$ $(\beta_3 - S_3)$ $\sinh\beta_3 l_2$	$-k_3'A_3G_3$ $(\beta_3 - S_3)$ $\cosh\beta_3 l_2$	0	0	0	0	0	0	0	B_{12} F_2
0	0	0	0	0	0	0	0	$\cosh\alpha_3 l_3$	$\sinh\alpha_3 l_3$	$\cosh\beta_3 l_3$	$\sinh\beta_3 l_3$	$-\cosh\alpha_4 l_3$	$-\sinh\alpha_4 l_3$	$-\cosh\beta_4 l_3$	$-\sinh\beta_4 l_3$	0	0	0	B_{13}
0	0	0	0	0	0	0	0	R_3 $\sinh\alpha_3 l_3$	R_3 $\cosh\alpha_3 l_3$	S_3 $\sinh\beta_3 l_3$	S_3 $\cosh\beta_3 l_3$	$-R_4$ $\sinh\alpha_4 l_3$	$-R_4$ $\cosh\alpha_4 l_3$	$-S_4$ $\sinh\beta_4 l_3$	$-S_4$ $\cosh\beta_4 l_3$	0	0	0	B_{14}
0	0	0	0	0	0	0	0	$-E_3I_3\alpha_3R_3$ $\cosh\alpha_3 l_3$	$-E_3I_3\alpha_3R_3$ $\sinh\alpha_3 l_3$	$-E_3I_3\beta_3S_3$ $\cosh\beta_3 l_3$	$-E_3I_3\beta_3S_3$ $\sinh\beta_3 l_3$	$E_4I_4\alpha_4R_4$ $\cosh\alpha_4 l_3$	$E_4I_4\alpha_4R_4$ $\sinh\alpha_4 l_3$	$E_4I_4\beta_4S_4$ $\cosh\beta_4 l_3$	$E_4I_4\beta_4S_4$ $\sinh\beta_4 l_3$	0	0	0	B_{15}
0	0	0	0	0	0	0	0	$-k_3'A_3G_3$ $(\alpha_3 - R_3)$ $\sinh\alpha_3 l_3$	$-k_3'A_3G_3$ $(\alpha_3 - R_3)$ $\cosh\alpha_3 l_3$	$-k_3'A_3G_3$ $(\beta_3 - S_3)$ $\sinh\beta_3 l_3$	$-k_3'A_3G_3$ $(\beta_3 - S_3)$ $\cosh\beta_3 l_3$	$k_4'A_4G_4$ $(\alpha_4 - R_4)$ $\sinh\alpha_4 l_3$	$k_4'A_4G_4$ $(\alpha_4 - R_4)$ $\cosh\alpha_4 l_3$	$k_4'A_4G_4$ $(\beta_4 - S_4)$ $\sinh\beta_4 l_3$	$k_4'A_4G_4$ $(\beta_4 - S_4)$ $\cosh\beta_4 l_3$	0	0	0	B_{16}
0	0	0	0	0	0	0	0	0	0	0	0	α_4R_4 $\cosh\alpha_4 l_4$	α_4R_4 $\sinh\alpha_4 l_4$	β_4S_4 $\cosh\beta_4 l_4$	β_4S_4 $\sinh\beta_4 l_4$	0	0	0	B_{17}
0	0	0	0	0	0	0	0	0	0	0	0	$(\alpha_4 - R_4)$ $\sinh\alpha_4 l_4$	$(\alpha_4 - R_4)$ $\cosh\alpha_4 l_4$	$(\beta_4 - S_4)$ $\sinh\beta_4 l_4$	$(\beta_4 - S_4)$ $\cosh\beta_4 l_4$	0	0	0	B_{18}
0	0	0	0	0	0	0	0	0	0	0	0	0	0	0	0	α_5R_5 $\cosh\alpha_5 l_5$	α_5R_5 $\sinh\alpha_5 l_5$	β_5S_5 $\cosh\beta_5 l_5$	β_5S_5 $\sinh\beta_5 l_5$	B_{19}
0	0	0	0	0	0	0	0	0	0	0	0	0	0	0	0	$(\alpha_5 - R_5)$ $\sinh\alpha_5 l_5$	$(\alpha_5 - R_5)$ $\cosh\alpha_5 l_5$	$(\beta_5 - S_5)$ $\sinh\beta_5 l_5$	$(\beta_5 - S_5)$ $\cosh\beta_5 l_5$	B_{20}

Note: Rows 2 and 17 were interchanged and rows 3 and 18 were interchanged for the reason given in the note of section 4.2.3.

Then the response of any point (X) of the motor could be found by computing the appropriate u_i, ψ_i :

Motor case:

$0 \leq X \leq l_1$ $\quad u_1(X,t)$, $\psi_1(X,t)$ were evaluated

$l_1 \leq X \leq l_2$ $\quad u_2(X,t)$, $\psi_2(X,t)$ were evaluated

$l_2 \leq X \leq l_3$ $\quad u_3(X,t)$, $\psi_3(X,t)$ were evaluated

Blast tube:

$l_3 \leq X \leq l_4$ $\quad u_4(X,t)$, $\psi_4(X,t)$ were evaluated

Propellant:

$0 \leq X \leq l_5$ $\quad u_5(X,t)$, $\psi_5(X,t)$ were evaluated

A programme was written to calculate the response of cartridge loaded motors using this analysis, the data required were:

F_1, F_2 ,

A_i, ρ_i, l_i, I_i, k'_i, ν_i, E^*_i for $i = 1,5$

Note: $A_1 = A_2 = A_3$, $\rho_1 = \rho_2 = \rho_3$, etc.

since they all refer to the motor case.

A_4, ρ_4, l_4 etc. refer to the blast tube

A_5, ρ_5, l_5 etc. refer to the propellant

E_i for $i = 1,4$ was real since the motor case and blast tube were elastic. E^*_5 was the complex modulus of the propellant; since it varied with frequency it was input for the necessary frequencies.

4.3.3 The solution when the accelerations at the forcing points are known

An analysis similar to that given in section 4.2.3 can be performed. The boundary conditions at $x = l_1$ and $x = l_2$ will be as given in equation 4.2.(3) otherwise the end conditions will be as given in equation 4.3.(2).

4.3.4 Longitudinal vibrations of a cartridge loaded motor

The mathematical model is given by:

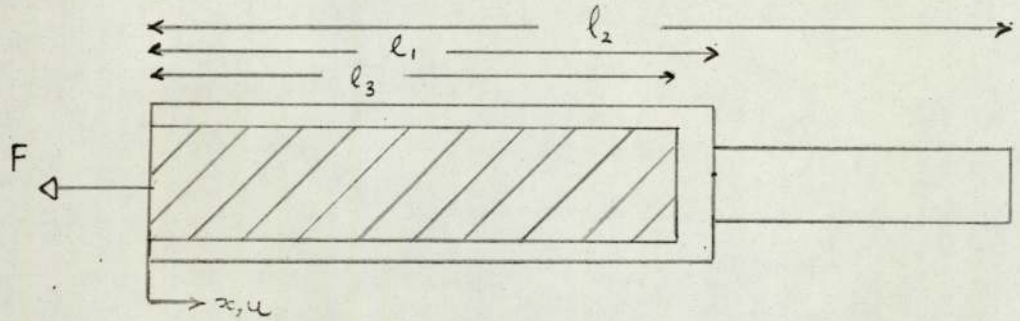

The displacement of beam i is given by (see reference (59)):

$$u_i = (B_i \cos \alpha_i x + C_i \sin \alpha_i x) e^{i\omega t}$$

where $$\alpha_i^2 = \omega^2 \sqrt{\frac{\rho_i}{E_i}}$$

The boundary conditions are:

at $x = 0$ $\quad \sigma_1 A_1 + \sigma_3 A_3 = -F, \quad u_1 = u_3$.

at $x = l_1$ $\quad \sigma_1 A_1 = \sigma_2 A_2, \quad u_1 = u_2$.

at $x = l_2$ $\quad \sigma_2 = 0$.

at $x = l_3$ $\quad \sigma_3 = 0$.

where $$\sigma_i = E_i \frac{\partial u_i}{\partial x}$$

i.e. six equations to solve for the unknown coefficients

$$B_1, B_2, B_3, C_1, C_2, C_3$$

Since the applied force varies sinusoidally with time then E_3 is replaced with E^*_3 since the propellant is viscoelastic.

then $$\alpha_3 = \omega \sqrt{\frac{\rho_3}{E^*_3}}$$

and $$\sigma_3 = E^*_3 \frac{\partial u_3}{\partial x}$$

If the acceleration at the forcing point is known (a_1) then the end conditions at x = 0 are given by:

$$u_1 = -a_1/\omega^2$$

$$u_3 = -a_1/\omega^2$$

4.3.5 Results of computer analyses and comparisons with measurements

Motor C

This was the design of motor which was damaged during the vibration trials in 1970 (see section 1.1.7). The general arrangement is shown in fig. (4.3) and the motors were mounted for the transverse vibrations as shown in fig. (4.8). Tests were performed at +40°C and -20°C. The vibration specification stated that the motor must be subjected to a sinusoidal vibration test consisting of a double sweep between 20 Hz and 500 Hz with the level of vibration (the average of the responses measured at the two clamping points) less than or equal to 1.5 g.

The motor was also to be subjected to random vibration, then the sinusoidal test was to be repeated. The 'before' and 'after' plots were compared for differences which might indicate that the motor had suffered damage.

The only measurements made were the responses of the control points; these could have been used to predict the response at any other point but this was not attempted since there were no experimental results available for comparison.

The program described in section 4.3.2 was utilised to calculate the responses of the propellant and the case assuming values for the applied forces (see fig. (4.9)). The relative displacement between the propellant and the case was then calculated. The system was assumed to be linear then the force necessary to cause impact of the propellant on the case could be calculated. The applied forces were

assumed to be equal.

The responses at various frequencies are given in fig. (4.10(a)) for the temperature at +40°C and in fig. 4.10(b) for the temperature at -20°C.

At 40°C it may be seen that impact is likely to occur when the forcing frequency is 10 Hz and the applied forces are approximately 25 N. The position of the impact is at a distance of 0.98 m from the bonded end.

Similarly at -20°C contact will occur when the forcing frequency is 50 Hz at 0.8 m from the bonded end when the applied forces are about 1 200 N. An estimate was made of the actual applied forces (based on the mass of the motor and the response at low frequencies when F = M a), it was calculated to be about 1 200 N. Thus it may be suggested that the damage would be more likely to occur at the high temperature than at -20°C; also the point of damage at 40°C would be about 1.0 m from the bonded end. This was in fact the case (see section 1.1.7).

Note that it has been assumed that the propellant remains as a straight beam with a constant clearance between it and the case; in practise when the propellant is warm it is very soft and will not support its own weight so will slump onto the case. The motor is periodically turned to combat this occurrence but it is unlikely that it is removed completely.

Motor D

This is a motor design which has not yet been subjected to vibration trials. The predicted responses at +50°C and -25°C are given in fig. (4.11). If the applied forces are more than 135 N then damage is likely to occur caused by the propellant impacting on the case when the forcing frequency is 90 Hz.

Note: The complex moduli used in these analyses were obtained from the relaxation moduli and then modified using the 'correction factor' q_T found empirically for propellant No. 1 for particular temperatures.

$$q_T = \left(\frac{E_{1m}}{E_{1R}} + i \frac{E_{2m}}{E_{2R}} \right)_T$$

where suffix m indicates measured value

suffix R indicates value obtained from relaxation modulus

T indicates a particular temperature

Table 4.1

Experimental results on Motor A

Trial No.	Frequency where acceleration was a maximum (Hz)	Maximum acceleration (g)
1	103	16
2	120	26
3	122	40
4	129	24
5	140	28
6	130	26
7	135	32
8	110	30
9	113	24
10	114	28
11	112	30
12	111	34
13	104	16
14	100	20
15	131	40
16	112	24
17	121	28
18	124	20
19	105	20
20	128	40
21	124	34
22	133	17
23	121	18
24	129	16
25	130	30
26	100	16
27	125	25
28	105	20
29	114	25
30	112	26
31	111	23
32	104	15
33	100	12
34	112	15
35	128	22
Average	117	24.6
Root mean square scatter: $\sqrt{\frac{1}{n}\sum_{i=1}^{n}(x_i - \bar{x})^2}$	11.3	7.5

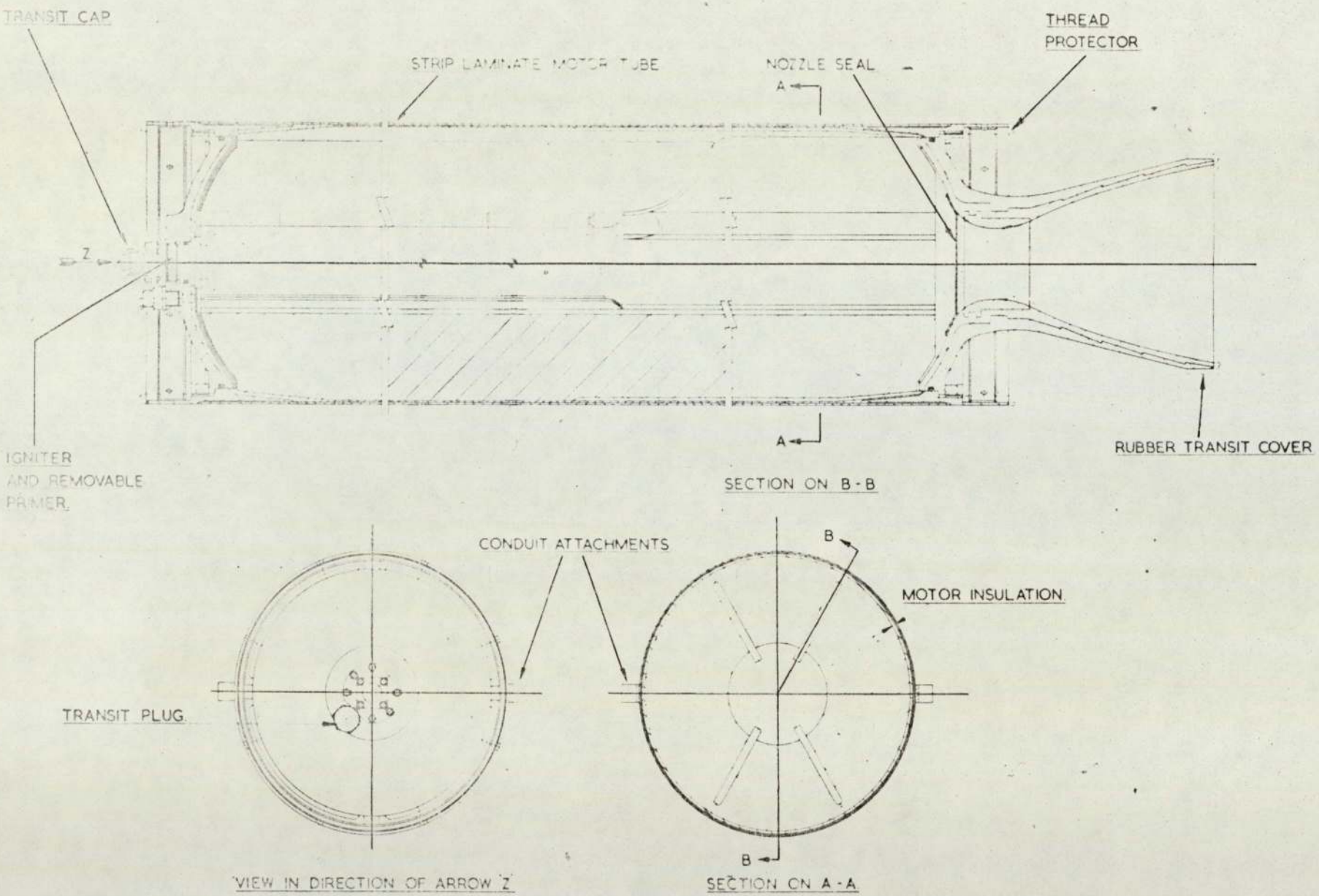

FIG 4.1 GENERAL ARRANGEMENT OF CASE BONDED MOTOR (A)

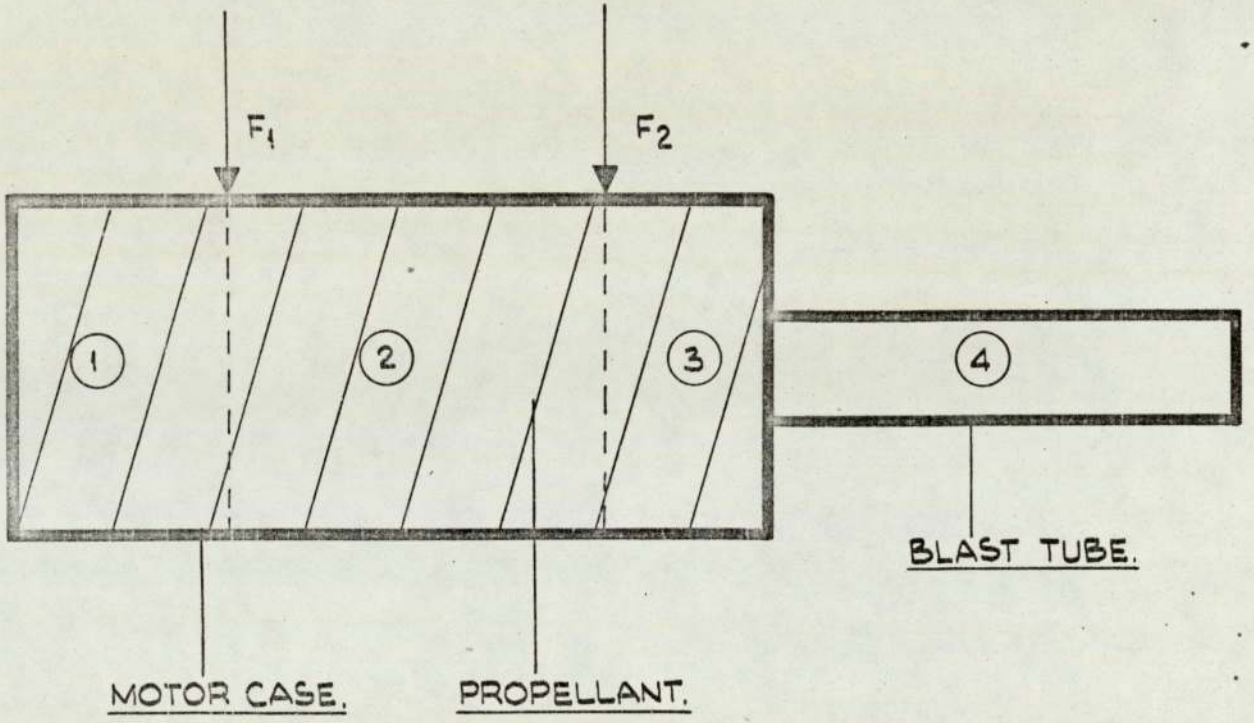

FIG. 4.2 MATHEMATICAL MODEL OF A CASE BONDED MOTOR.

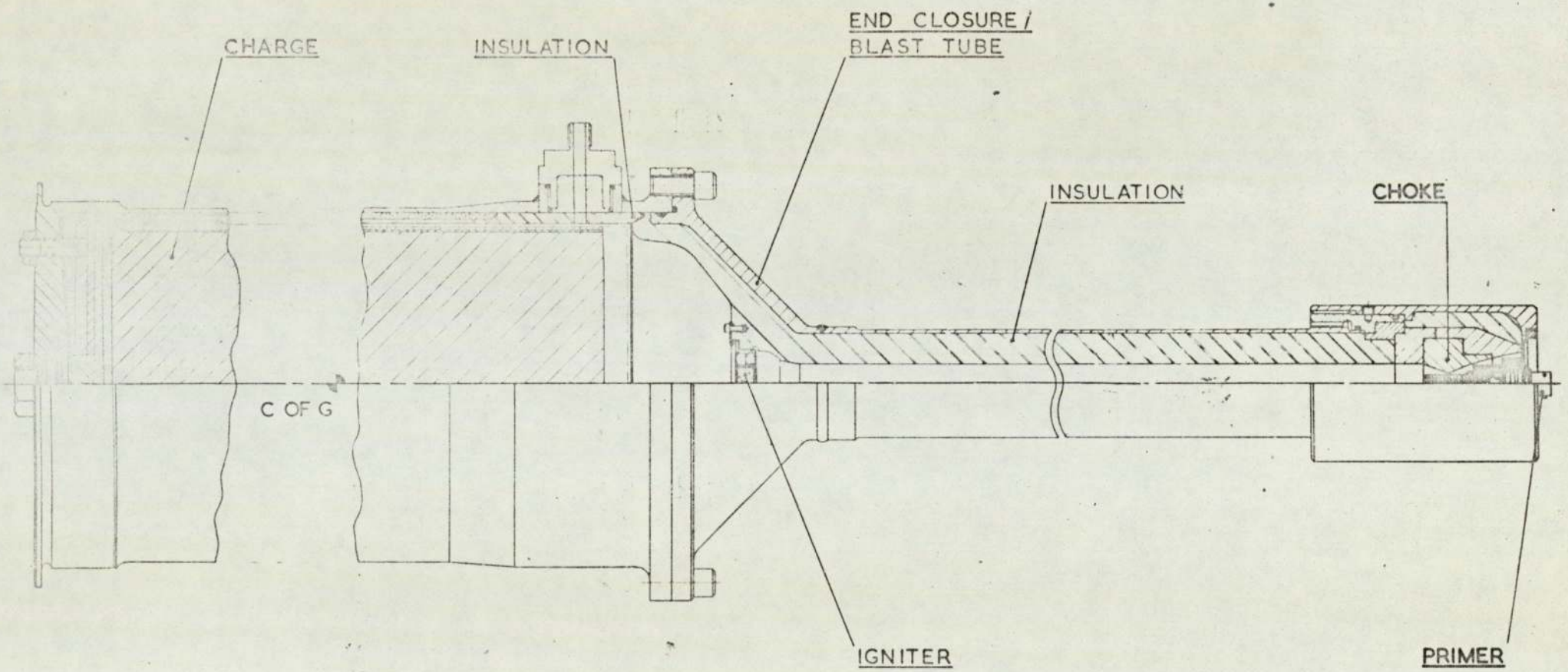

FIG. 4.3 GENERAL ARRANGEMENT OF CARTRIDGE LOADED MOTOR (C)

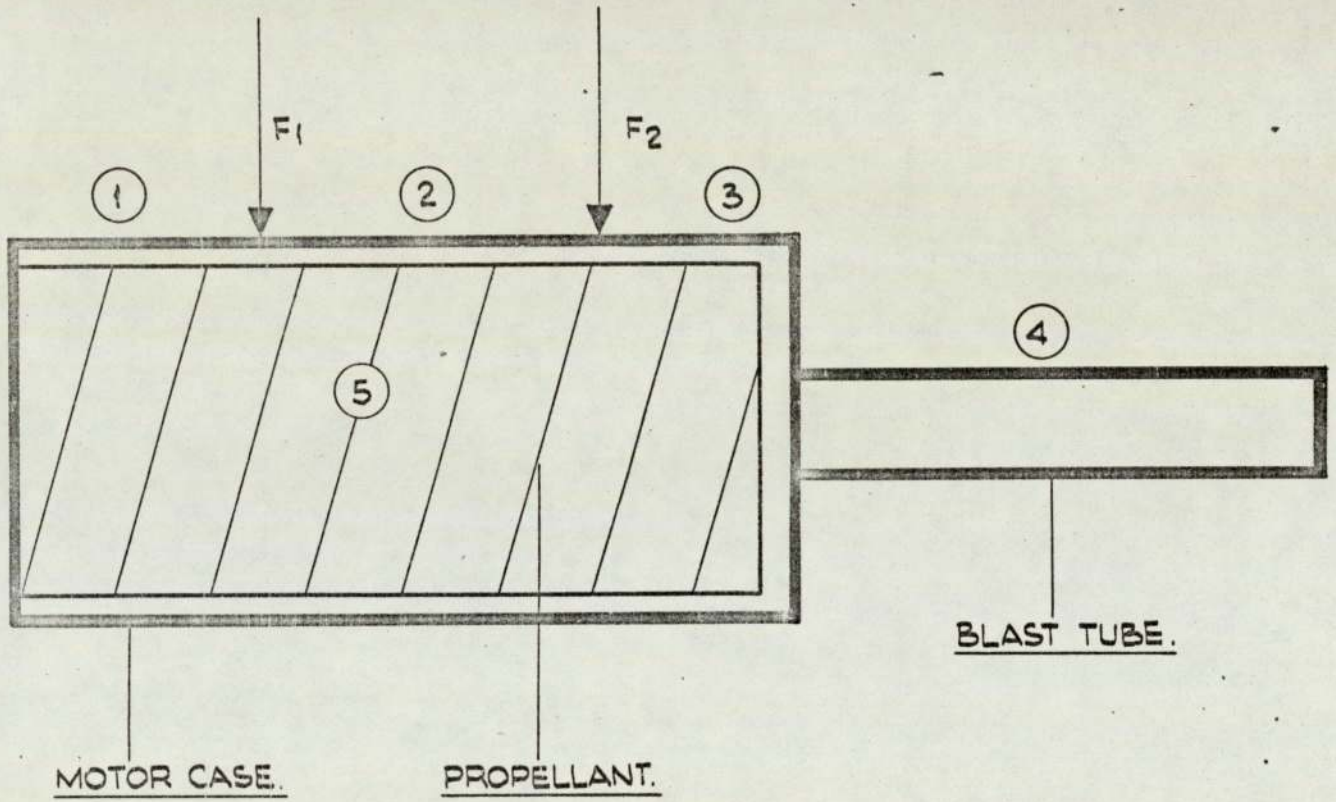

FIG. 4.4 MATHEMATICAL MODEL OF A CARTRIDGE LOADED MOTOR.

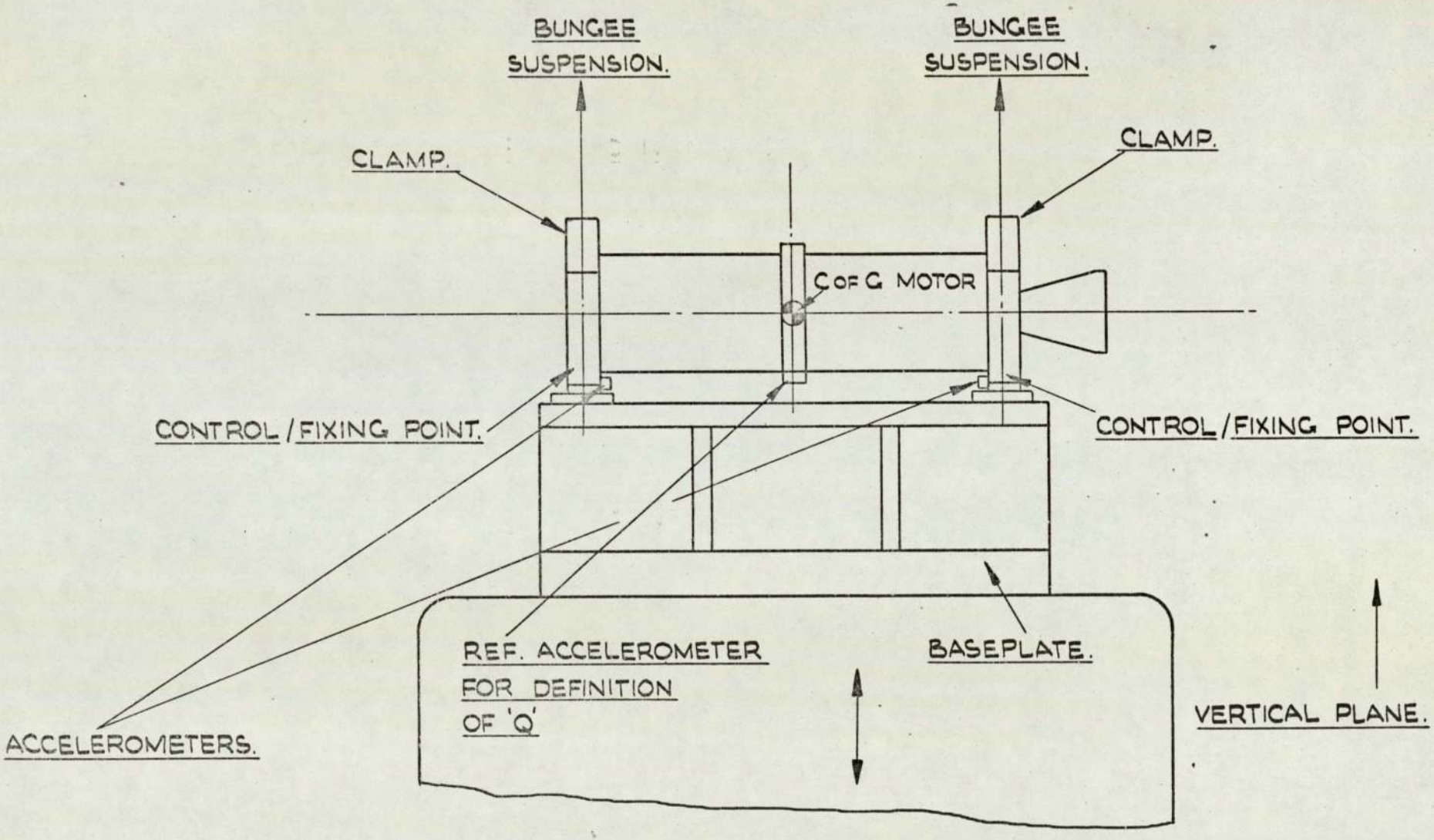

FIG. 4.5 MOTOR 'A' MOUNTING FOR TRANSVERSE VIBRATION.

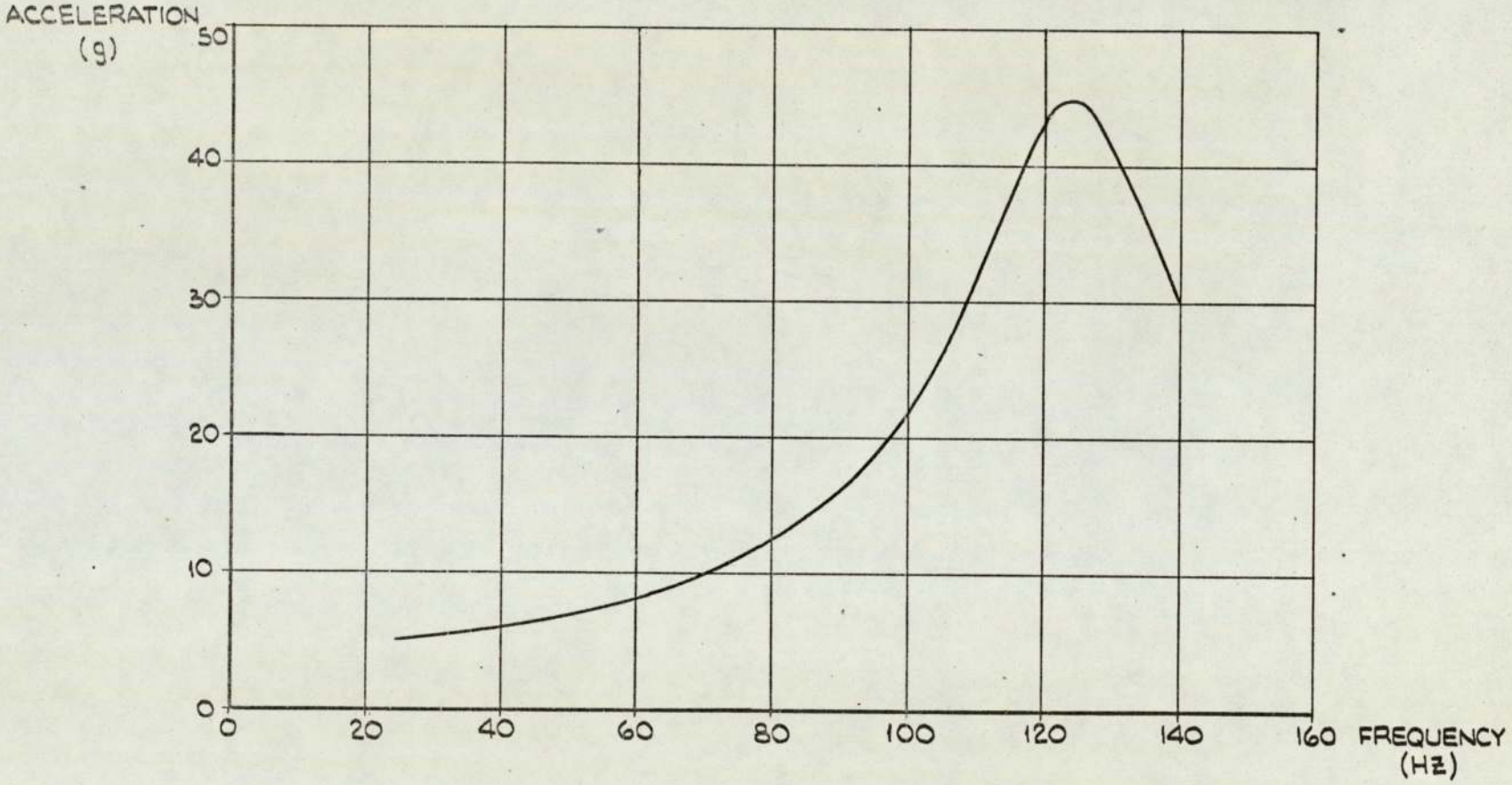

FIG. 4.6 ACCELERATION VS. FREQUENCY RESPONSE OF THE CENTRE OF GRAVITY OF MOTOR 'A'. (CONSTANT ACCELERATION OF 4g AT CONTROL POINTS)

(a) TEMPERATURE 30°C

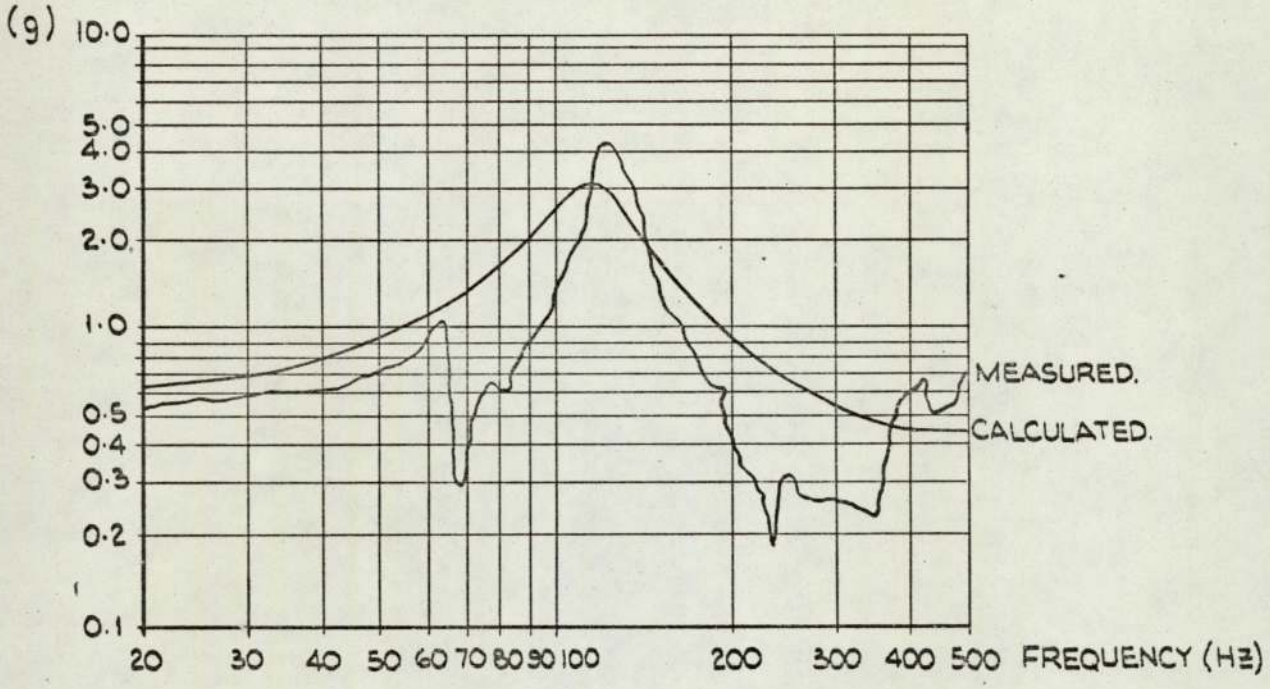

(b) TEMPERATURE -10°C.

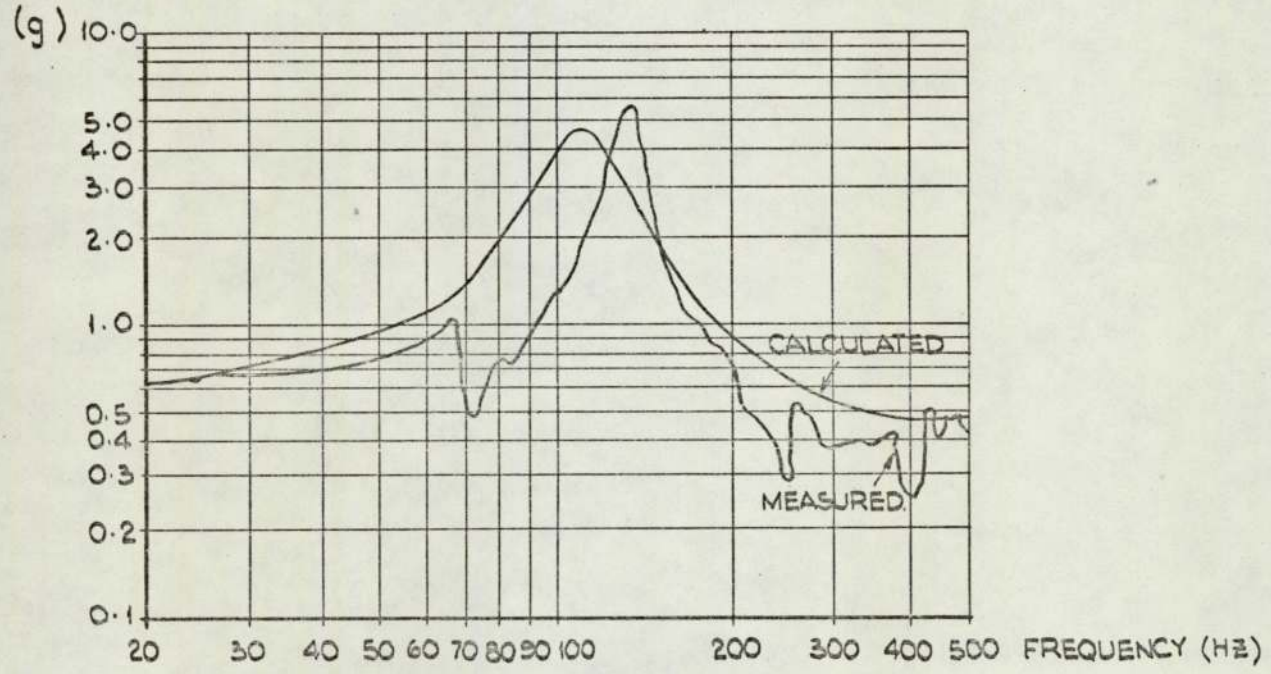

FIG. 4.7

COMPARISON OF PREDICTED AND MEASURED ACCELERATION VS. FREQUENCY RESPONSES OF THE CENTRE OF GRAVITY OF MOTOR 'B'.

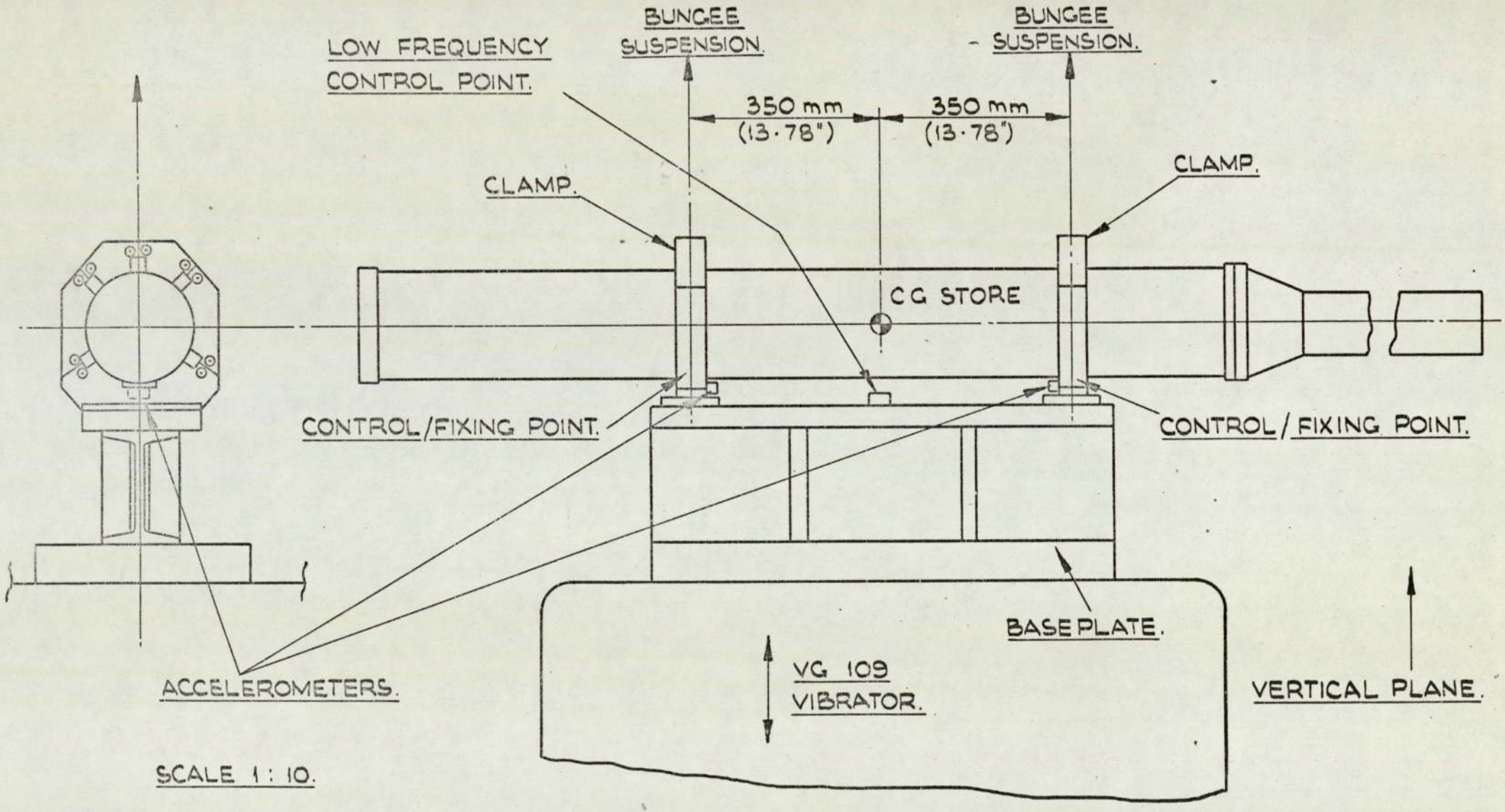

FIG. 4.8 MOTOR C MOUNTING FOR TRANSVERSE VIBRATION.

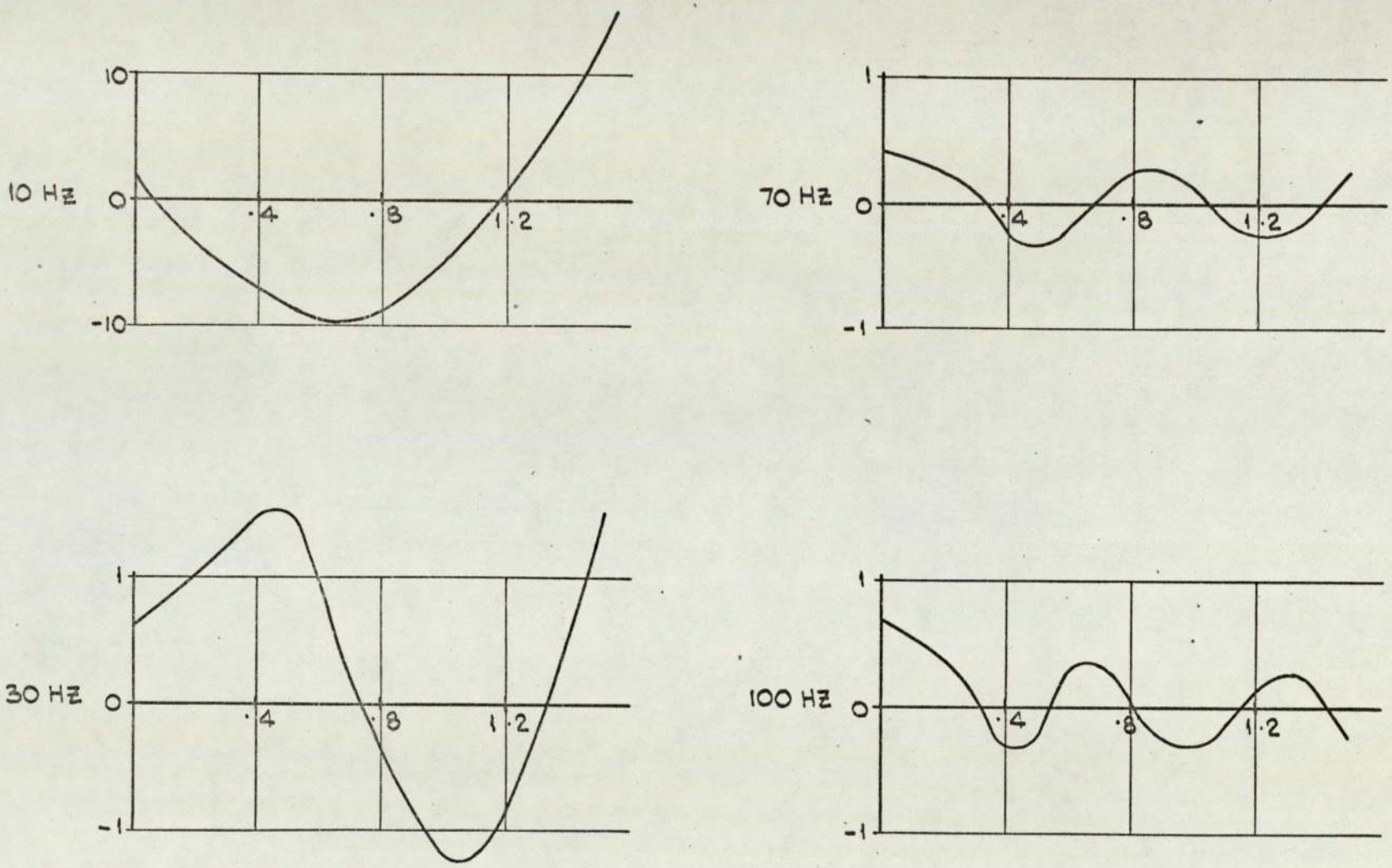

FIG. 4.9(a) RESPONSE OF THE PROPELLANT IN MOTOR C (20°C) DISPLACEMENT (mm) VS. DISTANCE ALONG THE PROPELLANT (m) AT VARIOUS FREQUENCIES. APPLIED FORCES :- 1000 N.

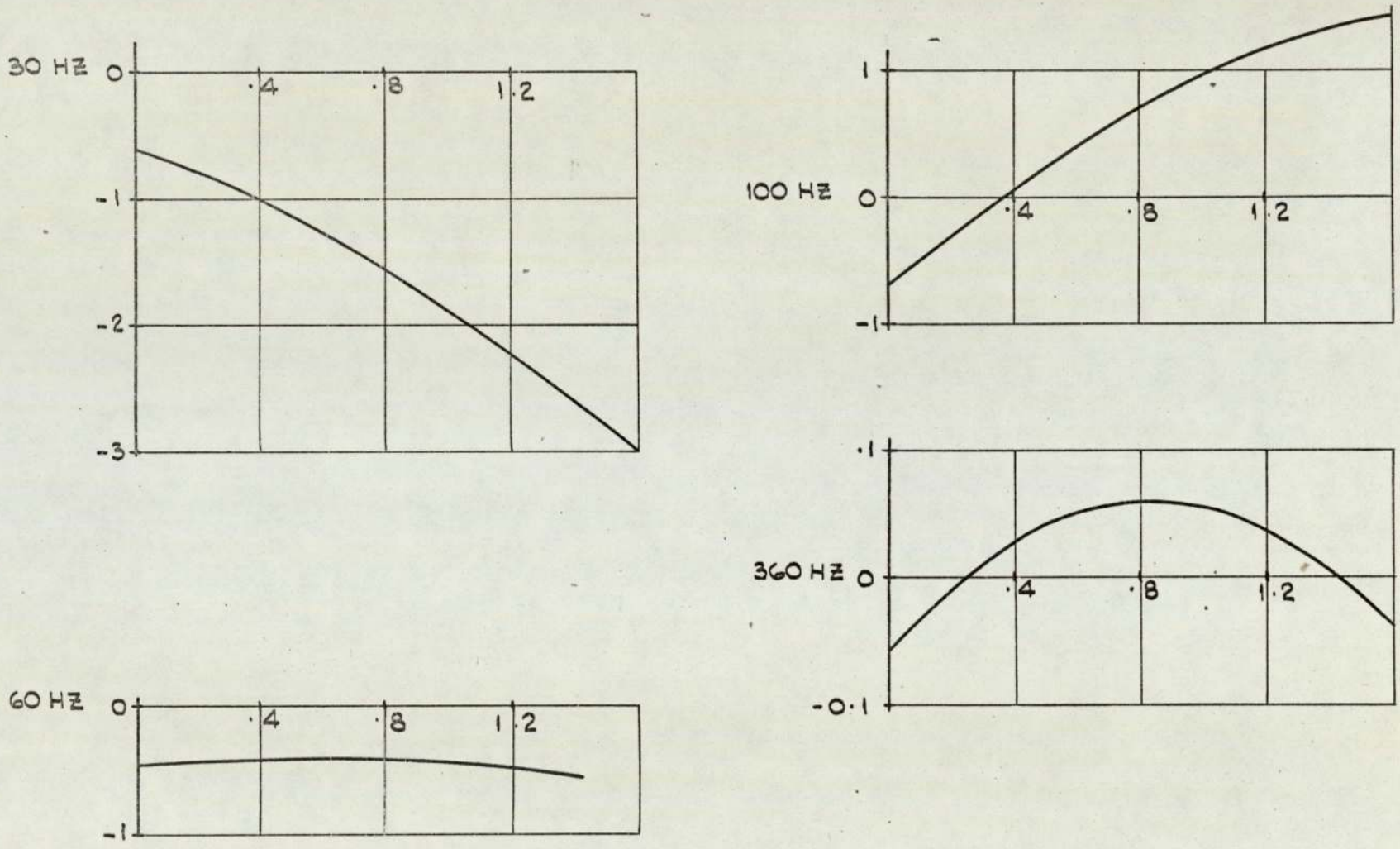

FIG. 4. 9(b) RESPONSE OF THE CASE OF MOTOR C (20°C)
DISPLACEMENT (mm) Vs. DISTANCE ALONG THE CASE (m)
AT VARIOUS FREQUENCIES. APPLIED FORCES :- 1000 N.

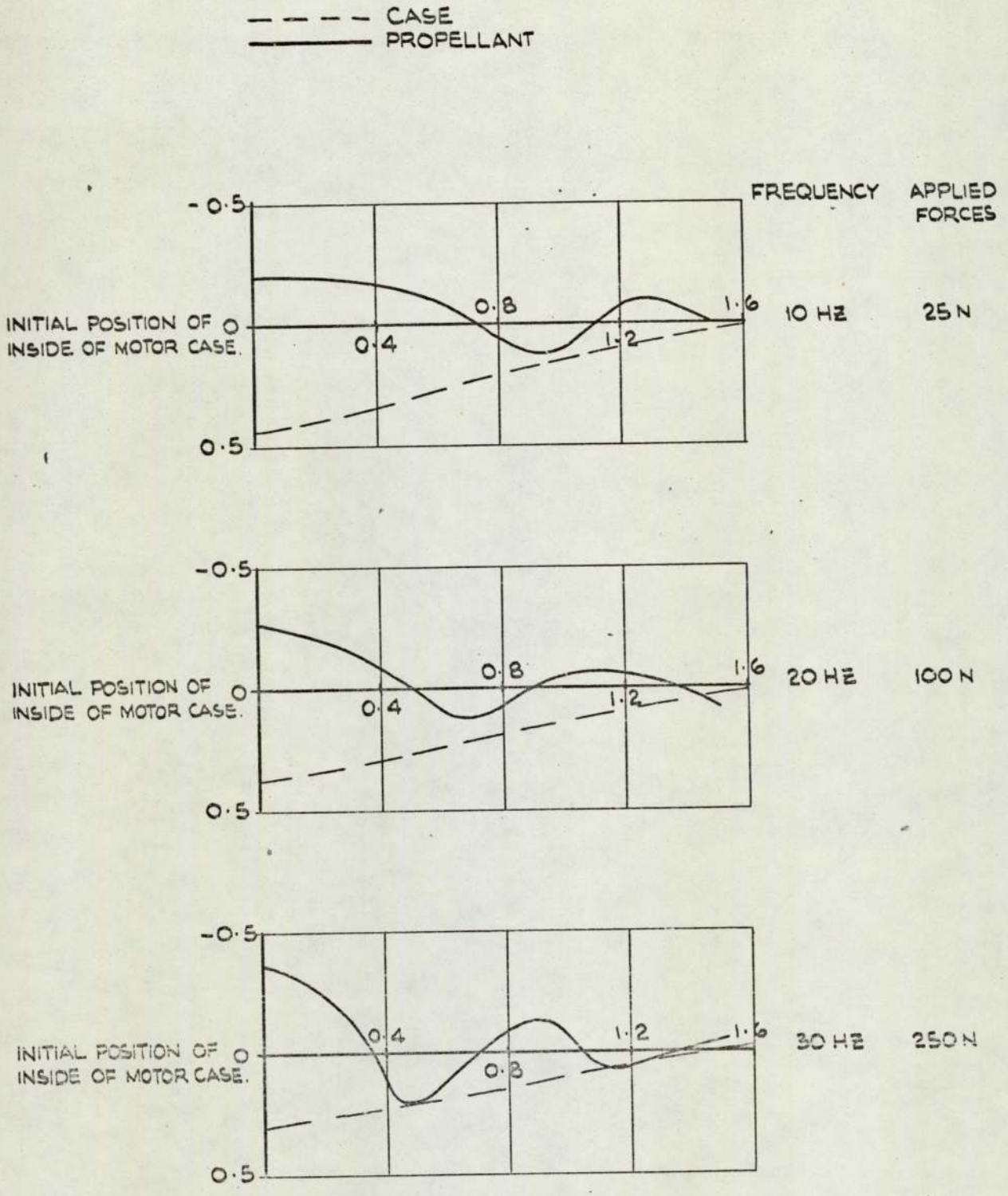

FIG. 4. 10(a) RESPONSE OF MOTOR C AT 40°C

DISPLACEMENT (mm) Vs. DISTANCE ALONG THE MOTOR (m)

(GAP BETWEEN PROPELLANT AND CASE INITIALLY :- ·64 mm)

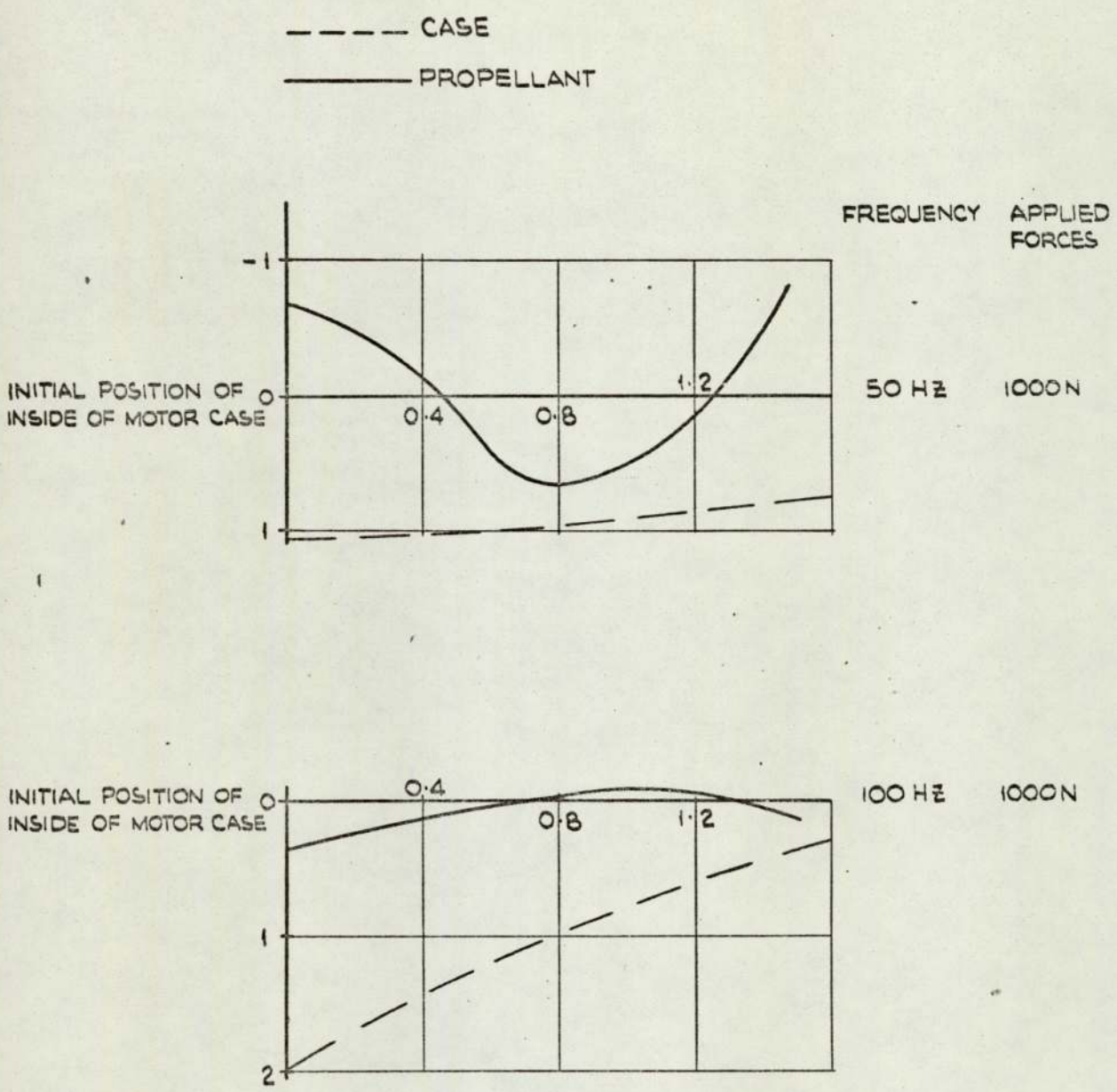

FIG. 4.10(b) RESPONSE OF MOTOR C AT -20°C
DISPLACEMENT (mm) VS. DISTANCE ALONG THE MOTOR (m)
(GAP BETWEEN PROPELLANT AND CASE :- 1·72 mm)

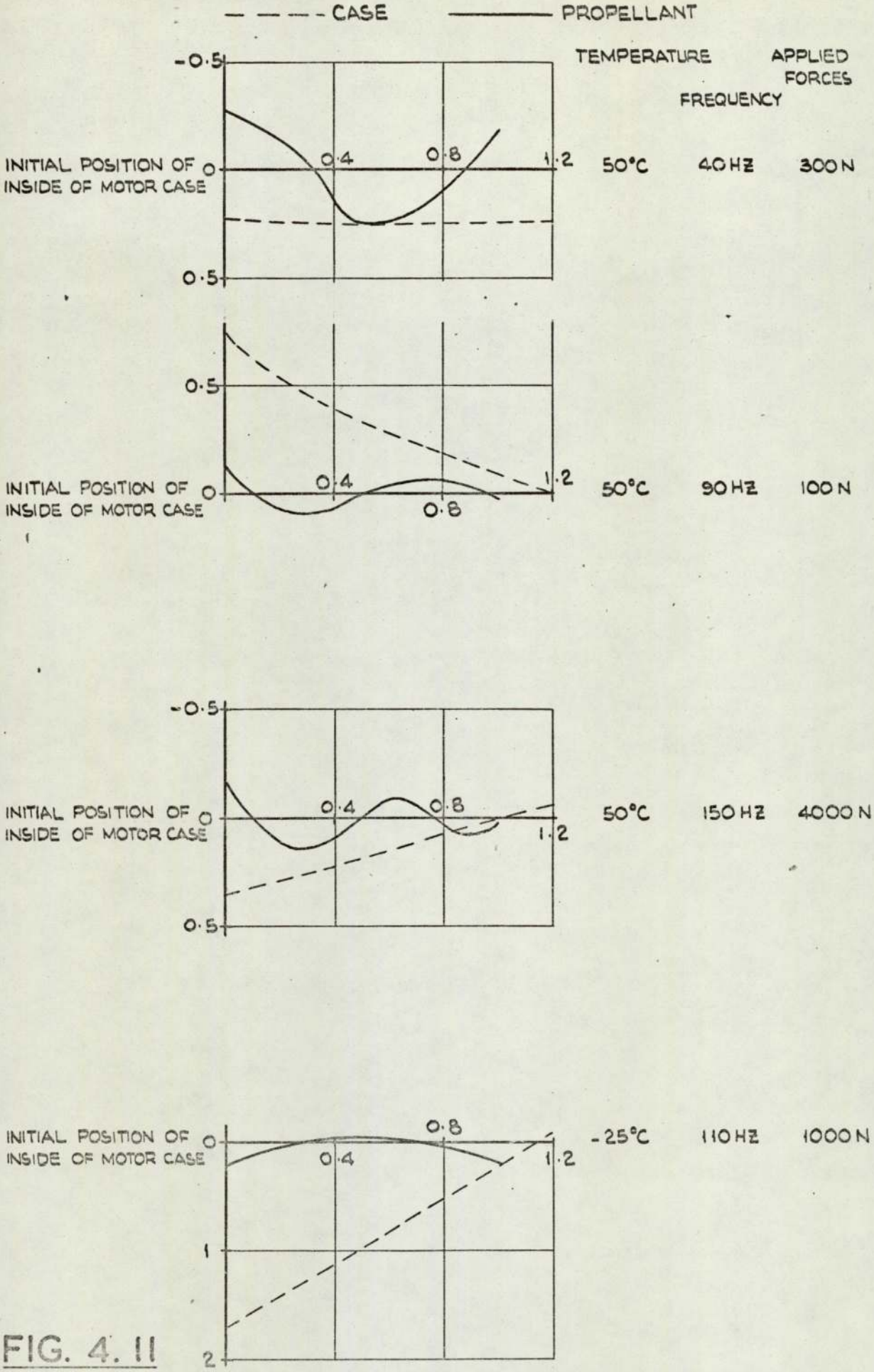

FIG. 4. 11

RESPONSE OF MOTOR D AT + 50°C AND -25°C.
DISPLACEMENT (mm) VS. DISTANCE ALONG THE MOTOR (m)
GAP BETWEEN CASE AND PROPELLANT AT 50°C :- 5 mm
GAP BETWEEN CASE AND PROPELLANT AT -25°C :- 1·5 mm

Chapter 5

CONCLUSIONS AND PROPOSALS FOR FURTHER WORK

5.1 Admittance method for measuring the complex modulus E*

The modulus was measured with 2 samples of propellant No. 1. It was shown that the modulus was dependent on frequency and temperature but independent of sample length (provided that the sample was long in relation to the cross section so that it could be assumed that the stress was constant over the cross section).

The measured complex was used to calculate:

(i) the acceleration and phase at the forced end of the test rod in longitudinal vibration

(ii) the acceleration and phase at both ends of the test rod in transverse vibration

(iii) the acceleration at 9 points along the length of the full scale sample

These were compared with measured data and were in good agreement.

The modulus was also measured at several temperatures where the value of E* ranged from 1 242(1 + i 0.33) MN/m^2 at 1 820 Hz and $-9^{\circ}C$ to 10.74 (1 + i 0.88) MN/m^2 at 200 Hz and $+39^{\circ}C$, so the method works within that range of modulus at least. The complex modulus of natural rubber was also measured and was found to be equal to 4.2 (1 + i 0.05) MN/m^2 at low frequencies. This agreed with the modulus measured by another technique so the admittance method works for a damping constant (E_2/E_1) at least as low as 0.05. There appears to be no upper limit because if a material is so heavily damped that no peaks in the acceleration vs frequency response are discernable then masses can be added to each end until the response does show a maximum. From the dimensions of the rod and the added masses an estimate for the complex modulus at the frequency of maximum acceleration may be made. This estimate is used as the initial guess for the iteration routine.

The fact that the method can be used for heavily damped materials is the most important point as there is no other simple technique which is applicable. (The other technique which does exist uses a viscoelastic/elastic beam in transverse vibration. The Euler-Bernoulli equations for transverse vibration are used, they are more complicated than the equations for longitudinal vibration and they are only valid over a limited frequency range when shear deformation and rotary inertia can be ignored. Then, having found the "composite" modulus, it is necessary to extract the complex modulus of the viscoelastic material).

The experimental set up for the admittance method contains only standard instruments and needs no special equipment; the experimental procedure is simple and quick (the measurements needed to calculate the complex modulus in the range of 100 Hz to 1 000 Hz are made in about 10 minutes); the rig can be easily adapted to measure the complex modulus at specific temperatures by surrounding the specimen with an oven/refrigerator thus not disturbing any other equipment.

The frequency range over which the method is valid is about 10 Hz to 5 000 Hz depending on modulus, sample size etc. The limits for a particular sample are determined by:

(a) The lower limit: When the rod moves as a rigid body (somewhat below the first "resonance"). The response is independent of complex modulus so the results from the iteration technique cannot be relied upon.
The lower limit can be reduced by increasing the added end masses thus decreasing the first "resonance".

(b) The upper limit: When the wave length is of the same order as the cross section the assumption that the stress is constant over the cross section is not valid.

The upper limit can be increased either by reducing the end masses or reducing the cross section area.

If the frequency - temperature superposition principle may be applied then the frequency range can be greatly extended.

The computer programme to calculate the complex modulus from the measurement is short and simple to use. It is easy to obtain a reasonable estimate of the modulus at the frequency where the acceleration is a maximum. With this as the initial estimate for the iterative process the programme will calculate E* for each frequency at which measurements were made.

5.2 Complex moduli of other propellants

It has been shown that the measured complex modulus was appreciably different from that obtained from the relaxation modulus for propellant No. 1. It is necessary to have the accurate complex modulus to give a reasonable prediction of the response of a rocket motor to forced vibration so the moduli of the other propellant should be measured too.

It may be found that the "correction factor" - q_T used in the present work (based on only one material) may be applicable for all propellants, if not, the complex moduli of each propellant will have to be measured.

There exist at SRS good facilities for maintaining the specimen at a constant temperature so it will be possible to determine the modulus at various temperatures. It will also be possible to assess the applicability of the temperature - frequency superposition principle for each propellant.

5.3 Rocket Motors

The analysis developed for analysing rocket motors have given very good results for the three of the studied motors for which experimental data are available (A, B and C).

No special experiments were carried out on a rocket motor for the present research and much more remains to be done both experimentally and theoretically. Tests are necessary with a more extensive monitoring system then conclusions could be reached on the applicability of the mathematical models.

It is necessary to

(i) measure input forces to the motor by including force transducers between the motor and the vibrator.

(ii) measure the effect of the clamps and specify the tightening torque to ensure repeatable trials

(iii) measure the phase difference between signals (applied forces, control accelerations etc) to give a more accurate representation of the constraints

(iv) Install more accelerometers along the motor

(v) (With a cartridge loaded motor) include accelerometers within the propellant to measure its response as well as the case - then it may be seen if the two are impacting

The theory of rocket motor vibration needs to be extended to include:

(i) the effect of forced random vibration (this is based on the response at specific frequencies)

(ii) the response of cartridge loaded motors when the propellant is not rigidly connected to the case

(iii) the response when the propellant has slumped onto the case

5.4 Transport vibration specifications

Although the transport vibration trials are specified by the customer it would seem useful to do some experiments on rocket motors - both packaged and when connected to the missile - to measure the vibrations that are encountered during transportation by road, air, sea etc. If the specifications were based on actual measurements then realistic vibration trials could be designed which would ensure that the motor would be safe to use and would obviate the necessity of designing a motor to withstand tests many times harsher than anything it would be subjected to in service.

5.5 Other applications of the present work

(a) The admittance method can be used to measure the complex modulus of any viscoelastic material as discussed in 5.1.

(b) The method developed for analysing the motors can be used to study the effect of a sinusoidal force on any system of rigidly connected beams - elastic or viscoelastic. The solution for each beam is standard and the set of end conditions are put into matrix form which is solved by the Gauss elimination technique to give the coefficients; the response of any part of the system can then be evaluated.

(c) The use of viscoelastic materials to damp out unwanted vibrations has been studied extensively (see references (17), (28), (33), (39), (40), and (41)). In the present work it has been shown that the effectiveness of a damping material is given by:

$$\xi = E_2/2E_1 \quad (\text{or } Q = E_1/E_2)$$

so for a viscoelastic material of known modulus it is possible to predict ξ (or Q) as above.

For an elastic/viscoelastic composite beam a composite E* must be evaluated (see references (3) and (61)), then the same equations may be used.

If the coating of viscoelastic material is more than five times the thickness of the elastic beam then

$$(E_2/E_1)_{\text{composite}} \simeq (E_2/E_1)_{\text{viscoelastic}}$$

5.6 The solution to The Problem

As mentioned in the introduction, the problem which initiated the present research was one particular design of motor which failed during the vibration trials. It has been shown in the present work that this was probably caused by the propellant hitting the case when the motor was subjected to low frequency vibration which excited the second "resonance" of the propellant. The damage occurred only at the high temperature because (a) the gap between the base and the propellant was small due to the high coefficient of expansion of the propellant and (b) the complex modulus was lower at the high temperature thus reducing the frequency of the "resonance" to a value where the displacement was of the same order as the gap.

The problem was overcome by inserting rubber strips along the length of the propellant thus connecting it to the case.

By connecting the case and the propellant in this way they are not able to vibrate separately so they become a composite structure similar to the case bonded motor.

The first "resonance" of the composite occurs between that of the propellant alone and that of the case alone since the case adds stiffness to the propellant thus increasing its natural frequency and the propellant adds mass to the case thus reducing its natural frequency. The propellant also adds damping so it considerably reduces the displacement of the case at the natural frequency.

Since the propellant and case cannot move independently no damage can be caused by vibration, the rubber support is in the form of strips to allow room for expansion so no thermal stresses are induced.

As this amendment is simple and inexpensive to incorporate it is probably the best solution possible.

APPENDICES

Appendix A

The Euler-Bernoulli Equations

(i) The Euler-Bernoulli equations for an elastic beam in bending

From elementary bending theory:

Bending moment

$$M = - EI \frac{\partial^2 u}{\partial x^2} \qquad A(1)$$

where $u = u(x,t)$ is the displacement of the neutral axis, u positive down.

Consider an element δx of the beam:

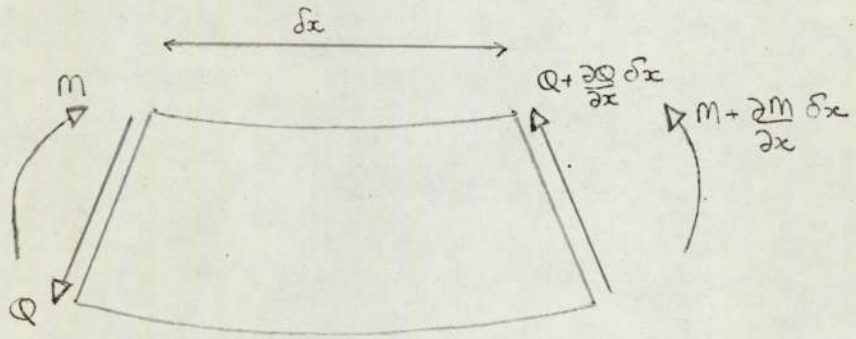

The equilibrium equations are:

$$Q = - \frac{\partial M}{\partial x}$$

and

$$\frac{\partial Q}{\partial x} = - \rho A \frac{\partial^2 u}{\partial t^2}$$

$\therefore$ by substituting for M from A(1), we have

$$EI \frac{\partial^4 u}{\partial x^4} = - \rho A \frac{\partial^2 u}{\partial t^2} \qquad A(2)$$

Consider the beam in forced vibration with an applied harmonic force $F = F_o e^{i\omega t}$. If it is assumed that the transients have died away and the beam is in the steady state condition, then it may be assumed:

$$u(x,t) = u_o(x)\, e^{i\omega t}$$

The equation A(2) becomes:

$$\frac{d^4 u_o}{dx^4} + \alpha^4 u_o = 0$$

where $\alpha^4 = \rho A \omega^2 / EI$ A(3)

Then the solution of A(3) is:

$$u_o = B_1 \cos \alpha x + B_2 \sin \alpha x + B_3 \cosh \alpha x + B_4 \sinh \alpha x \qquad A(4)$$

The four unknown coefficients B_1, B_2, B_3 and B_4 are found from the end conditions of the beam.

e.g. consider a free-free beam excited by the force F at the end x = l.

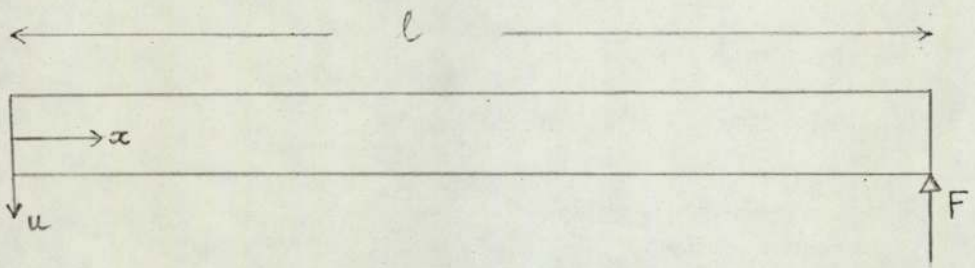

Then the conditions are:

at $x = 0$, $Q = 0$, $M = 0$.

at $x = l$, $Q = F$, $M = 0$.

where $Q = EI \dfrac{\partial^3 u}{\partial x^3}$ and $M = -EI \dfrac{\partial^2 u}{\partial x^2}$

Solving for the coefficients B_i gives

$$u = \frac{F_o e^{i\omega t}}{2EI\alpha^3(1 - \cos \alpha l \cosh \alpha l)} \quad x$$

$$(\cos \alpha x + \cosh \alpha x)(\sin \alpha l - \sinh \alpha l)+(\sin \alpha x + \sinh \alpha x)(\cos \alpha l - \cosh \alpha l) \qquad A(5)$$

(ii) <u>The Euler-Bernoulli equations for a viscoelastic beam in bending</u>

The second form of the Correspondence Principle (see section 1.2.7) is applied, then

u_o is as given in equation A(5) except that α is defined by:

$$\alpha^4 = \rho A\omega^2/E^*I$$

Appendix B

The Timoshenko Beam Equations

(i) The Timoshenko equations for an elastic beam in bending

From elementary bending theory:

Bending Moment $M = -EI \frac{\partial \psi}{\partial x}$ B(1)

Shear Force $Q = - k'AG \left(\frac{\partial u}{\partial x} - \psi\right)$ B(2)

where $u = u(x,t)$ is the deplacement of the neutral axis, u positive down and $\psi = \psi(x,t)$ is the slope of the neutral axis, ψ positive clockwise. E, I, k', A, G do not vary with x or t.

Consider an element δx of the beam

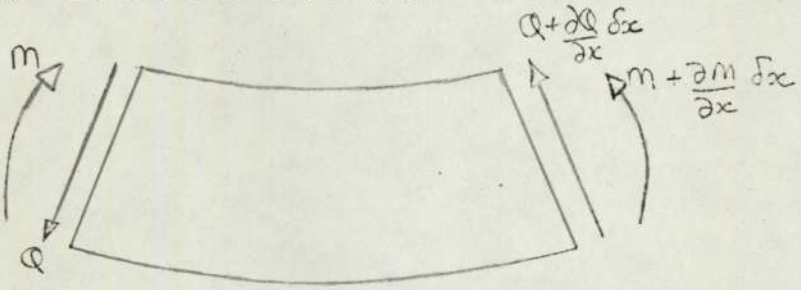

The equilibrium equations are:

$$Q - \left(Q + \frac{\partial Q}{\partial x} \delta x\right) = \rho A \delta x \frac{\partial^2 u}{\partial t^2} \qquad B(3)$$

$$M - \left(M + \frac{\partial M}{\partial x} \delta x\right) - Q \frac{\delta x}{2} - \left(Q + \frac{\partial Q}{\partial x} \delta x\right) \frac{\delta x}{2} = \rho I \, \delta x \frac{\partial^2 \psi}{\partial t^2} \qquad B(4)$$

From B(3)

$$\frac{\partial Q}{\partial x} + \rho A \frac{\partial^2 u}{\partial t^2} = 0$$

Substituting for Q from B(2):

$$-k'AG \left(\frac{\partial^2 u}{\partial x^2} - \frac{\partial \psi}{\partial x}\right) + \rho A \frac{\partial^2 u}{\partial t^2} = 0 \qquad B(5)$$

From B(4),

$$\frac{-\partial M}{\partial x} - Q = \rho I \frac{\partial^2 \psi}{\partial t^2}$$

Substituting for M and Q from B(1) and B(2):

$$EI \frac{\partial^2 \psi}{\partial x^2} + k'AG \left(\frac{\partial u}{\partial x} - \psi \right) = \rho I \frac{\partial^2 \psi}{\partial t^2} \qquad B(6)$$

B(5) and B(6) are the mixed differential equations of motion in u and ψ.

From B(5)

$$\frac{\partial \psi}{\partial x} = \frac{\partial^2 u}{\partial x^2} - \frac{\rho A}{k'AG} \frac{\partial^2 u}{\partial t^2} \qquad B(7)$$

$$\text{therefore } \frac{\partial^3 \psi}{\partial x \partial t^2} = \frac{\partial^4 u}{\partial x^2 \partial t^2} - \frac{\rho A}{k'AG} \frac{\partial^4 u}{\partial t^4} \qquad B(8)$$

$$\text{and } \frac{\partial^3 \psi}{\partial x^3} = \frac{\partial^4 u}{\partial x^4} - \frac{\rho A}{k'AG} \frac{\partial^4 u}{\partial t^2 \partial x^2} \qquad B(9)$$

Differentiating B(6) with respect to x gives

$$EI \frac{\partial^3 \psi}{\partial x^3} + k'AG \left(\frac{\partial^2 u}{\partial x^2} - \frac{\partial \psi}{\partial x} \right) = \rho I \frac{\partial^3 \psi}{\partial x \partial t^2}$$

Substituting B(7), B(8) and B(9) gives

$$EI \frac{\partial^4 u}{\partial x^4} - \left(\frac{EI\rho}{k'G} + \rho I \right) \frac{\partial^4 u}{\partial x^2 \partial t^2} + \rho A \frac{\partial^2 u}{\partial t^2} + \frac{\rho^2 I}{k'G} \frac{\partial^4 u}{\partial t^4} = 0 \qquad B(10)$$

From B(6),

$$\frac{\partial u}{\partial x} = \frac{1}{k'AG} \left(\rho I \frac{\partial^2 \psi}{\partial t^2} - EI \frac{\partial^2 \psi}{\partial x^2} \right) + \psi$$

$$\text{therefore } \frac{\partial^3 u}{\partial x^3} = \frac{\rho I}{k'AG} \frac{\partial^4 \psi}{\partial x^2 \partial t^2} - \frac{EI}{k'AG} \frac{\partial^4 \psi}{\partial x^4} + \frac{\partial^2 \psi}{\partial x^2} \qquad B(11)$$

$$\text{and } \frac{\partial^3 u}{\partial x \partial t^2} = \frac{\rho I}{k'AG} \frac{\partial^4 \psi}{\partial t^2} - \frac{EI}{k'AG} \frac{\partial^4 \psi}{\partial x^2 \partial t^2} + \frac{\partial^2 \psi}{\partial t^2} \qquad B(12)$$

Differentiating B(5) with respect to x gives

$$\rho A \frac{\partial^3 u}{\partial x \partial t^2} - k'AG \left(\frac{\partial^3 u}{\partial x^3} - \frac{\partial^2 \psi}{\partial x^2} \right) = 0$$

then substituting B(11) and B(12) gives

$$EI \frac{\partial^4 \psi}{\partial x^4} + \rho A \frac{\partial^2 \psi}{\partial t^2} - \left(\rho I + \frac{\rho EI}{k'G} \right) \frac{\partial^4 \psi}{\partial x^2 \partial t^2} + \frac{\rho^2 I}{k'G} \frac{\partial^4 \psi}{\partial t^4} = 0 \qquad B(13)$$

B(10) and B(13) are the separated differential equations of motion in u and ψ. Consider the beam in forced vibration with an applied harmonic force $F = F_o e^{i\omega t}$. If it is assumed that the transients have died away and the beam is in the steady state condition then it may be assumed:

$$u(x,t) = u_o(x) e^{i\omega t}$$

$$\psi(x,t) = \psi_o(x) e^{i\omega t}$$

Substituting in B(10) gives

$$\frac{d^4 u_o}{dx^4} + \frac{\omega^2}{EI} \left(\rho I + \frac{\rho EI}{k'G} \right) \frac{d^2 u_o}{dx^2} + \frac{1}{EI} \left(\frac{\rho^2 I \omega^4}{k'G} - \omega^2 \rho A \right) u_o = 0$$

or $$\frac{d^4 u_o}{dx^4} + C_1 \frac{d^2 u_o}{dx^2} + C_2 u_o = 0 \qquad B(14)$$

where $$C_1 = \frac{\omega^2}{EI} \left(\rho I + \frac{\rho EI}{k'G} \right)$$

and $$C_2 = \frac{1}{EI} \left(\frac{\rho^2 I \omega^4}{k'G} - \omega^2 \rho A \right)$$

Similarly from B(13),

$$\frac{d^4\psi_o}{dx^4} + C_1 \frac{d^2\psi_o}{dx^2} + C_2\psi_o = 0 \qquad B(15)$$

The general solutions of equations B(14) and B(15) are:

$$u_o = B_1 \cosh \alpha x + B_2 \sinh \alpha x + B_3 \cosh \beta x + B_4 \sinh \beta x \qquad B(16)$$

$$\psi_o = B_5 \cosh \alpha x + B_6 \sinh \alpha x + B_7 \cosh \beta x + B_8 \sinh \beta x \qquad B(17)$$

where $$\alpha^2 = \tfrac{1}{2}\left(-C_1 + \sqrt{C_1^2 - 4C_2}\right) \qquad B(18)$$

and $$\beta^2 = \tfrac{1}{2}\left(-C_1 - \sqrt{C_1^2 - 4C_2}\right)$$

Substituting B(16) and B(17) into B(6) gives

$$\begin{aligned} &EI(\alpha^2 B_5 \cosh \alpha x + \alpha^2 B_6 \sinh \alpha x + \beta^2 B_7 \cosh \beta x + \beta^2 B_8 \sinh \beta x) \\ &+ \rho I\omega^2 (B_5 \cosh \alpha x + B_6 \sinh \alpha x + B_7 \cosh \beta x + B_8 \sinh \beta x) \\ &+ k'AG((\alpha B_1 \sinh \alpha x + \alpha B_2 \cosh \alpha x + \beta B_3 \sinh \beta x + \beta B_4 \cosh \beta x) \\ &- (B_5 \cosh \alpha x + B_6 \sinh \alpha x + B_7 \cosh \beta x + B_8 \sinh \beta x)) = 0 \end{aligned}$$

Since x is arbitrary, the coefficients of cosh αx, sinh αx, cosh βx and sinh βx must all be independently equal to zero.

Therefore $(EI\,\alpha^2 - k'AG + \rho I\omega^2)\, B_5 + k'AG\,\alpha\, B_2 = 0$

or $$B_5 = R\, B_2$$

where $$R = -k'AG\,\alpha/(EI\,\alpha^2 - k'AG + \rho I\omega^2) \qquad B(19)$$

Similarly, $B_6 = R\ B_1$,

and $B_7 = S\ B_4$,

$B_8 = S\ B_3$,

where $S = -k'AG\beta/(EI\beta^2 - k'AG + \rho I\omega^2)$. B(20)

Thus there are only four independent unknown coefficients.

therefore $u=(B_1 \cosh \alpha x + B_2 \sinh \alpha x + B_3 \cosh \beta x + B_4 \sinh \beta x)e^{i\omega t}$

and $\psi=(R\,B_2 \cosh \alpha x + R\,B_1 \sinh \alpha x + S\,B_4 \cosh \beta x + S\,B_3 \sinh \beta x)e^{i\omega t}$

The end conditions of the beam give four equations which are used to solve for B_1, B_2, B_3 and B_4.

e.g. for a free-free beam the bending moment and shear force are zero at $x = 0$ and $x = l$.

(ii) <u>The Timoshenko equations for a viscoelastic beam in bending</u>

The second form of the Correspondence Principle is applied (see section 1.2.7) then,

$$u=(B_1 \cosh \alpha x + B_2 \sinh \alpha x + B_3 \cosh \beta x + B_4 \sinh \beta x)e^{i\omega t}$$

$$\psi=(R\ B_2 \cosh \alpha x + R\ B_1 \sinh \alpha x + S\ B_4 \cosh \beta x + S\ B_3 \sinh \beta x)e^{i\omega t}$$

where $$C_1 = \frac{\omega^2}{E^*I}\left(\rho I + \frac{\rho E^* I}{k'G^*}\right)$$

and $$C_2 = \frac{1}{E^*I}\left(\frac{\rho^2 I\omega^4}{k'G^*} - \omega^2 \rho A\right)$$

then α^2 and β^2 are given by equation B(18).

and $R = -k'AG^*\alpha / (E^*I\alpha^2 - k'AG^* + \rho I\omega^2)$;

$$S = -k'AG^*\beta / (E^*I\beta^2 - k'AG^* + \rho I\omega^2)$$

Note: G^* is given by $G^* = \dfrac{E^*}{2(1+\nu^*)}$

It was assumed that the material was incompressible,

then $\nu^* = \frac{1}{2}$

and $G^* = E^*/3$

Note: Figure (B.1) shows a comparison of the responses calculated using the Euler-Bernoulli theory and the Timoshenko theory. The dimensions of the beam were:

cross section - 0.025 m x 0.025 m

length - 0.2 m

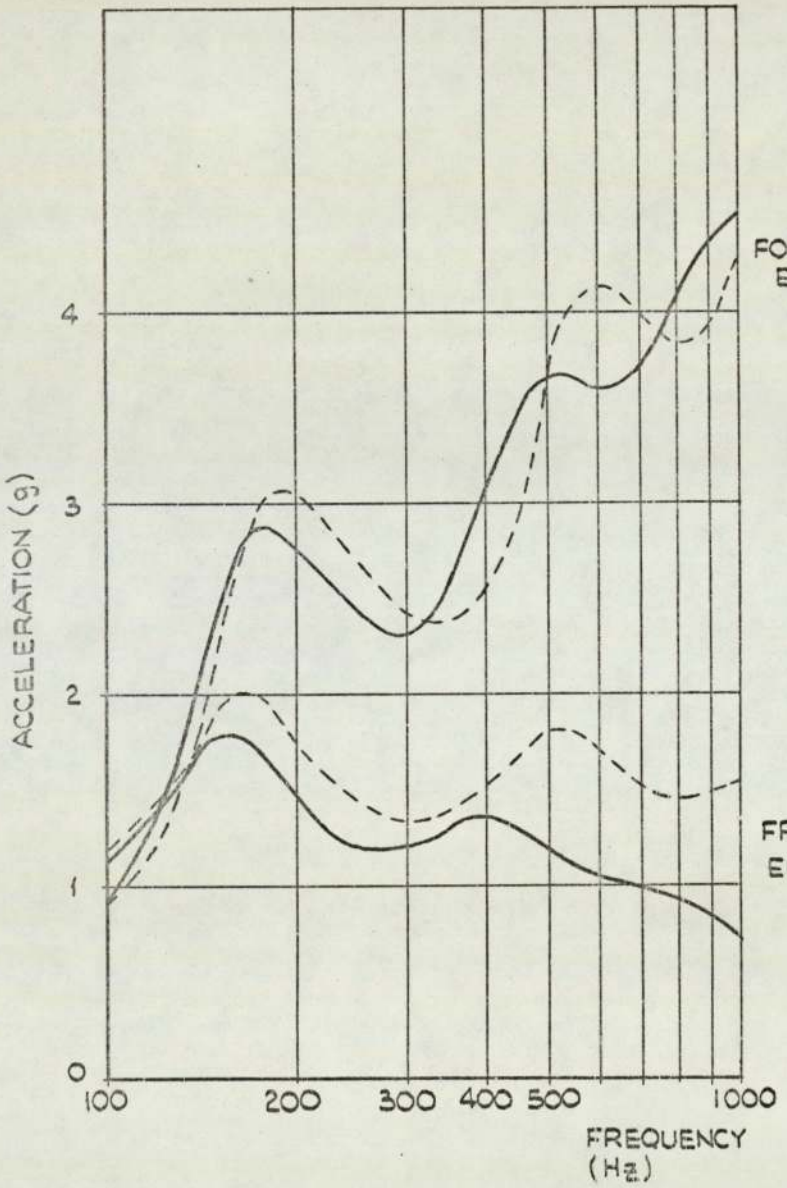

FIG. B.1

COMPARISON OF TIMOSHENKO AND EULER-BERNOULLI EQUATIONS FOR TRANSVERSE VIBRATIONS OF A BEAM.

—— TIMOSHENKO

--- EULER-BERNOULLI

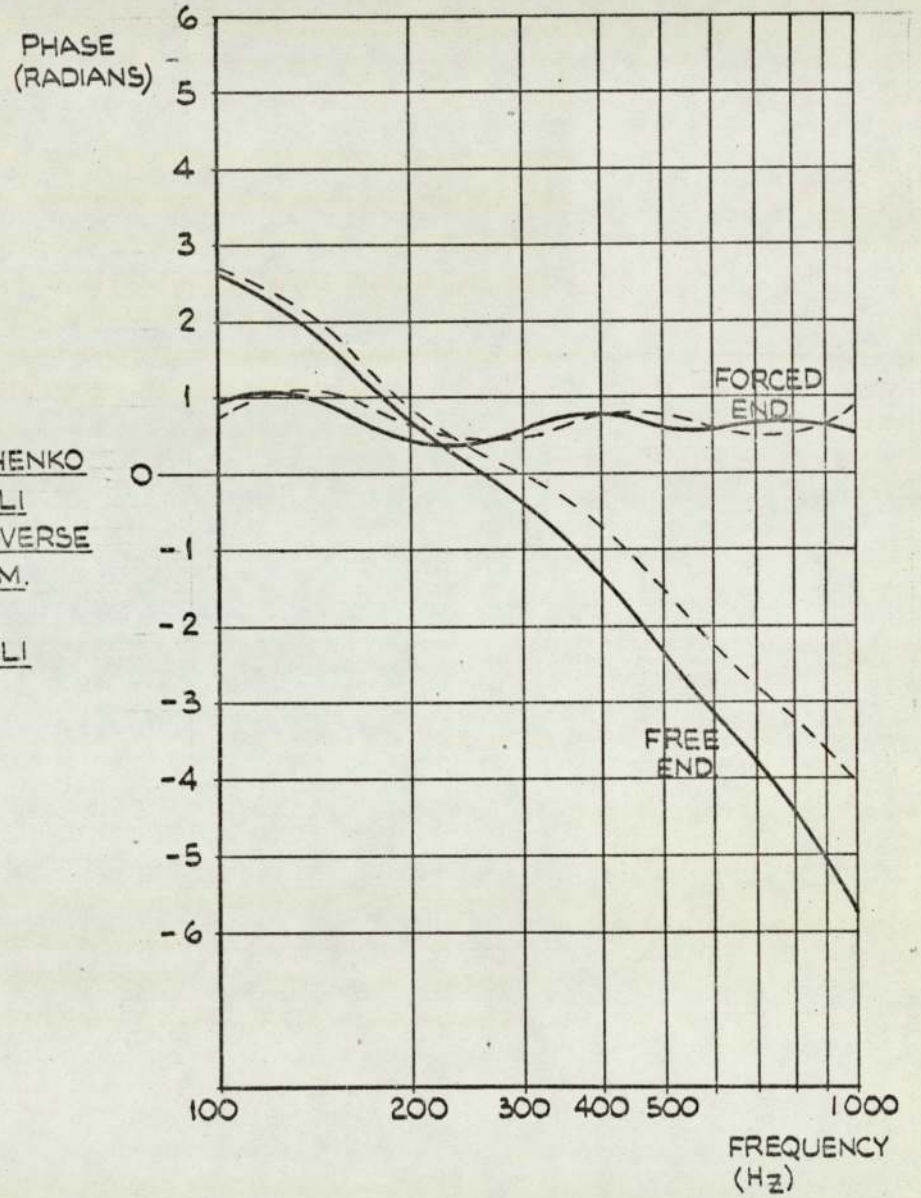

Appendix C

Comparison of the 'direct' and 'modal analysis' methods

There are two methods for solving a forced vibration problem :

(i) The direct method, where the applied forces are used as boundary conditions.

(ii) The modal analysis method where the displacement is expressed as a sum of the normal modes.

In the following, a problem will be solved using both methods and it will be shown that the results are the same.

The problem is a free-free beam forced at $x = l$ in transverse vibrations by a harmonically varying force $F = F_o e^{i\omega t}$.

The differential equation of motion is:

$$EI \frac{\partial^4 u}{\partial x^4} = -\rho A \frac{\partial^2 u}{\partial t^2} \qquad C(1)$$

The Direct Method

The problem is solved by the direct method in Appendix A, the solution for the displacement $u(x,t)$ is given by:

$$u = \frac{F_o e^{i\omega t}}{2EI\alpha^3(1 - \cos \alpha l \cosh \alpha l)} \times$$

$$(\cos \alpha x + \cosh \alpha x)(\sin \alpha l - \sinh \alpha l) + (\sin \alpha x + \sinh \alpha x)(\cos \alpha l - \cosh \alpha l) \qquad C(2)$$

where $\alpha^4 = \rho A \omega^2 / EI$

Modal Analysis

The solution of equation C(1) is assumed to be:

$$u(x,t) = \sum_{n=1}^{\infty} X_n \phi_n$$

where X_n are the normal functions for a free-free beam,

and ϕ_n are the generalised coordinates.

(a) The Normal Functions X_n of a free-free beam

Assume $u = X_n e^{i\omega_n t}$,

then the solution of equation C(1) is given by:

$$u = X_n e^{i\omega_n t} =$$

$$(B1_n \cos \alpha_n x + B2_n \sin \alpha_n x + B3_n \cosh \alpha_n x + B4_n \sinh \alpha_n x)\, e^{i\omega_n t}$$

where $\alpha_n^4 = \rho A\, \omega_n^2 / EI$ C(3)

The boundary conditions are:

$$\left.\begin{array}{lll} \text{at } x = 0 & -EI \dfrac{\partial^2 u}{\partial x^2} = 0 \quad \text{and} & EI \dfrac{\partial^3 u}{\partial x^3} = 0 \\ \text{at } x = l & -EI \dfrac{\partial^2 u}{\partial x^2} = 0 \quad \text{and} & EI \dfrac{\partial^3 u}{\partial x^3} = 0 \end{array}\right\} \quad C(4)$$

Substituting C(3) into C(4) gives the frequency equation (from which ω_n is calculated) and the Normal Functions:

The frequency equation is

$$\cos \alpha_n l \cosh \alpha_n l = 1$$

then $$\omega_n = \alpha_n^2 l \sqrt{\frac{EI}{\rho A l^2}}$$

The Normal Functions are given by:

$$X_n = \frac{B1_n}{\sinh \alpha_n l - \sin \alpha_n l}$$

$$(\cos \alpha_n l - \cosh a_n l)(\sin \alpha_n x + \sinh \alpha_n x) + (\sinh \alpha_n l - \sin \alpha_n l)(\cos \alpha_n x + \cosh \alpha$$

C(5)

Normal Functions are defined such that

$$\int_0^l X_n^2 \, dx = 1 \qquad C(6)$$

and $$\int_0^l X_n X_m \, dx = 0$$

Substituting C(5) into C(6) gives

$$Bl_n = \frac{\sinh \alpha_n l - \sin \alpha_n l}{\sinh \alpha_n l \cos \alpha_n l - \sin \alpha_n l \cosh \alpha_n l}$$

$$\text{therefore } X_n = \frac{(\cos\alpha_n l - \cosh\alpha_n l)(\sin\alpha_n x + \sinh\alpha_n x) + (\sinh\alpha_n l - \sin\alpha_n l)(\cos\alpha_n x + \cosh\alpha_n x)}{\sinh \alpha_n l \cos \alpha_n l - \sin \alpha_n l \cosh \alpha_n l}$$

It may be shown (see reference 59 , p. 364) that the generalised coordinates ϕ_n for forced transverse vibrations of a beam excited at $x = l$ by a force $F = -F_o e^{i\omega t}$, are given by

$$\phi_n = \frac{F(X_n)_{x=l}}{\rho A l(\omega_n^2 - \omega^2)}$$

$$\text{therefore } u = -F_o e^{i\omega t} \frac{1}{\rho A l} \sum_{n=1}^{\infty} \frac{X_n (X_n)_{x=l}}{\omega_n^2 - \omega^2}$$

$$\text{therefore } u = \frac{-2F_o e^{i\omega t}}{EIl} \sum_{n=1}^{\infty} \frac{X_n}{\alpha_n^4 - \alpha^4} \qquad C(7)$$

Comparison of the two results

Consider the solution using the direct method, i.e. equation C(2);

Let $f(x) = (\sinh\alpha l - \sin\alpha l)(\cosh\alpha x + \cos\alpha x) - (\cosh\alpha l - \cos\alpha l)(\sinh\alpha x + \sin\alpha x)$

Then $$u = -F_o e^{i\omega t} \frac{f(x)}{2EI\alpha^2(1-\cos\alpha l \cosh\alpha l)}$$

Since $\{X_n\}$ is a complete set of orthogonal functions in the range 0 to l, it is possible to express $f(x)$ as an infinite sum in terms of these functions,

i.e. $$f(x) = \sum_{n=1}^{\infty} a_n X_n$$

then $$a_n = \int_o^l f(x)\, X_n\, dx \Big/ \int_o^l X_n^2\, dx$$

$$= 1/l\ (1 - \cos\alpha l \cosh\alpha l) \frac{4\alpha^3}{\alpha_n^4 - \alpha^4}$$

therefore $$f(x) = \sum_{n=1}^{\infty} \frac{(1 - \cos\alpha l \cosh\alpha l)\, 4\alpha^3}{l(\alpha_n^4 - \alpha^4)} X_n$$

therefore $$u = \frac{-2F_o e^{i\omega t}}{EIl} \sum_{n=1}^{\infty} \frac{X_n}{\alpha_n^4 - \alpha^4}$$

which is identical to equation C(7).

Appendix D

Gauss Elimination

If there are m simultaneous equations in m unknowns to be solved then they can be written in matrix form and solved using the Gauss Elimination technique. Let the matrix equation be

$$(A)\ \{x\} = \{y\}$$

The method consists of manipulating the matrices (A) and $\{y\}$ by equivalence operations to convert (A) into upper triangular form

$$(A')\ \{x\} = \{y'\}$$

i.e.
$$\begin{bmatrix} 1 & a_{12}' & a_{13}' & a_{14}' & \cdot & \cdot & \cdot & \cdot \\ 0 & 1 & a_{23}' & a_{24}' & \cdot & \cdot & \cdot & \cdot \\ 0 & 0 & 1 & a_{34}' & \cdot & \cdot & \cdot & \cdot \\ 0 & 0 & 0 & 1 & a_{45}' & \cdot & \cdot & \cdot \\ \cdots & \cdots & \cdots & \cdots & \cdots & \cdots & \cdots & \cdots \\ \cdots & \cdots & \cdots & \cdots & \cdots & \cdots & \cdots & \cdots \\ 0 & 0 & 0 & 0 & \cdots & 0 & 0 & 1 \end{bmatrix} \begin{bmatrix} x_1 \\ x_2 \\ x_3 \\ x_4 \\ \cdot \\ \cdot \\ x_{m-1} \\ x_m \end{bmatrix} = \begin{bmatrix} y_1' \\ y_2' \\ y_3' \\ y_4' \\ \cdot \\ \cdot \\ y_{m-1}' \\ y_m' \end{bmatrix} \quad D($$

then $\{x\}$ is found by back substitution.

The procedure is: divide all elements in the first row (including y_1) by a_{11}

Then the zeros in positions (2,1)(3,1)(4,1) etc are formed by performing the equivalence operations :

$$a_{ni} = a_{ni} - a_{n1}\, a_{11}, \quad \text{for } i = 1,m \text{ and for } n = 2,m$$

and $$y_n = y_n - a_{n1} y_1 \qquad \text{for } n = 2,m$$

The first column is then in the form given in equation D(1)
The procedure is then repeated for column 2, i.e. all elements in row 2 (including y_2) are divided by a_{22}; elements (3,2),(4,2),(5,2), etc are put equal to zero by the equivalence operations:

$$a_{ni} = a_{ni} - a_{n2}\, a_{2i} \qquad \text{for } i = 2,m \text{ and } n = 3,m$$

and $$y_n = y_n - a_{n2} y_2 \qquad \text{for } n = 3,m$$

Similarly for columns 3 to m until the matrix is in the form D(1).
Consider the m^{th} equation: $x_m = y_m$

" " $(m-1)^{th}$ " $x_{m-1} + a_{m-1,m} x_m = y_{m-1}$; hence x_{m-1}

" " $(m-2)^{th}$ " $x_{m-2} + a_{m-2,m-1} x_{m-1} + a_{m-2,m} x_m = y_{m-2}$; hence x_{m-2} etc

A flow diagram for the technique is given on the following pages

ss elimination technique

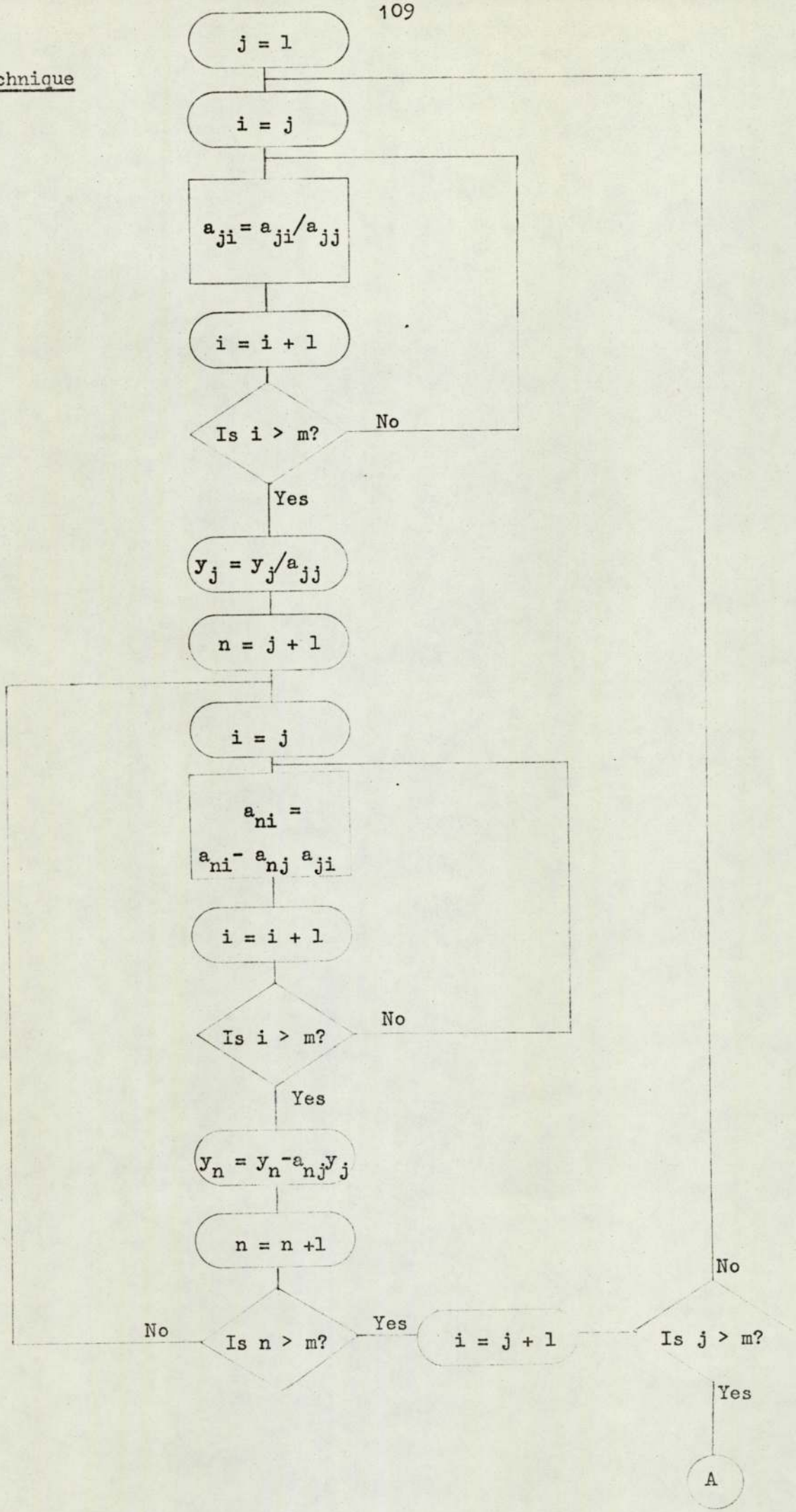

Back substitution

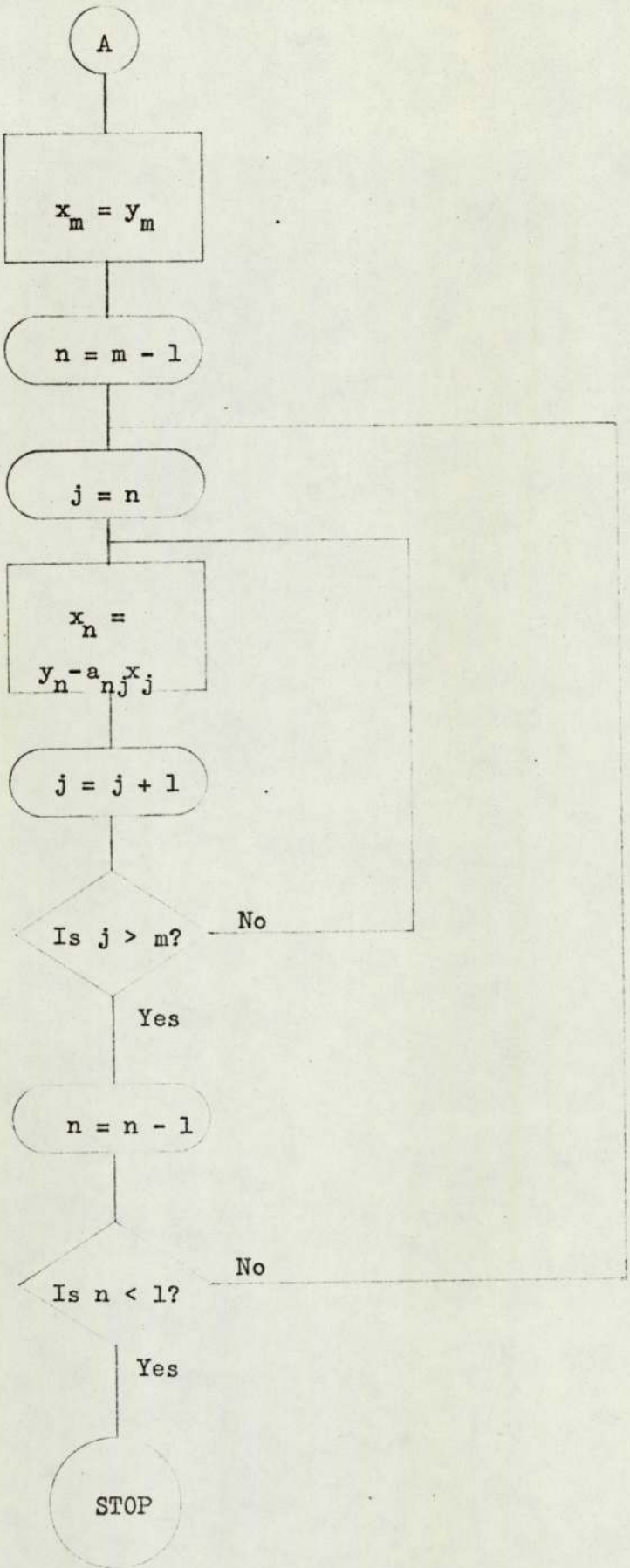

Appendix E

```
      IMPLICIT REAL*8  (A-H,O-Z)
      OPEN (5,INPUT,PROMPT'FILE 5')
      OPEN (6,OUTPUT*T)
      DOUBLE PRECISION COMPLEX BO,BR,AC,A,E,S,C
      DOUBLE PRECISION COMPLEX V,D1,D2,F,FD,T
      DOUBLE PRECISION COMPLEX X1,X2
      REAL*8 M1,M2
      TEN 6=1ØØØ.*1ØØØ.
      PI=4.*ATAN(1.)
      EP1=.ØØ1
 7Ø   WRITE(Ø,65)
 65   FORMAT(//'INPUT BR')
      ACCEPT BR
 8Ø   READ(5,1Ø)AR,RO,EL,EF
      WRITE(6,11)
      WRITE(6,1Ø)AR,RO,EL,EF
 83   READ(5,1Ø)M1,M2
      WRITE(6,19)
      WRITE(6,1Ø)M1,M2
 89   WRITE(6,21)
 9Ø   READ(5,2Ø)FR,X,Y
      X=X*9.8Ø665
      IF(FR)99,99,1ØØ
1ØØ   OM=2.*PI*FR
      A=DCMPLX(X*DCOS(Y),X*DSIN(Y))
      A1=(M1+M2)/(RO*EL*EL)
      A2=AR*AR*RO
      C1=EF/(AR*EL*RO)
      C2=AR*RO*EL
      X1=EF*RO*AR
      X2=(M1+M2)*AR*RO
      X3=AR*AR*RO*RO*EL
      X4=M1*M2/EL
11Ø   S=CDSIN(BR)
      C=CDCOS(BR)
      T=S/C
      V=X2*C+(X3/BR-X4*BR)*S
      E=X1/V-A
      FD=X1*(X2*S-(X3/BR-X4*BR)*C+(X3/(BR*BR)+X4)*S)/(V*V)
      BR=-F/FD+BR
      AC=X1/(X2*CDCOS(BR)+(X3/BR-X4*BR)*CDSIN(BR))
119   IF(DABS(DREAL(AC)-X*DCOS(Y))-EP1)12Ø,12Ø,11Ø
12Ø   IF(DABS(DIMAG(AC)-X*DSIN(Y))-EP1)13Ø,13Ø,11Ø
13Ø   E=(OM*OM*EL*EL*RO)/(BR*BR)
      E=E/TEN6
      WRITE(6,5Ø)FR,E
 1    CONTINUE
      GO TO 9Ø
 99   CONTINUE
      CLOSE(6)
      STOP
 1Ø   FORMAT(4D1Ø.4)
 11   FORMAT(//3X,'AREA',5X,'DENSITY',4X,'LENGTH',2X,'RMS FORCE')
 19   FORMAT(//3X,'MASS 1', 4X, 'MASS 2')
 20   FORMAT(5F1Ø.4)
 21   FORMAT(//1X,'FREQUENCY',4X,'E1',6X,'E2')
 5Ø   FORMAT(2X,7F8.2)
      END
```

References

1 DILLON, J.H., I.B. PRETTYMAN and G.L. HALL. Hysteretic and elastic properties of rubberlike materials under dynamic shear stresses. J. Applied Physics. 15 309 April 1944.

2 DILLON, J.H. and S.D. GEHMAN. Hysteresis and methods for its measurement in rubber-like materials. India Rubber World. 115 (1) 61 October 1946.

3 OBERST, H. and K. FRANKENFELD. Über die Dämpfung der Biegeschwingungen dünner Bleche durch fest haftende Beläge. Acustica 2 AB181 1952.

4 FITZGERALD, E.R. and J.D. FERRY. Method for determining the dynamic mechanical behaviour of gels and solids at audio-frequencies; comparison of mechanical and electrical properties. J. Colloid Science 8 1 1953.

5 BLAND, D.R. and E.H. LEE. Calculation of the complex modulus of linear viscoelastic materials from vibrating reed measurements. J. Applied Physics 26(12) 1497 December 1955.

6 KOPPELMANN, J. Über die Bestimmung des dynamischen Elastizitätsmoduls und des dynamischen Schubmoduls im Frequenzbereich von 10^{-5} bis 10^{-1} Hz. Rheologica Acta 1 20 1958.

7 HUANG, T.C. The effect of rotatory inertia and of shear deformation on the frequency and normal mode equations of uniform beams with simple end conditions. Trans. of the ASME. J. Applied Mechanics 28 579 December 1961

8 SCHAPERY, R.A. Approximate methods of transform inversion for viscoelastic stress analysis.
Proc. 4th U.S. National Congress of Applied Mechanics 2 1075 1962.

9 MILES, D.O. Sinusoidal shear generator for study of viscoelasticity.
J. Applied Physics 33(4) 1422 April 1962.

10 BURTON, J.D., W.B. JONES and J.D. FRAZEE. Viscoelastic vibrations.
Bulletin 3rd Meeting ICRPG Working Group on Mechanical Behaviour.
p. 191 1964.

11 WILLIAMS, M.L. Structural analysis of viscoelastic materials.
AIAA J. 2(5) 785 May 1964.

12 ACHENBACH, J.D. Dynamic response of a long case-bonded viscoelastic cylinder.
AIAA J. 3(4) 673 April 1965.

13 HUNTER, S.C. The solution of boundary value problems in linear viscoelasticity.
Proc. 4th Symposium on Naval Structural Mechanics. Mechanics and chemistry of solid propellants. p. 257 April 1965.

14 BALTRUKONIS, J.H. The dynamics of solid propellant rocket motors.
Proc. 4th Symposium on Naval Structural Mechanics. Mechanics and chemistry of solid propellants. p. 297 April 1965.

15 ACHENBACH, J.D. Thickness-shear vibrations of an ablating rocket.
Northwestern University TR/65/3 July 1965.

16 ACHENBACH, J.D. Forced vibrations of a burning rocket.
AIAA J. 3(7) 1333 July 1965.

17 DiTARANTO, R.A. Theory of vibratory bending for elastic and viscoelastic layered finite-length beams.
Trans. ASME. J. Applied Mechanics. 881 December 1965.

18 HENRY, L.A. and A.M. FREUDENTHAL. Forced vibrations of a finite viscoelastic cylinder case-bonded to a thin shell.
AIAA J. 4 313 1966.

19 DAVIS, J.L. Dynamical aspects of viscoelasticity.
Trans. of the Society of Rheology. 10(2) 449 1966.

20 PAN, H-H. Vibration of a viscoelastic Timoshenko beam.
J. Engineering Mechanics Division. Proc. ASCE EM2 213 April 1966.

21 ACHENBACH, J.D. Dynamic response of a viscoelastic cylinder with ablating inner surface.
Trans. ASME J. Applied Mechanics. 275 June 1966

22 COWPER, G.R. The shear coefficient in Timoshenko's beam theory.
Trans. ASME J. Applied Mechanics. 335 June 1966.

23 ADKINS, R.L. Design considerations and analysis of a complex modulus apparatus.
Experimental Mechanics. 6 362 July 1966

24 VALANIS, K.C. Exact and variational solutions to a general viscoelasto-kinetic problem.
Trans. ASME J. Applied Mechanics. 888 December 1966

25 NASHIF, A.D. New method for determining damping properties of viscoelastic materials.
Proc. 36th Symposium on shock and vibration. p. 37 1967.

26 NICHOLAS, T. and R.A. HELLER. Determination of the complex shear modulus of a filled elastomer from a vibrating sandwich beam.
Experimental Mechanics. 7 110 March 1967.

27 ACHENBACH, J.D. Vibrations of a viscoelastic body.
AIAA J. 5(6) 1213 June 1967.

28 AGBASIERE, J.A. and P. GROOTENHUIS. Flexural vibration of symmetrical multi-layer beams with viscoelastic damping.
J. Mechanical Engineering Science. 10 (3) 269 1968.

29 SOWERS, J.D. Forced response of lumped-parameter system with applications to missile dynamics.
Shock and Vibration Bulletin. 38(3) 95 1968.

30 CANNON, C.M., A.D. NASHIF and D.I.G. JONES. Damping measurements on soft viscoelastic materials using a tuned damper technique.
Shock and Vibration Bulletin. 38(3) 151 1968.

31 NICHOLAS, T. The effects of rotatory inertia and shear deformation on the flexural vibrations of a two-layered viscoelastic-elastic beam.
Shock and Vibration Bulletin. 38(3) 13 1968.

32 PARSONS, J.S., W. YATER and F. SCHLOSS. The measurement of dynamic properties of materials using a transfer impedance technique.
Dept. of Navy. Naval ship research and development centre.
Report 2981 April 1969.

33 JONES, D.I.G. Material damping.
J. of Environmental sciences 12 20 June 1969

34 KORITES, B.J. and F.C. NELSON. The influence of dissipative heating on the loss factor of a viscoelastically damped beam.
Trans. ASME J. Engineering for Industry 91 975 November 1969.

35 SHAFFER, B.W. and R.I. SANN. Forced transverse vibration of a solid viscoelastic cylinder bonded to a thin casing.
ASME Paper No. 69-WA/APM - 20 November 1969.

36 DUDEK, T.J. Determination of the complex modulus of viscoelastic two-layer composite beams.
J. Composite Materials 4 74 January 1970.

37 COST, T.L. and E.B. BECKER. A multidata method of approximate Laplace Transform inversion.
International Journal for Numerical Methods in Engineering 2 207 1970

38 NORRIS, D.M. and W.C. YOUNG Complex modulus measurement by longitudinal vibration testing.
Experimental Mechanics 10 93 February 1970.

39 GROOTENHUIS, P. The control of vibrations with viscoelastic materials.
J. Sound and Vibration 11(4) 421 1970

40 BAUMGARTEN, J.R. and B.K. PEARCE. The damping effects of viscoelastic materials. Part I - Transverse vibrations of beams with viscoelastic coatings.
Trans. ASME J. Engineering for Industry 93 645 May 1971

41 CHATTERJEE, A. and J.R. BAUMGARTEN. An analysis of viscoelastic damping characteristics of a simply supported sandwich beam. Trans. ASME J. Engineering for Industry 93 1239 November 1971.

42 ROBERTSON, S.R. Using measured material parameters in solving forced motion problems in viscoelasticity. J. Sound and Vibration 19(1) 95 1971.

43 HUANG, T.C. and C.C. HUANG. Free vibrations of viscoelastic Timoshenko beams. Trans. ASME J. Applied Mechanics 38 515 1971

44 COOTE, C.T. Measurement of the damping properties of silicone-based elastomers over wide temperature ranges. J. Sound and Vibration 21(2) 133 1972

45 ROBERTSON, S.R. Forced motion of isotropic and transversely isotropic viscoelastic Timoshenko beams using measured material. J. Sound and Vibration 23(2) 157 1972

46 BERT, C.W. Material damping. An introductory review of mathematical models, measures and experimental techniques. J. Sound and Vibration 29(2) 129 1973

47 JONES, D.I.G. Temperature-frequency dependence of dynamic properties of damping materials. J. Sound and Vibration 33(4) 451 1974

48 FERRY, J.D. Viscoelastic properties of polymers. 2nd Edition John Wiley and Sons., Inc. 1970

49 FLÜGGE, W. Viscoelasticity Blaisdell Publishing Co. 1967

50 HUANG, C.C. PhD Thesis University of Wisconsin 1967

51 FOX, L. An introduction to numerical linear algebra.
Clarendon Press Oxford 1964

52 KOLSKY, H. Experimental studies of the mechanical behaviour of linear viscoelastic solids.
Proc. 4th Symposium on Naval Structural Mechanics.
Mechanics and chemistry of solid propellants. p. 357 1965

53 ZAVERI, K. and H.P. OLESEN. Measurement of elastic modulus and loss factor of asphalt.
Brüel and Kjaer Technical Review No. 4 1972

54 SACK, H.S., J. MOTZ, H.L. RAUB and R.N. WORK
Elastic losses in some high polymers as a function of frequency and temperature
J. Applied Physics 18(5) 450 1947

55 HORIO, H. and S. ONOGI Forced vibration of a reed as a method of determining viscoelasticity
J. Applied Physics 22(7) 977 1951

56 NOLLE, A.W. Methods for measuring dynamic mechanical properties of rubber-like materials
J. Applied Physics 19(8) 753 1948

57 KLINE, D.E. A recording apparatus for measuring the dynamic mechanical properties of polymers
J. Polymer Science 22 449 1956

58 ROBINSON, D.W. An apparatus for the measurement of dynamic mechical properties of polymers over a wide temperature range.
J. Scientific Instruments 32 2 1955

59 TIMOSHENKO, S. Vibration problems in engineering. 3rd edition
D. Van Nostrand Co. Inc.

60 ARMENÀKAS, A.E., D.C. GAZIS and G. HERRMANN Free vibrations of circular cylindrical shells. Pergamon Press 1969.

61 DALQUIST, C.A. A family of viscoelastic materials for diverse damping applications ASME Publication 71-Vibr-47

62 RALSTON, A. A first course in numerical analysis.
McGraw-Hill 1965

Acknowledgements

The author wishes to acknowledge the help given by the following:

Prof. E. Downham, for his help and guidance throughout the research especially regarding the experimental work.

Mr. N.J. Kerruish, for help with the mathematical problems.

Mr. H.M. Darwell, Mr. H. Badham, Dr. F.R. Wallis and Mr. J.H.B. Pearce, for assistance, especially with problems on rocket motors.

Mrs. M. Fishbourne, for help in coding several computer programs.

Mr. B. Muddyman, for his assistance with the laboratory experiments.

Mr. D.J. Finch and Mr. C.S. Sunnersjö, for many helpful discussions.

Mrs. Brenda Jones, for typing the manuscript.

Mrs. I. Pitcher, for tracing the figures.

Mr. G. Panting, my father, for checking the manuscript for errors in grammar and spelling.

Mr. G. Edwards, my husband, for his help, encouragement and patience during the past three years.